New Signal Transduction Methods for Cucurbit[*n*]uril-Based Chemosensors

Zur Erlangung des akademischen Grades einer

DOKTORIN DER NATURWISSENSCHAFTEN

(Dr. rer. nat.)

von der KIT-Fakultät für Chemie und Biowissenschaften

des Karlsruher Instituts für Technologie (KIT)

genehmigte

DISSERTATION

von

M. Sc. Nilima Manoj Kumar

1. Referent: Priv.-Doz. Dr. Frank Biedermann
2. Referent: Prof. Dr. Stefan Bräse

Tag der mündlichen Prüfung: 16. Juli 2024

Declaration

I, Nilima Manoj Kumar, declare that this thesis entitled **"New Signal Transduction Methods for Cucurbit[n]uril-Based Chemosensors"** and the work presented in it are my own and the work was undertaken under the supervision of Priv.-Doz. Dr. Frank Biedermann at the Institute of Nanotechnology (INT), at the Karlsruhe Institute of Technology (KIT). I confirm that:

- This work was done wholly while in candidature for a research degree at KIT.
- The whole thesis was written by me, and no other sources other than the specified were used.
- The rules for ensuring good scientific practice of the Karlsruhe Institute of Technology (KIT) have been used, and the submission and archiving of the primary data in accordance with section A(6) of the rules for ensuring good scientific practice of KIT have been ensured.
- The electronic version of the work is consistent with the written version.
- Where I have consulted the published work of others, this is always clearly attributed.
- I have acknowledged all main sources of help.
- Where the thesis is based on work done by myself jointly with others, I have clarified exactly what was done by others and what I have contributed myself.
- Furthermore, I declare that I did not undertake any previous doctoral studies and that I am currently not enrolled in any other ongoing doctoral procedure.

Nilima Manoj Kumar

Deklaration

Ich, Nilima Manoj Kumar, erkläre, dass diese Arbeit mit dem Titel **"New Signal Transduction Methods for Cucurbit[*n*]uril-Based Chemosensors"** und die darin vorgestellten Ergebnisse meine eigenen sind. Die Arbeit wurde unter der Leitung von Priv.-Doz. Dr. Frank Biedermann am Institut für Nanotechnologie (INT), am Karlsruher Institut für Technologie (KIT) angefertigt. Ich bestätige:

- Diese Arbeit wurde vollständig während der Kandidatur für ein Forschungsstudium am KIT durchgeführt.
- Die gesamte Arbeit wurde von mir verfasst und es wurden keine anderen Quellen als die angegebenen verwendet.
- Es wurden Maßnahmen zur Sicherstellung einer guten wissenschaftlichen Praxis des Karlsruher Instituts für Technologie (KIT) angewendet und die Übermittlung und Archivierung der Primärdaten gemäß Abschnitt A(6) der Regeln zur Sicherstellung einer guten wissenschaftlichen Praxis des KIT sichergestellt.
- Die elektronische Fassung des Werkes entspricht der schriftlichen Fassung.
- Im Fall, dass ich die veröffentlichten Arbeiten anderer konsultiert habe, wird dies immer eindeutig zugeordnet.
- Ich habe alle wichtigen Hilfsquellen zur Kenntnis genommen.
- Wenn die Arbeit auf Arbeiten basiert, die ich gemeinsam mit anderen geleistet habe, habe ich kenntlich gemacht, was von anderen geleistet wurde und was ich selbst beigesteuert habe.
- Des Weiteren erkläre ich, dass ich kein vorheriges Promotionsstudium absolviert habe und mich derzeit nicht in einem anderen laufenden Promotionsverfahren befinde.

Nilima Manoj Kumar

With heartfelt gratitude and love, I dedicate this work to my beloved family and dearest friends.

Table of Contents

1. Abstract

Molecular recognition of bioactive analytes plays a vital role in various fields, including clinical diagnostics, pharmaceuticals, and environmental monitoring. Although conventional instrument-based analytical methods such as high-performance liquid chromatography (HPLC), NMR, and mass spectrometry are available for molecular analysis, their execution is cumbersome, requires expensive instrumentation, and is time-consuming. Additionally, these challenges restrict their use in home or point-of-care units for routine diagnosis. Therefore, chemosensors based on supramolecular host-guest chemistry are a promising alternative for the selective and sensitive detection of analytes, offering a low-cost and fast-responding sensing platform for diagnostics and sensing applications. These chemosensors comprise an artificial receptor as a molecular recognition motif and a molecular signalling component for reporting the recognition event. To date, several macrocyclic hosts and their derivatives have been investigated as artificial receptors to develop robust chemosensors. Among these macrocyclic hosts, cucurbit[n]urils have a prominent role due to their exceptional binding affinities for a wide variety of analytes and hence, cucurbit[n]uril-based chemosensors have been extensively researched for analyte sensing. In most examples, cucurbit[n]uril-based chemosensors utilize fluorescence as the signal transduction mechanism. Fluorescent species require an external light source to produce emission signals. Consequently, fluorescent chemosensors encounter major challenges, such as background fluorescence from other emissive components in the sample, light source instability, light scattering, and photobleaching. These challenges result in a suboptimal signal-to-noise ratio, thereby limiting their practical applications. Hence, new design principles for cucurbit[n]uril-based chemosensors are necessary.

Designing chemiluminescent chemosensors would be advantageous because chemiluminescence is generated through a chemical reaction and does not depend on an external light source for signal generation. Chemiluminescent chemosensors can thus circumvent the drawbacks of fluorescent chemosensors by providing a comparatively low background signal and superior signal-to-noise ratio. Another approach is to develop electrochemical sensors that produce electrochemical responses as detectable signals. These sensors serve as a useful complement to existing fluorescent chemosensors, particularly at

emergency sites where fast and accurate detection is essential. Additionally, electrochemical-based detection methods hold the potential for designing compact and portable sensors.

In this thesis, novel signal transduction methods for cucurbit[*n*]uril-based chemosensors are developed by investigating chemiluminescence- and electrochemical- based detection strategies. In addition, proof-of-concept solutions for realizing their practical applications in molecular diagnostics are described.

The first research project presents the design and development of a chemiluminescent chemosensor utilizing cucurbit[8]uril as the macrocyclic host and phenoxy 1,2-dioxetane as the chemiluminescent indicator. This chemosensor enabled the detection of drugs at low micromolar concentrations in biofluids such as human urine and human serum. In addition, it was found that cucurbit[8]uril can act as a chemiluminescent enhancer of commercially available chemiluminescent substrates such as CDP-Star. This shows the potential of cucurbit[8]uril to improve the chemiluminescent diagnostic assay by providing a non-toxic and cost-effective substitute to existing performance enhancers like surfactant-dye adducts that are chemically unstable. Finally, a chemiluminescence resonance energy transfer-based assay is developed employing a cucurbit[7]uril-dye conjugate and a phenoxy 1,2-dioxetane to detect the herbicide paraquat in aqueous media. Although literature examples of chemiluminescent host-guest type chemosensors for cell imaging and the detection of reactive oxygen species have been reported, this research project represents the first study of a chemiluminescent host-guest type chemosensor for the detection of small organic molecules, such as drugs, in biofluids.

The second research project demonstrates a novel design principle of an electrochemical chemosensor utilizing cucurbit[7]uril as the macrocyclic host and electrochemically active platinum(II) compound as the redox indicator for the detection of redox-inactive analytes. Specifically, this chemosensor exhibited low micromolar detection of pancuronium bromide drug, a known muscle relaxant, in aqueous solutions and human urine samples. This is the first chemosensor capable of detecting pancuronium bromide *via* host-guest interactions. Unlike existing electrochemical chemosensors, this design eliminates the need for cumbersome immobilization processes on the electrode surface. Notably, it is adaptable to perform with commercially available screen-printed electrodes and requires minimal sample volumes for measurements. This design strategy thus provides potential possibilities for developing miniaturized, disposable, and portable sensors for molecular diagnostics.

Abstract

In summary, this doctoral thesis focuses on designing novel signal transduction strategies to develop cucurbit[n]uril-based chemosensors by exploiting chemiluminescence and electrochemical-based detection methods for the sensitive detection of biologically relevant analytes in biofluids. These designs can pave the way for the future development of cost-effective and fast-response chemosensors based on host-guest chemistry, with improved practical applications in molecular diagnostics.

2. Zusammenfassung / Abstract in German

Die molekulare Erkennung bioaktiver Analyten spielt in verschiedenen Bereichen eine wichtige Rolle, darunter in der klinischen Diagnostik, der Pharmazie und der Umweltüberwachung. Obwohl für die molekulare Analyse herkömmliche instrumentenbasierte Analysemethoden wie Hochleistungsflüssigkeitschromatographie (HPLC), NMR und Massenspektrometrie zur Verfügung stehen, ist ihre Durchführung umständlich, erfordert teure Instrumente und ist zeitaufwändig. Darüber hinaus beschränken diese Herausforderungen ihre Verwendung in Heim- oder Point-of-Care-Einheiten für die Routinediagnose. Daher sind Chemosensoren auf Basis supramolekularer Wirt-Gast-Chemie eine vielversprechende Alternative für die selektive und empfindliche Erkennung von Analyten und bieten eine kostengünstige und schnell reagierende Sensorplattform für Diagnostik- und Sensoranwendungen. Diese Chemosensoren umfassen einen künstlichen Rezeptor als molekulares Erkennungsmotiv und eine molekulare Signalkomponente zur Meldung des Erkennungsereignisses. Bisher wurden mehrere makrozyklische Wirte und ihre Derivate als künstliche Rezeptoren untersucht, um robuste Chemosensoren zu entwickeln. Unter diesen makrozyklischen Wirten spielen Cucurbit[n]urile aufgrund ihrer außergewöhnlichen Bindungsaffinitäten für eine Vielzahl von Analyten eine herausragende Rolle, und daher wurden Chemosensoren auf Cucurbit[n]uril-Basis intensiv für die Analyterkennung erforscht. In den meisten Fällen nutzen Chemosensoren auf Cucurbit[n]uril-Basis Fluoreszenz als Signalübertragungsmechanismus. Fluoreszierende Spezies benötigen eine externe Lichtquelle, um Emissionssignale zu erzeugen. Daher stehen fluoreszierende Chemosensoren vor großen Herausforderungen, wie Hintergrundfluoreszenz von anderen emittierenden Komponenten in der Probe, Instabilität der Lichtquelle, Lichtstreuung und Photobleichung. Diese Herausforderungen führen zu einem suboptimalen Signal-Rausch-Verhältnis und begrenzen so ihre praktischen Anwendungen. Daher sind neue Designprinzipien für Chemosensoren auf Cucurbit[n]uril-Basis erforderlich.

Die Entwicklung chemilumineszierender Chemosensoren wäre von Vorteil, da Chemilumineszenz durch eine chemische Reaktion erzeugt wird und für die Signalerzeugung nicht auf eine externe Lichtquelle angewiesen ist. Chemilumineszierende Chemosensoren können somit die Nachteile fluoreszierender Chemosensoren umgehen, indem sie ein vergleichsweise niedriges Hintergrundsignal und ein besseres Signal-Rausch-Verhältnis bieten.

Ein anderer Ansatz ist die Entwicklung elektrochemischer Sensoren, die elektrochemische Reaktionen als erkennbare Signale erzeugen. Diese Sensoren dienen als nützliche Ergänzung zu vorhandenen fluoreszierenden Chemosensoren, an denen eine schnelle und genaue Erkennung unerlässlich ist. Darüber hinaus bieten elektrochemische Erkennungsmethoden das Potenzial für die Entwicklung kompakter und tragbarer Sensoren.

In dieser Arbeit werden neuartige Signalübertragungsmethoden für Cucurbit[*n*]uril-basierte Chemosensoren entwickelt, indem chemilumineszenz- und elektrochemische Detektionsstrategien untersucht werden . Darüber hinaus werden Proof-of-Concept-Lösungen für die Realisierung ihrer praktischen Anwendung in der molekularen Diagnostik beschrieben.

Das erste Forschungsprojekt präsentiert den Entwurf und die Entwicklung eines chemilumineszierenden Chemosensors, der Cucurbit[8]uril als makrozyklischen Wirt und Phenoxy-1,2-dioxetan als chemilumineszierenden Indikator verwendet. Dieser Chemosensor ermöglichte die Erkennung von Arzneimitteln in niedrigen mikromolaren Konzentrationen in Bioflüssigkeiten wie menschlichem Urin und menschlichem Serum. Darüber hinaus wurde festgestellt, dass Cucurbit[8]uril als chemilumineszierender Verstärker von kommerziell erhältlichen chemilumineszierenden Substraten wie CDP-Star wirken kann. Dies zeigt das Potenzial von Cucurbit[8]uril, den chemilumineszierenden diagnostischen Test zu verbessern, indem es einen ungiftigen und kostengünstigen Ersatz für vorhandene Leistungsverstärker wie Tensid-Farbstoff-Addukte bietet, die chemisch instabil sind. Schließlich wird ein auf Chemilumineszenz-Resonanzenergietransfer basierender Test entwickelt, der ein Cucurbit[7]uril-Farbstoff-Konjugat und ein Phenoxy 1,2-dioxetan verwendet, um das Herbizid Paraquat in wässrigen Medien zu erkennen. Obwohl in der Literatur bereits Beispiele für chemilumineszierende Chemosensoren vom Wirt-Gast-Typ für die Zellbildgebung und die Erkennung reaktiver Sauerstoffspezies beschrieben wurden, handelt es sich bei diesem Forschungsprojekt um die erste Untersuchung eines chemilumineszierenden Chemosensors vom Wirt-Gast-Typ für die Erkennung kleiner organischer Moleküle, wie etwa Arzneimittel, in Bioflüssigkeiten.

Das zweite Forschungsprojekt demonstriert ein neuartiges Designprinzip eines elektrochemischen Chemosensors, der Cucurbit[7]uril als makrozyklischen Wirt und eine elektrochemisch aktive Platin(II)-Verbindung als Redoxindikator zur Erkennung redoxinaktiver Analyten verwendet. Insbesondere zeigte dieser Chemosensor eine Erkennung des Arzneimittels Pancuroniumbromid im niedrigen mikromolaren Bereich in wässrigen

Lösungen und menschlichen Urinproben. Dies ist der erste Chemosensor, der Pancuroniumbromid über Wirt-Gast-Wechselwirkungen erkennen kann. Im Gegensatz zu bestehenden elektrochemischen Chemosensoren macht dieses Design aufwändige Immobilisierungsprozesse auf der Elektrodenoberfläche überflüssig. Es ist insbesondere an handelsübliche, im Siebdruckverfahren hergestellte Elektroden anpassbar und erfordert nur minimale Probenvolumina für Messungen. Diese Designstrategie bietet somit potenzielle Möglichkeiten für die Entwicklung miniaturisierter, tragbarer Einwegsensoren für die Molekulardiagnostik.

Zusammenfassend konzentriert sich diese Doktorarbeit auf die Entwicklung neuartiger Signalübertragungsstrategien zur Entwicklung von Chemosensoren auf Cucurbit[*n*]uril-Basis unter Nutzung von Chemilumineszenz und elektrochemischen Nachweismethoden für die empfindliche Erkennung biologisch relevanter Analyten in Bioflüssigkeiten. Diese Entwürfe können den Weg für die zukünftige Entwicklung kostengünstiger und schnell reagierender Chemosensoren auf Basis der Wirt-Gast-Chemie ebnen, mit verbesserten praktischen Anwendungen in der Molekulardiagnostik.

3. General Introduction

3.1. Supramolecular chemistry based on molecular recognition

Supramolecular chemistry has attained increasing attention over the past decades due to the broad range of possibilities for practical applications, especially in medical diagnostics and sensing.[1-5] To date, well-known instrument-based methods such as high-performance liquid chromatography (HPLC), nuclear magnetic resonance (NMR) spectroscopy, and mass spectrometry have been employed for clinical analysis. Despite their potential for sensing applications, their implementation for routine diagnostics at home or point-of-care units is challenging due to technical sophistication, high costs, and high time consumption. Moreover, the capacity for high-throughput screening is restricted.

In this context, the advent of supramolecular chemistry based on molecular recognition strategy has emerged as a promising research area towards diagnostic and sensing applications.[6] Molecular recognition involves the specific and selective binding between the recognition element and the target analyte through non-covalent interactions such as hydrogen bonds, ionic bonds, hydrophobic interactions, and van der Waals forces.[7] Extensive research has been conducted in this direction to develop functional units called chemosensors and to investigate their potential for sensing analytes.[5, 6, 8, 9] A typical chemosensor consists of a recognition element or receptor to perform molecular recognition of the target analytes and a signal transducer to report the recognition event by producing a detectable signal such as optical, electrochemical, magnetic or thermal response (Figure 3.1).[10] The target binding specificity of the chemosensor is attained from the complementary structural and chemical features of the
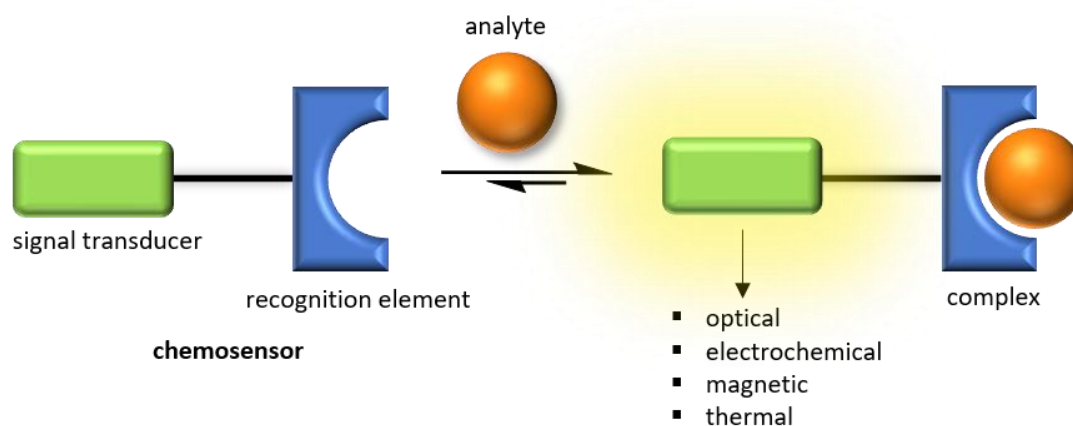
Figure 3.1 Schematic representation of a chemosensor.

recognition element. Due to their selective and sensitive detection of analytes, chemosensor-based research can offer further opportunities in diagnostics and sensing applications.

Chemosensors based on biological recognition elements such as antibodies, enzymes, and nucleic acids are termed biosensors and have shown promising results in molecular recognition-based diagnostics.[11-13] The following section explains various biosensors and the challenges associated with their practical implementations. Chemosensors based on host-guest chemistry as an alternative sensing platform for molecular recognition-based diagnostics, where artificial receptors act as recognition elements, are described in Section 3.1.2.

3.1.1. Biosensors

Biosensors are chemosensors with a biological recognition element that specifically interacts with the target analyte and a transducer that generates quantifiable signals.[14, 15] Clark and Lyons first elucidated the concept of biosensors in the 1960s for the detection of glucose.[16] Based on the nature of the recognition process, biosensors are classified as biocatalytic sensors and affinity sensors.[17] Biocatalytic sensors use biological catalysts, such as enzymes, to catalyze a reaction with the target analyte. Affinity sensors rely on specific binding between a target analyte and a recognition element, such as antibodies or nucleic acids.

In enzyme-based biosensors, enzymes are used as recognition elements due to their specific binding capabilities and catalytic properties, which allow them to convert specific substrate molecules (or target analytes) into products (Figure 3.2a).[18, 19] Several analyte recognition mechanisms have been employed in these biosensors: (1) detection of the product generated by the enzymatic conversion of the analyte, (2) detection of analyte-induced inhibition or
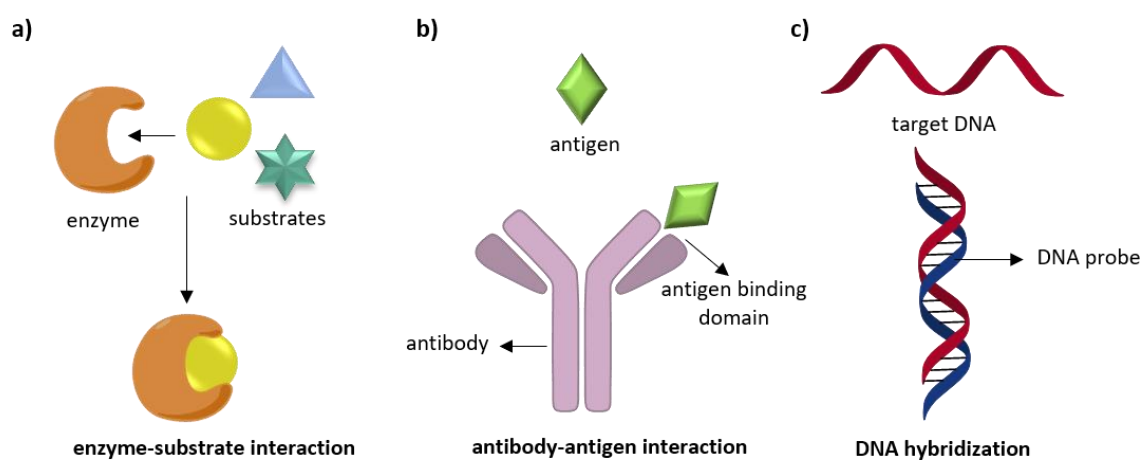

Figure 3.2 Schematic representation of analyte recognition by biological recognition elements. (a) enzyme, (b) antibody, and (c) nucleic acids.

activation of enzyme, or (3) monitoring changes in enzyme properties resulting from the interaction with the analyte.[20] For instance, various changes occurring during the enzymatic reaction can be monitored, including proton concentration (H^+), the release or uptake of gases (CO_2, NH_3, O_2), light absorption and emission.[21] Signal transducers then convert these changes into measurable signals.[22] The substrate-binding site of the enzyme is arranged with amino acids, which enable the enzyme to selectively bind to the specific substrate.[23] In some cases, enzymes work along with nonprotein chemical groups such as cofactors to attain substrate specificity.[17] In order to maintain the enzyme activity, immobilizing enzymes onto the sensor surface is necessary in enzyme-based biosensors.[24] The catalytic activity and specificity of enzyme-based biosensors have enabled these sensors to achieve high sensitivity.[25] Enzyme-based biosensors have been applied for the quantitative and qualitative analysis of target analytes in various fields such as environment, biomedicine, food quality control, agriculture, and pharmaceuticals.[26, 27] Many enzyme-based biosensors use a class of enzymes known as oxidoreductases.[28] The most widely investigated enzyme-based biosensors are glucose biosensors, which are used in clinical diagnostics to monitor blood glucose levels.[29] Additionally, other enzyme-based biosensors, such as lactate biosensors, are used in sports medicine for monitoring lactate accumulation during exercise, while urea biosensors are used in clinical diagnostics for monitoring kidney function.[30, 31] Similarly, numerous enzyme-based biosensors have been developed, commercialized, and utilized for various applications. Although enzyme-based biosensors have found practical applications, they have major drawbacks, such as a lack of selective enzymes for analytes of interest, enzyme instability, challenges associated with enzyme immobilization methods, reduced selectivity for *in vivo* analysis due to the presence of interferents in the sample matrix, and high costs.[32, 33]

Biosensors with antibody-based recognition elements, commonly referred to as immunosensors, exploit the high sensitivity and specificity of the antibody-antigen interactions.[24, 34] Antibodies are Y-shaped proteins with antigen-binding domains (Figure 3.2b).[24] The amino acid sequence in the antibody binding site determines the specificity of the antibody-antigen interaction. The sensing principle of the immunosensors is that the formation of a specific antibody-antigen complex enables the detection of analytes based on the resulting signal changes, such as optical, electrochemical or other physical properties at the immunosensor surface.[35] In immunosensors, the immobilization of antibodies onto the sensor surface is necessary to maintain the proper conformation and orientation required for optimal binding with the target analyte (antigen).[36] Antibody-based recognition offers numerous

advantages, such as high specificity, sensitivity, non-invasive ability, and direct recognition capability. Due to these properties, immunosensors have been widely employed in clinical diagnostics, pharmaceuticals, environmental monitoring, and food analysis to detect various target analytes, including bacteria, viruses, hormones, drugs, tumour biomarkers, and pesticides.[25, 35, 37] While there are promising approaches, antibody-based recognition has certain limitations, including cross-reactivity, thermal and chemical instability, long assay times, high production costs, regeneration difficulties, and challenges in antibody immobilization.[24, 33] In addition, antibodies face challenges in real-time monitoring of endogenously occurring target molecules because of the challenges involved in the internalization of antibodies into cells.[25, 38]

Nucleic acids are another type of biological recognition element, which exploit the complementary binding patterns of ribonucleic acid (RNA) or single-stranded deoxyribonucleic acid (ssDNA) (Figure 3.2c).[13, 24] Nucleic acid-based biosensors are also called genosensors and are used to detect specific sequences of RNA or ssDNA.[24] To achieve this, RNA or ssDNA fragments complementary to the target sequence can be artificially designed and immobilized to the sensor surface.[39, 40] Specificity in detection is attained through the complementary recognition nature between the target sequence and the immobilized RNA or ssDNA fragment.[24, 41] Since genosensors are based on sequence-specific interactions, they have a significant role in many fields, particularly clinical, environmental, and food analysis. Genosensors have been widely employed for the detection of bacterial pathogens, tumour markers, environmental pollutants, and food contaminants.[42-45] In addition, they are used for the detection of point mutations and other genetic variations.[42, 46, 47] Nevertheless, genosensors have a limited scope of applications, as their use is restricted to designing sensors targeting nucleic acids.[33] Furthermore, major drawbacks are encountered, including challenges in synthesizing and modifying nucleic acids, issues with nucleic acid stability, and the high cost of production.[33]

Despite the advantages associated with each biological recognition element, the mentioned challenges significantly affect the performance and practical implementation of biosensors. The search for new recognition elements to develop robust, simple, cost-effective, and rapid sensors is of constant interest. In this context, chemosensors based on host-guest chemistry that utilize artificial receptors as recognition elements are extensively investigated as an alternate approach.[6, 48] The following section provides an overview of chemosensors based on host-guest chemistry.

3.1.2. Chemosensors based on host-guest chemistry

Host-guest chemistry is a branch of supramolecular chemistry that describes the complexation of two or more molecules through non-covalent interactions and has been broadly researched across many fields, ranging from molecular recognition to drug delivery.[2, 5, 49-54]
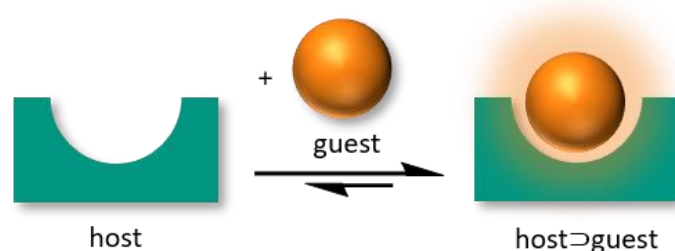

Figure 3.3 Schematic representation of a typical chemosensor based on host-guest chemistry.

Chemosensors based on host-guest chemistry are functional molecules that contain a synthetically derived molecule as a recognition element (host) (Figure 3.3). The host molecules are equipped with a binding cavity in which the specific guest molecules are encapsulated.[55] The underlying non-covalent interactions involved in host-guest binding include hydrogen bonding, electrostatic interactions, van der Waals forces, π-π stacking, and hydrophobic interactions.[56] In these chemosensors, host molecules bind reversibly with the guests (or analytes), forming host-guest inclusion complexes (Figure 3.3). Subsequently, these complex formations alter the physical, chemical, redox or spectroscopic properties of the guest or host, which serve as the basis for chemosensor design.[6, 48] To date, a wide variety of macrocyclic host molecules such as cyclodextrins, calix[n]arenes, cucurbit[n]urils, and pillar[n]arenes (Figure 3.4) have been extensively researched for developing novel host-guest type chemosensors due to their analyte-recognition property.[57-59]
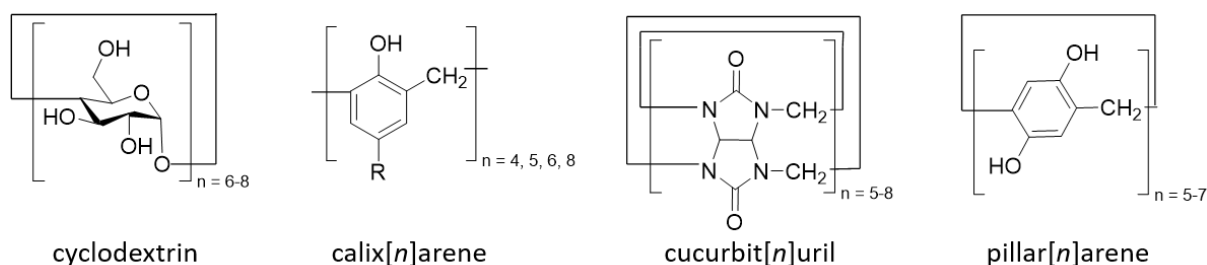

Figure 3.4 Chemical structures of macrocyclic host molecules.

Macrocyclic host molecules can be tailored in accordance with the target analyte.[48] Their structural and recognition properties are determined by their respective building blocks.[60] In addition, they are thermally and chemically robust and enable real-time monitoring of analytes with rapid response times.[48] Several macrocyclic hosts, such as cyclodextrins, calix[*n*]arenes, cucurbit[*n*]urils, and pillar[*n*]arenes (Figure 3.4) have been reported to bind with a wide range of analytes in aqueous media.[58, 61-63] Moreover, many macrocyclic hosts can be synthesized from low-cost, commercially available starting materials. Owing to these features, macrocyclic host molecules as a recognition element are gaining significant attention for developing host-guest type chemosensors for various applications, including drug delivery, cell imaging, photodynamic therapy, monitoring and detection of biologically and environmentally relevant analytes.[5, 6, 64-69] The following section discusses the signal generation strategies utilized in chemosensors based on host-guest chemistry.

3.1.3. Signal generation strategies for chemosensors

In chemosensors based on host-guest chemistry, the binding interaction between the macrocyclic host and analyte has to be coupled to a signal transduction event.[6, 70, 71] Different signal generation strategies are employed in designing chemosensors to achieve selective and sensitive detection of analytes. Direct binding assay (DBA), indicator displacement assay (IDA), guest displacement assay (GDA), and associative binding assay (ABA) are major signal generation strategies applied in chemosensor-based sensing assays.[6]
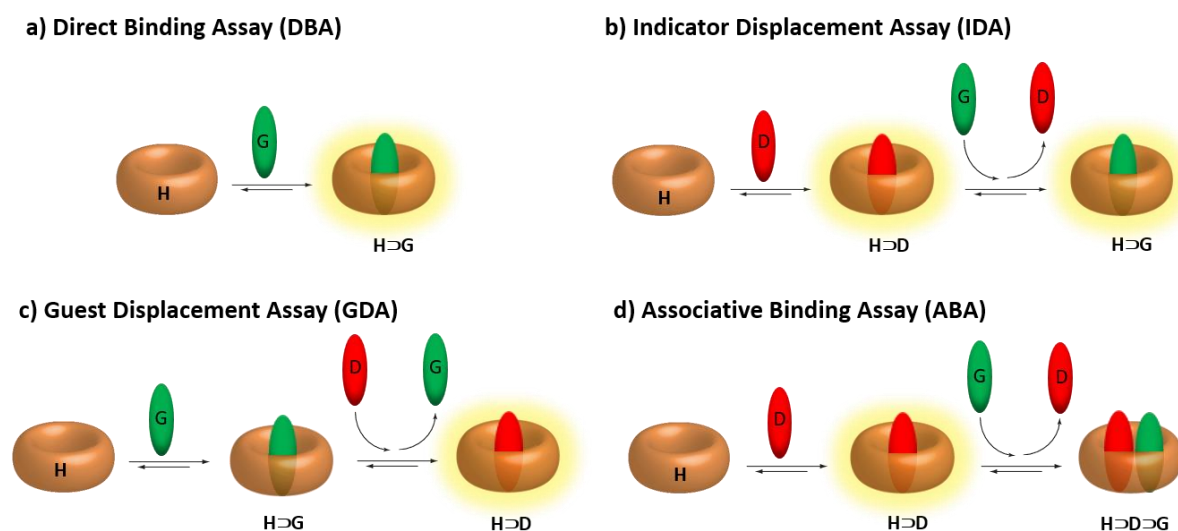

Figure 3.5 Schematic representation of different signal generation strategies. (a) DBA, (b) IDA, (c) GDA, and (d) ABA. Here, host (H) represents the macrocyclic host molecule, guest (G) represents the target analyte, and dye (D) represents the indicator molecule.

In a DBA, the interaction between the host and the guest (analyte) molecule results in an easily quantifiable signal change (Figure 3.5a).[6] DBA is applied in cases where the host or analyte is emissive/chromophoric/redox active such that the host-guest binding generates a significant signal change. Implementing a DBA-based chemosensor is often the most convenient and feasible option. Specifically, when the target analyte in DBA produces a unique signal response upon binding, allowing for differentiation from signals induced by cross-reactive analytes or interferents.[6]

IDA is applied for those host or guest (analyte) that are not emissive/chromophoric/redox-active or that do not produce a significant response upon guest binding (Figure 3.5b).[6, 72] IDA depends on indicator molecules, which change their spectroscopic (dyes) or electrochemical (redox active molecules) characteristics upon binding to a host molecule. The addition of a competitive binding guest leads to the displacement of the indicator (the indicator is shown as a dye in Figure 3.5b) from the host by forming the host-guest complex (H⊃G) accompanied by the recovery of the spectroscopic or electrochemical properties of the unbound indicator, which forms the basis for analyte detection. An ideal indicator should show distinct signal response changes for its free and bound state. Moreover, a crucial prerequisite for this assay to work is that the affinity between the indicator and the host should be comparable to that between the guest and the host.[73] Here, affinity refers to the degree to which the guest is bound to the host compared to the indicator and depends on the binding constant and concentration of the host, guest, and indicator, which are essential for achieving the effective displacement of the indicator and the subsequent signal response.[73, 74] This competitive approach is extensively employed in various molecular sensing applications.[6, 70, 73]

For analytes having low binding affinity for the host and poor aqueous solubility, GDA, a competitive binding assay is utilized (Figure 3.5c).[6, 75] In a GDA, the guest (analyte) first forms a complex with the host (H⊃G), and the encapsulation of the guest in the host cavity leads to a solubility enhancement. Subsequently, the addition of the indicator (the indicator is shown as a dye in Figure 3.5c) results in the displacement of the guest from the host cavity by forming the host-dye complex (H⊃D), which is accompanied by a change in the signal response. As a complementary approach to IDA, the GDA method is superior for insoluble and weakly binding guests.[75]

In cases where the host molecules can simultaneously bind the indicator and the guest (analyte) in their cavity, ABA can be established to perform analyte detection (Figure 3.5d).[6, 74, 76] ABA

involves the complex formation between the host and the aromatic indicator (the indicator is shown as a dye in Figure 3.5d) followed by the associative binding of the guest (aromatic analyte), leading to the formation of a 1:1:1 hetero-ternary complex (H⊃D⊃G) accompanied by a responsive signal. The face-to-face π-π stacking orientation between the aromatic indicator and the aromatic guest inside the host cavity facilitates electronic coupling phenomena, such as the emergence of a charge transfer band or changes in the emission spectra. This unique binding assay provides possibilities for distinguishing analytes from each other based on the resulting analyte-specific signal response (fingerprints) that is generated from the interaction between the analyte and the indicator within the host cavity.

Selecting an appropriate signal transduction method for the detection of the target analyte is very important for the success of chemosensors based on the aforementioned signal generation strategies. The following section gives an overview of different signal transduction methods employed in chemosensor-based sensing assays.

3.2. Signal transduction methods

In chemosensors, the generation of signal upon analyte binding is important for the detection of analytes. Therefore, choosing the appropriate signal transduction method is essential for the effective implementation of the developed chemosensors. Absorbance, fluorescence, chemiluminescence, electrochemical techniques, NMR, and mass spectrometry are some examples of the detection methods employed for signal transduction.[74, 77] The following sections provide a brief introduction to the commonly used detection methods, which include fluorescence, chemiluminescence, and electrochemical. In addition, the advantages of chemiluminescence and electrochemical detection methods over fluorescence are described.

3.2.1. Fluorescence-based detection methods

Fluorescence is the emission of photons by a molecule from its excited singlet state to the singlet ground state during a light absorption process.[78] Molecules in the excited states can also relax by non-radiative processes, in which excitation energy is not converted into photons but instead dissipated by thermal processes.[78] The Jablonski diagram (Figure 3.6a) offers a convenient representation of the excited state structure and possible processes.[78, 79]

In the Jablonski diagram, S_0, S_1, and S_2 represent the singlet ground state and the first and the second singlet electronic excited states, respectively. T_1 and T_2 represent the first and second triplet electronic excited states, respectively. Each electronic state is associated with vibrational
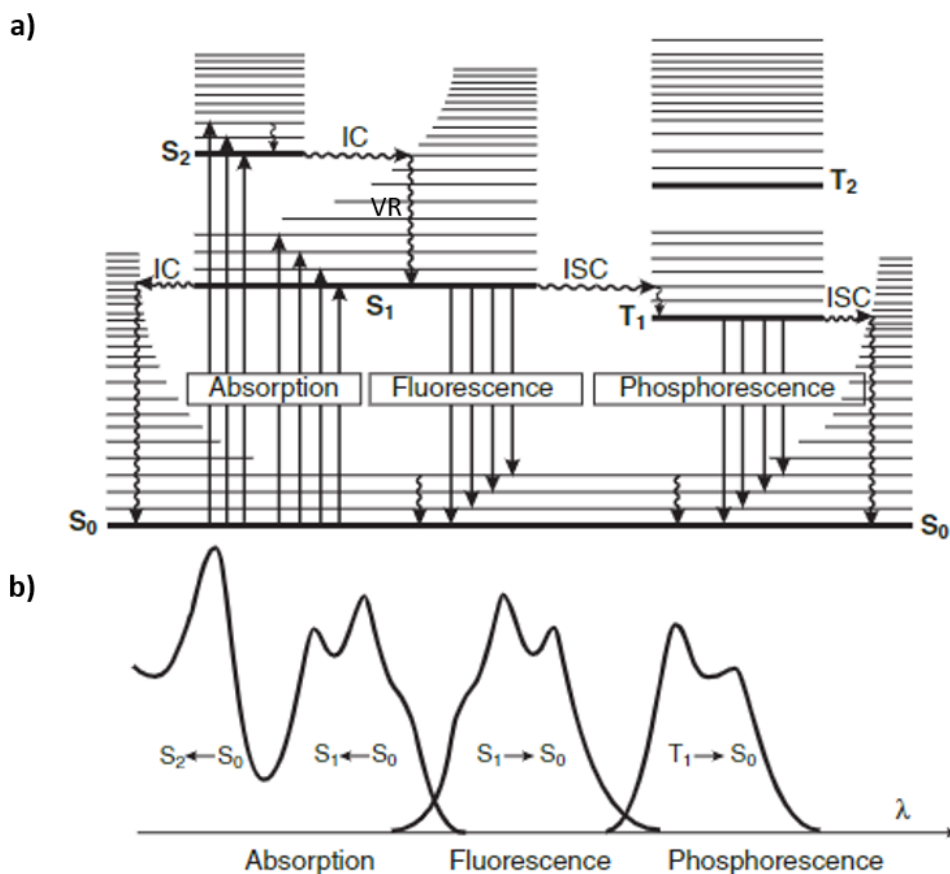
a)

b)

Figure 3.6 (a) Jablonski diagram illustrating relative positions of absorption, fluorescence, and phosphorescence spectra. Radiative and non-radiative processes are denoted as straight and wavy arrows, respectively. (b) Represenative absorbance, fluorescence, and phosphorescence spectra. Reprinted (adapted) with permission from ref.[79] Copyright 2012 Wiley-VCH Verlag GmbH & Co. KGaA.

levels. This diagram demonstrates that a molecule absorbs light from the lowest vibrational level of S_0 to a range of vibrational levels in the singlet electronic excited states (S_1, S_2). The wavelength of the absorbed light depends on the energy gap between the ground state and the excited state of the molecule. After absorbing light, transitions occur in the range of 10^{-15} s, and various processes start to take place. If a molecule becomes excited to an energy level higher than the lowest vibrational state of S_1, a non-radiative process called vibrational relaxation (VR, 10^{-12} s - 10^{-10} s) directs the excited molecule towards the lowest vibrational level of the S_1. If the singlet excited state is above S_1 (for example, S_2), a non-radiative process called internal conversion (IC, 10^{-11} s - 10^{-9} s) occurs. The molecule undergoes relaxation from the S_1 to S_0 by radiative decay process, emitting photons as fluorescence (10^{-10} s - 10^{-7} s). According to Kasha's rule, fluorescence occurs from the lowest vibrational level of the S_1 excited state.[80] Molecules can also undergo a spin-forbidden transition from S_1 to T_1 *via* a non-radiative pathway called intersystem crossing (ISC, 10^{-10} s - 10^{-8} s). The relaxation of

molecules from T_1 to S_0 by a radiative pathway with the emission of photons is termed phosphorescence (10^{-6} s - 10 s).

Due to energy dissipation in the excited state through non-radiative pathways, fluorescence emission is located at higher wavelengths than the absorption (Figure 3.6b). The difference in wavelengths of maximum emission and maximum absorption is referred to as the Stokes shift.[81] The transition from a triplet state to a singlet state is spin-forbidden, resulting in a longer lifetime for phosphorescence compared to spin-allowed fluorescence.[82] Consequently, the longer lifetime for the triplet excited state allows for more energy dissipation *via* non-radiative pathways. As a result, the phosphorescence spectrum is located at longer wavelengths compared to the fluorescence spectrum (Figure 3.6b).

Chemosensors generating fluorescence response as a recognition event for analyte detection are termed fluorescent chemosensors.[67, 70, 71] Therefore, these chemosensors depend on a photophysically active component, the fluorophore, to exhibit measurable signal changes upon analyte binding. When the target analyte is recognized by the host molecule, the fluorescence signal can be observed in the form of quenching, enhancement, or shift in the fluorescence maxima due to either electron transfer, charge transfer, or energy transfer processes.[65, 70, 83] The Figure 3.7 illustrates two cases for fluorescent chemosensors based on IDA, where the addition
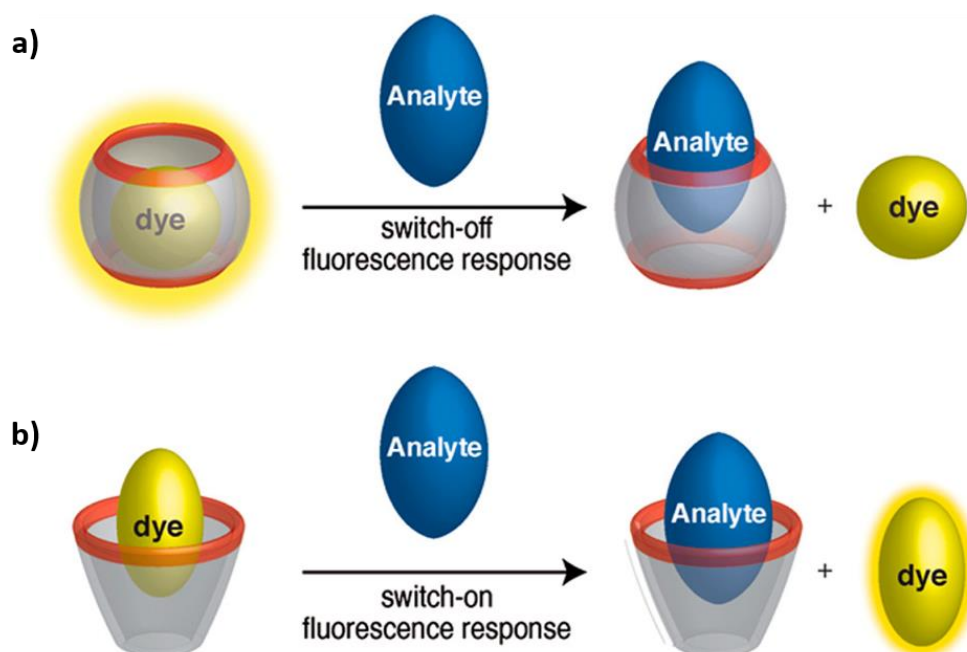

Figure 3.7 Schematic representation of fluorescent chemosensors based on IDA. The addition of an analyte either causes (a) a fluorescence decrease or (b) a fluorescence increase due to the displacement of the dye from the macrocyclic host. Reprinted (adapted) with permission from ref.[84] Copyright 2014 American Chemical Society.

of a target analyte either causes a switch-off fluorescence response (Figure 3.7a) or a switch-on fluorescence response (Figure 3.7b). For example, in macrocyclic hosts such as cyclodextrins and cucurbit[n]urils, the fluorescence of the encapsulated dye is enhanced due to the relocation of the dye into a more hydrophobic and solvent-protected environment of the macrocyclic host cavity.[63, 84] In contrast, for electron-rich macrocyclic hosts such as calix[n]arenes, the fluorescence of the encapsulated dye is quenched due to the charge-transfer process.[63, 84] Therefore, analyte addition results in fluorescence decrease (Figure 3.7a) or fluorescence increase (Figure 3.7b) due to the analyte-induced displacement of the dye from the host cavity.

Until now, a diverse range of fluorescent chemosensors have been developed for the detection of various analytes.[6, 67, 70, 85, 86] Despite progress in this field, several problems and challenges still exist. Fluorescence-based detection methods rely on an external light source to generate an excited state, which can lead to issues such as light scattering, instability of the light source, and photo-bleaching. In addition, high background signals from other emissive molecules may occur, especially when chemosensors are applied in biofluids. Hence, these issues can affect the performance of the chemosensor, leading to a reduced signal-to-noise ratio.

In this aspect, developing chemosensors that employ chemiluminescence as a detection method would be advantageous because this method does not rely on photoexcitation. Instead, chemiluminescence produces emission as a result of chemical reactions (chemiexcitation), resulting in a low background signal compared to fluorescence and an improved signal-to-noise ratio. Another alternative signal readout method for chemosensors is the electrochemical-based detection technique. This approach offers the potential to design sensors that can be miniaturized and made portable to use in on-site sensing applications. In the following sections, an overview of the chemiluminescence and electrochemical-based detection methods are described.

3.2.2. Chemiluminescence-based detection methods

Chemiluminescence (CL) is the light emission derived from a chemical reaction in which chemically excited molecules relax to the electronic ground state with the emission of photons.[87-89] Bioluminescence is a type of chemiluminescence produced by living organisms such as fireflies.[90]

Since an external light source is not required for the CL emission, the major drawbacks associated with fluorescence, such as light source instability, light scattering, photobleaching, and phototoxicity, are eliminated. In addition, the background signal is extremely low, providing high sensitivity and enhanced signal-to-noise ratio.[91] Due to these advantageous properties of CL over fluorescence, CL has been employed in a broad range of analytical applications, such as in immunoassays, DNA sequencing, cell imaging, photodynamic therapy, and drug discovery.[92-101]

Most CL reactions involve the chemical activation of molecules through oxidation. The activated molecule undergoes chemical transformation, leading to the formation of an unstable intermediate.[88, 102] The decomposition of this intermediate produces an excited luminogenic species (C^* or D^*) that decays to its ground state through the emission of light (direct CL, Figure 3.8a) or by transferring energy to an adjacent fluorophore (E) (indirect CL, Figure 3.8b) *via* chemiluminescence resonance energy transfer (CRET). This oxidation mechanism is
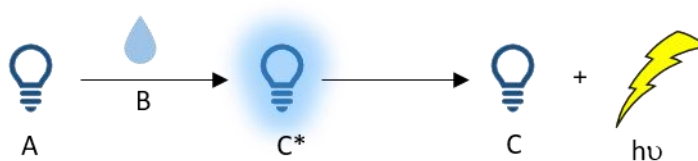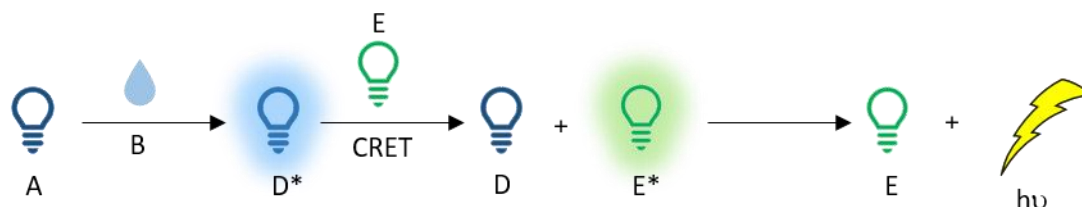

Figure 3.8 Schematic representation of (a) direct and (b) indirect CL. A and B represent the chemical reactants. E represents the fluorophore. Reprinted (adapted) with permission from ref.[108] Copyright 2020 Royal Society of Chemistry.
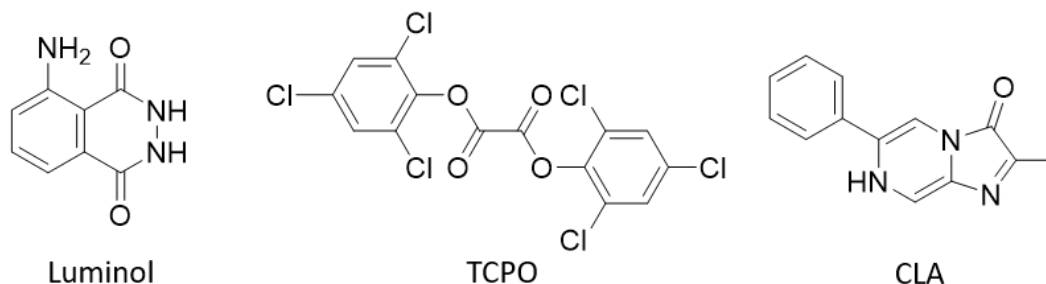
Figure 3.9 Chemical structures of common chemiluminescent substrates that produce CL *via* oxidative pathway.

followed by the common chemiluminescent substrates such as luminol,[103] oxalate esters (*e.g.* bis(2,4,6-trichlorophenyl)oxalate, TCPO),[104] and *Cypridina* luciferin analog (*e.g.* 2-methyl-6-phenyl-3,7-dihydroimidazo[1,2-α]pyrazin-3-one, CLA) (Figure 3.9).[105] Hence, these substrates have been used to analyse biological processes involving increased levels of oxidative species.[106-108]

Schaap and co-workers reported a non-oxidative pathway for CL activation based on triggerable phenoxy 1,2-dioxetanes (PDOs, Figure 3.10).[109] They showed that the chemiexcitation of PDOs bearing a protected phenolic group at the *meta* position could be initiated by deprotection of the protecting group, either chemically or enzymatically.[110-113] The mechanism involves the removal of a protecting group in the presence of specific enzymes or analytes of interest to produce the phenolate-dioxetane intermediate (**1**) (Figure 3.10). Subsequently, the intermediate decomposes through a chemically initiated electron exchange luminescence (CIEEL) process to generate the electronically excited benzoate ester (**4**), which decays to its ground state by emitting light in the blue wavelength region.

The proposed CIEEL mechanism pathways to form the excited benzoate ester (**4**) are shown in Figure 3.10.[114-116] Both pathways start with a single electron transfer from the phenolate anion to the antibonding orbital of the oxygen-oxygen bond of dioxetane, resulting in heterolytic cleavage of the peroxide bond. Thus, biradical intermediates (**2a** and **2b**) are formed. In pathway **A**, proposed by Liu and co-workers, **2a** decomposes to anionic biradical species (**3a**) and adamantanone.[115] Subsequently, **3a** undergoes intramolecular back electron transfer (BET) to form excited benzoate ester (**4**). In pathway **B**, where **2b** decomposes to a solvent-caged radical ion pair (**3b**). Followed by the intermolecular BET between solvent-caged pair in **3b**, resulting in excited benzoate ester (**4**).
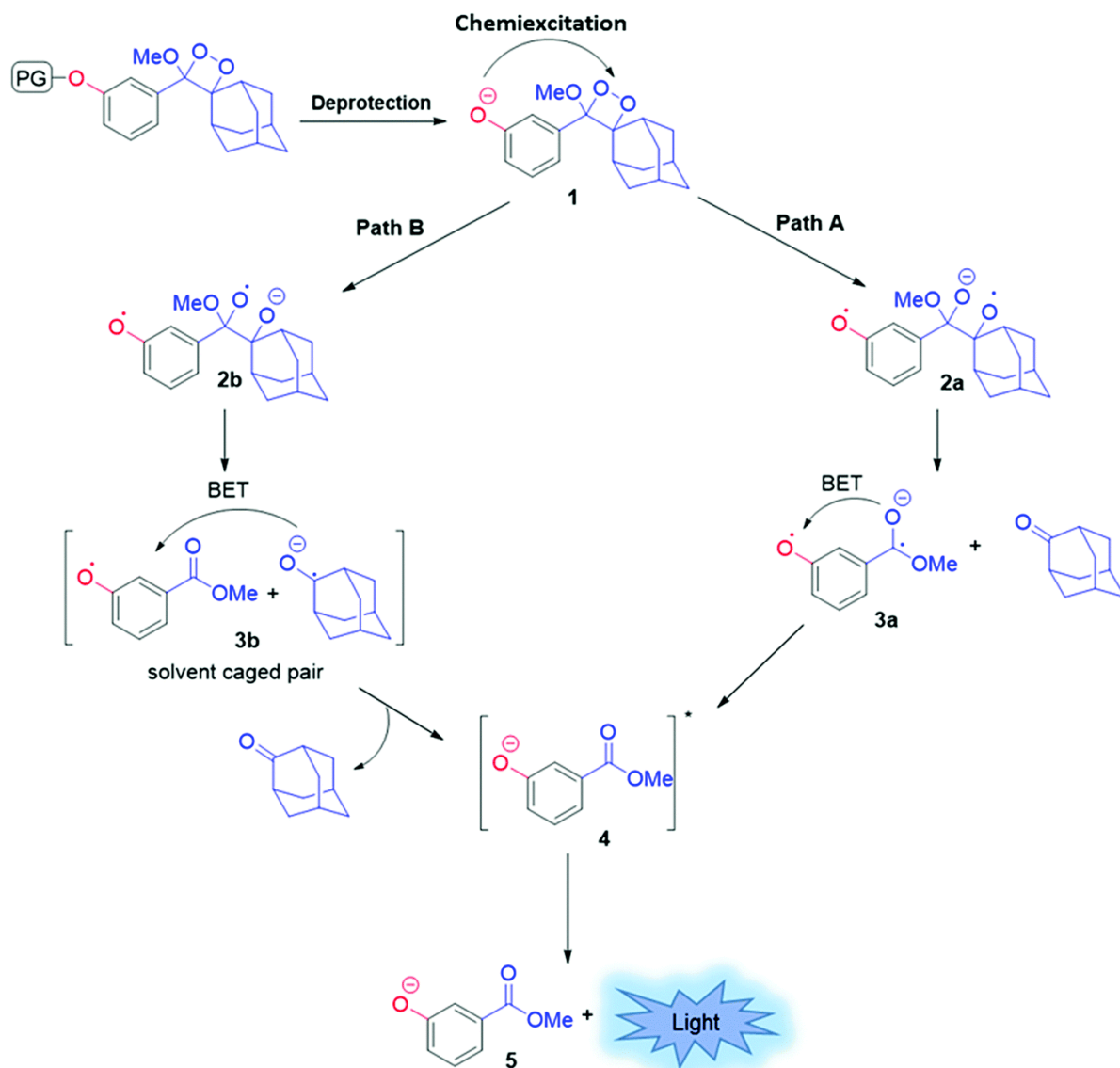
Figure 3.10 Proposed CIEEL mechanistic pathways for PDOs. Reprinted (adapted) with permission from ref.[116] Copyright 2018 Royal Society of Chemistry.

Adam and co-workers proposed that if excited state formation occurs *via* the intermolecular BET process, CL emission efficiency should be influenced by a solvent cage effect and, thus, should be dependent on viscosity. They experimentally observed an increase in CL emission with increasing solvent viscosity, thus showing the viscosity dependence of CL emission.[114] Mechanistically, high-viscosity solvents restrict the diffusive separation of the solvent-caged radical ion pair and thereby prevent non-radiative deactivation.[114] This suggests that the intermolecular BET process is involved in the CIEEL mechanism, supporting pathway **B**, which is the more widely accepted mechanism.

As PDOs are equipped with an enzyme or analyte-responsive protecting group (PG), they offer several possibilities for sensing applications. PDOs have efficient CL emission in organic

solvents like DMSO due to the high viscosity of DMSO. However, PDOs have relatively low CL quantum yields in aqueous media, thereby limiting their use in biologically relevant applications.[117] Hence, there is much research in this direction to enhance the emissive nature of PDOs in aqueous media.

Shabat and co-workers have reported promising studies that improved the emissive nature of PDOs in physiological conditions. Following are some representative examples of their work: By conjugating a fluorophore to dioxetane, dioxetane effectively transfers CL energy to the fluorophore (CRET), resulting in an amplified signal.[118] In addition, the wavelength of the emitted light can be tuned by choice of the fluorophore (Figure 3.11a). In another approach, they reported the modification of PDOs by introducing electron-withdrawing groups (EWGs), such as methyl acrylate and acrylonitrile substituents, at the *ortho* position of the protected phenolic group (Figure 3.11b).[96] These EWGs stabilize the intermediate *via* resonance delocalization, leading to enhanced CL emission in aqueous conditions.[96, 119] They also developed the first chemiluminescent PDOs that emit light in the near-infrared region under physiological conditions and applied them for *in vivo* imaging.[120]

All of these approaches enabled the generation of efficient chemiluminescent PDO probes for detecting various enzymes, reactive species, and even pathogens.[97, 116, 121] Some representative literature examples of PDOs and their applications are shown in Table 3.1.
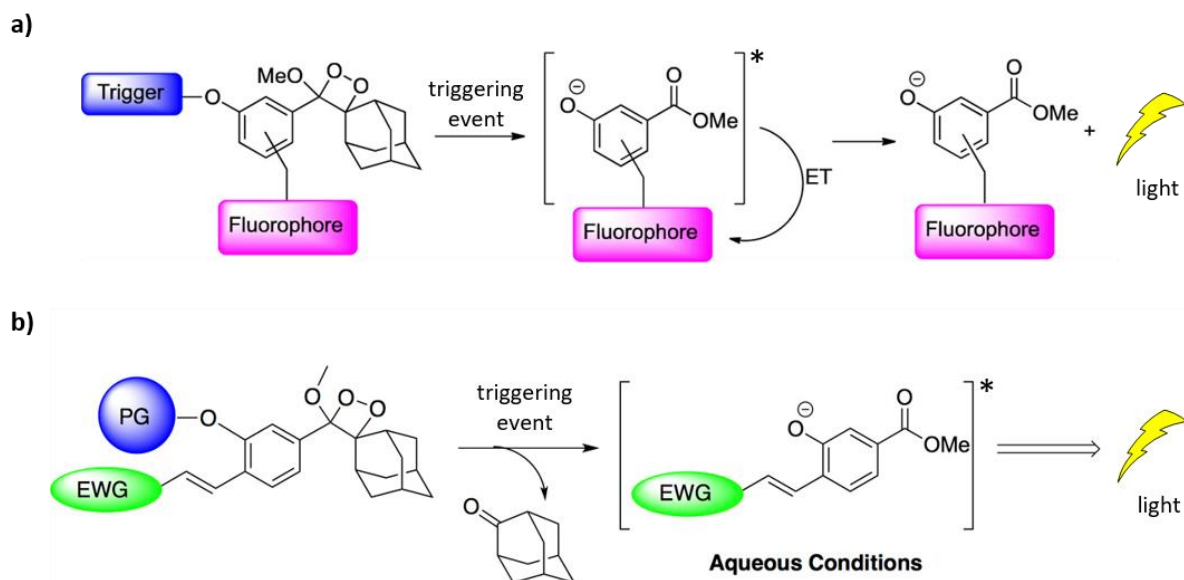
Figure 3.11 Different approaches to enhance the CL of PDOs in aqueous conditions. (a) Enhancement by energy transfer (ET) from the dioxetane to the fluorophore conjugate. Reprinted (adapted) with permission from ref.[118] Copyright 2016 American Chemical Society. (b) Direct CL amplification by introducing an EWG. Reprinted (adapted) with permission from ref.[96] Copyright 2017 American Chemical Society.

Table 3.1 Chemical structures of different PDO probes and their applications.

PDO probes	Applications	Ref.
	detection of fluoride ions *in vitro* and *in vivo*	122
	detection of alkaline phosphatase enzyme activity	123
	in vitro detection of protease activity	124
	in vivo imaging of β-galactosidase enzyme activity	125
	in vivo imaging of H_2S	126
	detection and imaging of nitroreductase enzyme *in vivo*	127
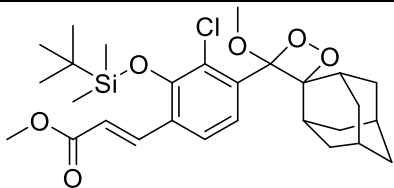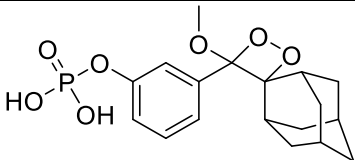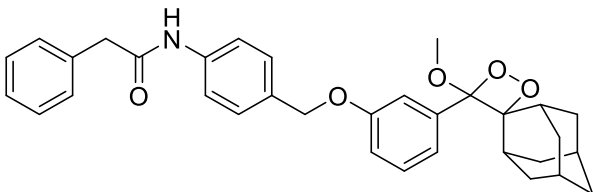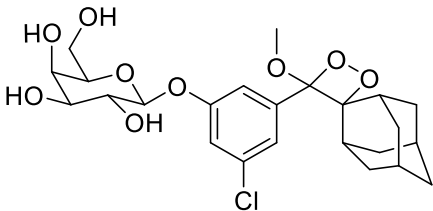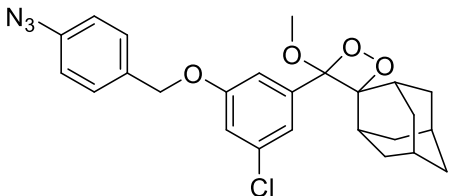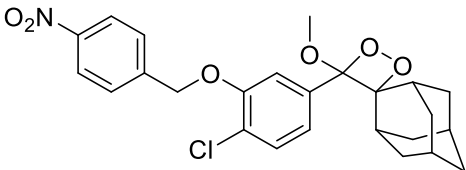
Figure 3.12 Schematic representation of the host-guest complex formation between PDO and TMCD leading to enhanced CL emission in aqueous medium. Reprinted (adapted) with permission from ref.[128] Copyright 2019 Royal Society of Chemistry.

Chemiluminescent probes play a significant role in developing chemiluminescent chemosensors, which generate CL response in the presence of the target analytes. In chemiluminescent chemosensors based on host-guest chemistry, the host-mediated complexation of the target analyte is coupled to a detectable CL signal change.
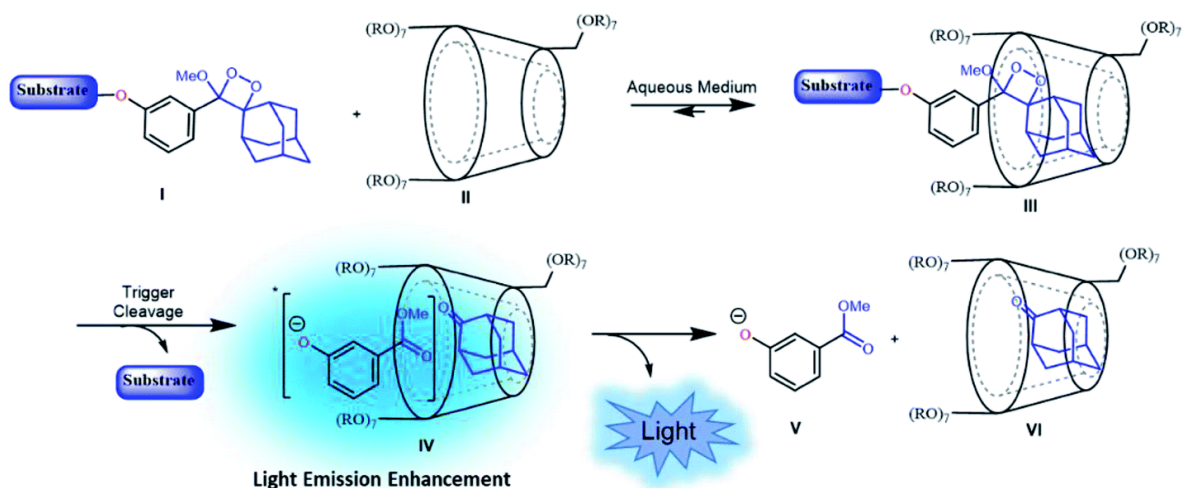
Shabat and co-workers reported the first host-guest complex formation of PDOs with trimethyl β-cyclodextrin (TMCD) to image enzymatic activity and reactive oxygen species *in vitro* and *in vivo*.[128] They showed that the CL emission of PDOs amplified upon complex formation with TMCD in the aqueous medium. This enhancement occurs because the hydrophobic cavity of the CD shields the PDOs from the surrounding water molecules (Figure 3.12). They have also investigated the CL enhancement of PDOs using other CD derivatives, and the largest CL enhancement was observed with TMCD. This explanation is based on the structural arrangement where the secondary alcohols of the CD are positioned close to the adamantyl-dioxetane moiety encapsulation site. This proximity may facilitate hydrogen bond formation with the dioxetane and its excited state intermediate, leading to quenched emission. In contrast, the secondary alcohols are methylated in TMCD, thus avoiding the hydrogen bond quenching effect.[128] Huang and co-workers developed a β-cyclodextrin (β-CD)-based host-guest complex of $CoFe_2O_4$ magnetic nanoparticles and applied them as catalysts for luminol-hydrogen peroxide CL reaction.[129] They also studied the detection of hydrogen peroxide in water.

However, until now, there have been no reports on chemiluminescent chemosensors based on host-guest chemistry for sensing biologically relevant small organic molecules such as drugs in biofluids. In the present thesis, novel chemiluminescent chemosensors based on host-guest

chemistry have been investigated for the detection of drugs in biofluids. The first part of my thesis focuses on the design and development of a CB8-based chemiluminescent chemosensor using PDO as the CL probe and describes its ability to detect drugs in biofluids.

3.2.3. Electrochemical-based detection methods

Electrochemical detection measures the changes in an electrical signal resulting from the electrochemical reaction occurring on the electrode surface.[130] Based on the electrical signal generated, electrochemical detection methods can be classified as potentiometry, voltammetry, and amperometry. Potentiometry measures changes in electrical potential, voltammetry involves measuring current as a function of the applied potential, and amperometry monitors current changes over time at a constant applied potential. This section briefly describes all these detection methods.

In potentiometry, the potential difference between two electrodes is measured using a high-impedance voltmeter over a nearly zero-current state (Figure 3.13).[131] One electrode is the indicator electrode, whose potential changes in response to the redox reaction of the analytes in the measuring solution, and the other one is the reference electrode, which has a constant potential (Figure 3.13). Both electrodes are immersed in the measuring solution. The Nernst equation (Eq. 3.1) governs the relationship between the measured potential and the concentration of the analyte ions.[132] Potentiometric methods are commonly applied in various fields such as environmental, agricultural, drug analysis, and determination of many organic and inorganic ions.[133-136]
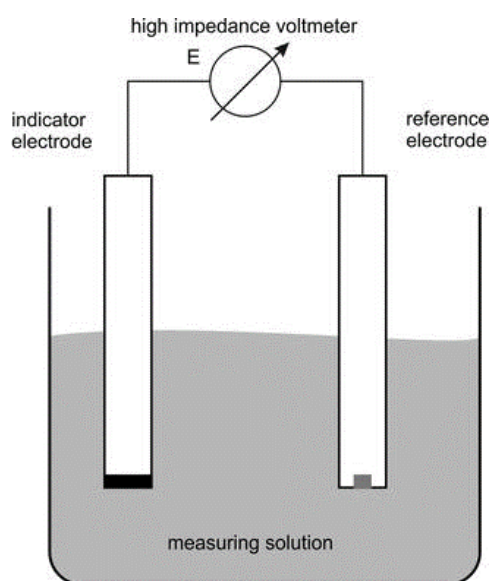

Figure 3.13 Schematic representation of a potentiometric measuring cell. Reprinted (adapted) with permission from ref.[132] Copyright 2014 Springer Science Business Media New York.

$$E = E^0 - \frac{RT}{nF} \ln Q \qquad \text{Eq. 3.1}$$

where E is the measured potential (potential difference between the indicator and the reference electrode); E^0 is the standard potential; R is the universal gas constant; T is the temperature in Kelvin; n is the number of electrons in the redox reaction; F is the Faraday constant; and Q is the reaction quotient (ratio of concentrations of products and reactants in the redox reaction).

In voltammetry, a varying potential is applied to a working electrode, which produces a characteristic current response as a measurable quantity. Cyclic voltammetry (CV), differential pulse voltammetry (DPV), and staircase voltammetry (SCV) are some examples of voltammetric methods.

In CV, the potential of the working electrode is scanned in a triangular potential waveform (as shown in Figure 3.14a), starting from a potential E_S to a switching potential (E_{Sw}).[137] At E_{Sw}, the direction of the potential changes and then the potential is scanned back to a final potential (E_F). The measurement result obtained is called a cyclic voltammogram, which shows the current variation as a function of the applied electrode potential.[130] See Figure 3.14b for a typical cyclic voltammogram of a redox-active species where the current resulting from the oxidation (anodic current, I_A) and the reduction (cathodic current, I_C) process is shown against the changing potential. For an electrochemically reversible process, the halfway potential ($E_{1/2}$) between anodic and cathodic peak potentials corresponds to the formal reduction potential ($E^{\circ\prime}$)
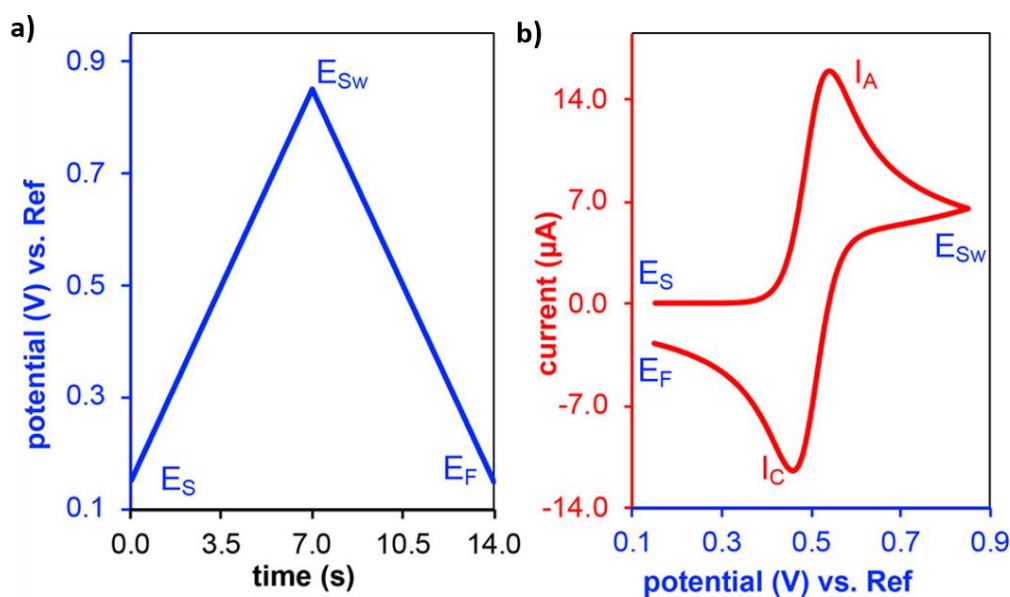

Figure 3.14 (a) Example of a triangular potential waveform applied in CV and (b) the resulting cyclic voltammogram of a redox-active species. Reprinted (adapted) with permission from ref.[137] Copyright 2021 American Chemical Society and Division of Chemical Education, Inc.

of the redox reaction.[138] The shape of the resulting voltammogram depends on the type of redox system studied and the conditions of the measurement. Based on the analysis, a full cycle, a partial cycle, or a series of cycles can be performed in CV measurements. CV provides information about the underlying electrochemical processes and is often used to determine the chemical characteristics of the compounds, monitor reaction intermediates, and stability measurements of reaction products.[139, 140]

In DPV, a series of potential pulses is applied to the working electrode and the current is measured once before the pulse application (I_1) and at the end of the pulse (I_2) (Figure 3.15a).[131] The DPV curve is the difference between the two measured currents plotted against the applied electrode potential. Since the current is measured at two points, this effectively reduces the background current, offering high sensitivity.[139, 141] The background current refers to the capacitive current that arises from the charging and discharging processes at the electrode surface. This current decays much faster and is negligible at the pulse end.[142] Thus, the resulting current difference primarily corresponds to the current from the redox process. Hence, DPV facilitates the detection of analytes at a low concentration range compared to the CV method. DPV has been used for measuring trace levels of pharmaceutical drugs.[143] Moreover, DPV can discriminate analytes with similar oxidation potentials.[144]

In SCV, a series of potential steps is applied to the working electrode and the current is measured at the end of each potential step (I_C) (Figure 3.15b) where the capacitive current is reduced to a negligible value.[131] SCV allows stepwise analysis of the electrochemical process.[145]
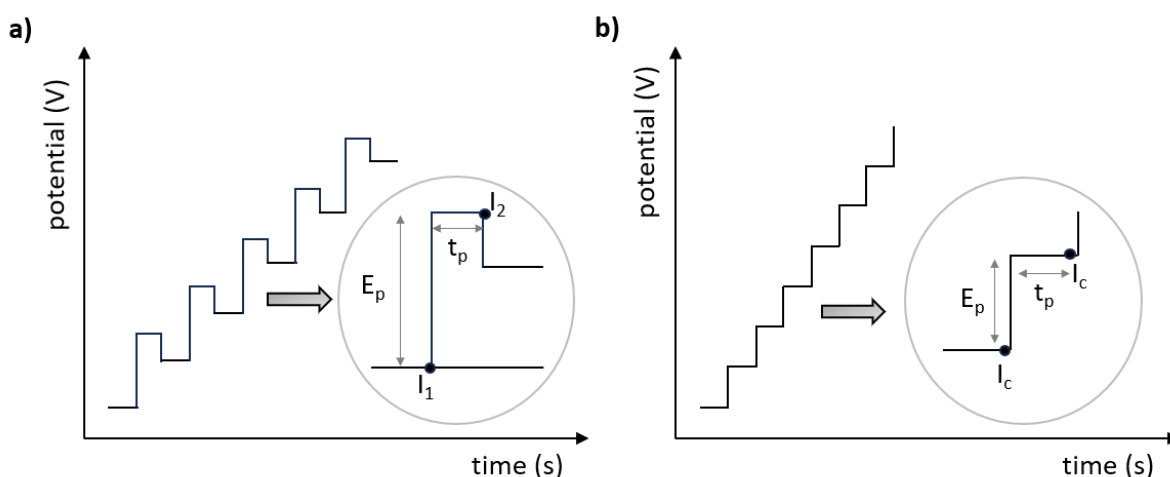

Figure 3.15 Typical potential signal of (a) DPV (I_1 and I_2 = two current measuring points) and (b) SCV (I_c = current measuring point). E_p = pulse height, t_p = pulse time. Reprinted (adapted) with permission from ref.[131] Copyright 2010 Springer-Verlag Berlin.
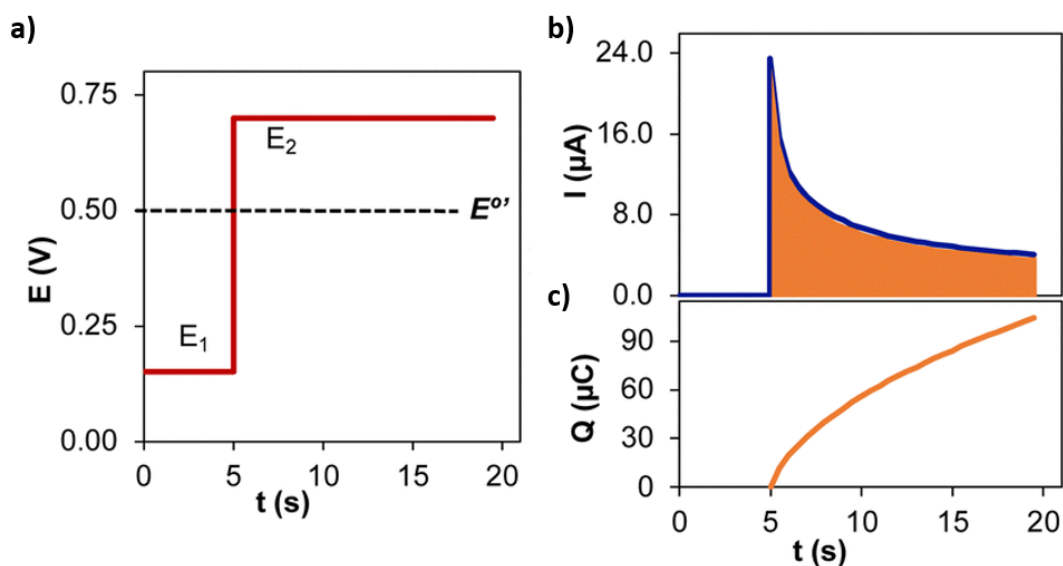
Figure 3.16 (a) Example of a potential-time waveform applied in a chronoamperometric experiment and the (b) resulting chronoamperogram and (c) chronocoulogram of a redox-active species. Reprinted (adapted) with permission from ref.[148] Copyright 2024 Royal Society of Chemistry.

Amperometry involves the measurement of current over time by applying a constant potential.[146] The current generated is directly proportional to the concentration of the redox-active species and thus, this method is extensively used for the quantitative analysis of redox-active analytes.[146, 147] In chronoamperometry, the variation in current response is recorded over time under stepwise applied potential.[148] In a chronoamperometry experiment, the potential of the working electrode is pulsed from a potential (E_1) at which no redox process occurs to a potential (E_2) exceeding the formal potential ($E^{\circ\prime}$) of the redox-active species. For example, Figure 3.16a illustrates the potential-time waveform applied to a redox-active species ($E^{\circ\prime} = 0.5$ V). Since E_2 is more positive than $E^{\circ\prime}$, the potential pulse leads to the oxidation of the species. The resulting chronoamperogram shown in Figure 3.16b depicts a gradual decrease in the current over time and this decrease depends on the concentration of the redox-active species. The integration of the obtained chronoamperogram gives the chronocoulogram (Figure 3.16c). This method offers additional selectivity because the oxidation or reduction potential applied in the measurement is typically characteristic of the target analyte.[149]

In electrochemical sensors, DPV, SCV, or chronoamperometry is commonly used as the detection method because these methods reduce the occurrence of capacitive current charges by applying a series of regular potential pulses, leading to enhanced sensitivity.[139, 141] Electrochemical detection methods offer an appealing detection approach due to their superior sensitivity, reproducibility, ease of use, portability, low cost, and the requirement of very small sample volumes.

Screen-printed electrodes (SPEs) are commercially available cheap electrodes that are popular for sensing purposes due to their ease of fabrication and cost-effectiveness. They consist of reference electrode (R.E.), counter electrode (C.E.), and working electrode (W.E.) that are printed on a solid substrate, as shown in Figure 3.17. In addition, they can be further functionalized according to the specific needs. Electrochemical detection methods, in combination with SPEs, have significantly contributed to the development of portable and affordable electrochemical sensors for various applications.[17, 150-153]
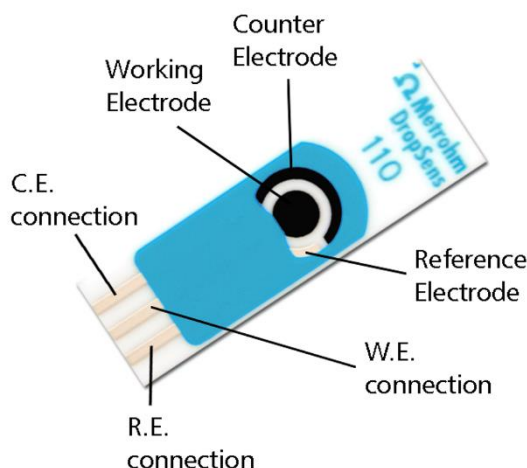

Figure 3.17 Illustration of an SPE consisting of a reference, counter, and working electrode. Reprinted with permission from Metrohm DropSens.

Electrochemical sensors based on host-guest chemistry have been widely explored due to the molecular recognition properties exhibited by the macrocyclic host molecules.[52, 154-157] Therefore, these host molecules assist in the accumulation of electroactive target analytes on the electrode surface, which improves the selectivity and sensitivity of detection.

Quintana and co-workers reported the development of an electrochemical sensor based on cucurbit[8]uril (CB8) as the macrocyclic host for tryptophan determination at low concentration levels.[155] They have used a CB8 glassy carbon-modified electrode for this purpose. The electrochemical measurement results showed that the complex formation of tryptophan with CB8 generates a potential shift to more positive values and a decrease in the oxidation current due to the interaction of tryptophan with CB8. They were also successful in applying the sensor in human serum for the detection of tryptophan. In addition, the sensor enabled the selective determination of tryptophan in the presence of other possible interferents, such as acetylcholine, ascorbic acid, and uric acid. In another work by the same authors, they proposed an electrochemical sensor using a CB8 glassy carbon-modified electrode to detect

the neurotransmitter dopamine in the nanomolar range, even in the presence of interferents such as ascorbic acid.[154]

Fragoso and co-workers presented a novel approach to develop a biosensor by modifying gold surfaces with an electropolymerized pyrrole-β-CD film for the detection of antibodies.[157] However, all these proposed strategies require electrochemically active analytes that undergo electron transfer reactions called redox reactions, leading to either oxidation or reduction of the analytes.

In this context, Yu and co-workers have introduced a competitive binding approach for the detection of electrochemically inactive (or redox-inactive) analytes using cucurbit[7]uril (CB7) as the macrocyclic receptor and ferrocene (Fc) as the redox indicator (Figure 3.18a).[158] They have shown that the oxidation potential of Fc that is immobilized on the gold electrode surface is shifted to more positive values upon forming a complex with CB7 (CB7⊃Fc) (Figure 3.18b, graph A). Upon increasing the concentration of redox-inactive analytes, the potential responses gradually shift back to the original potential of unbound Fc groups (to more negative potential) (Figure 3.18b, graph B). This indicates the presence of lower amount of CB7⊃Fc inclusion complexes as most of the CB7 competitively form inclusion complexes with the analytes.
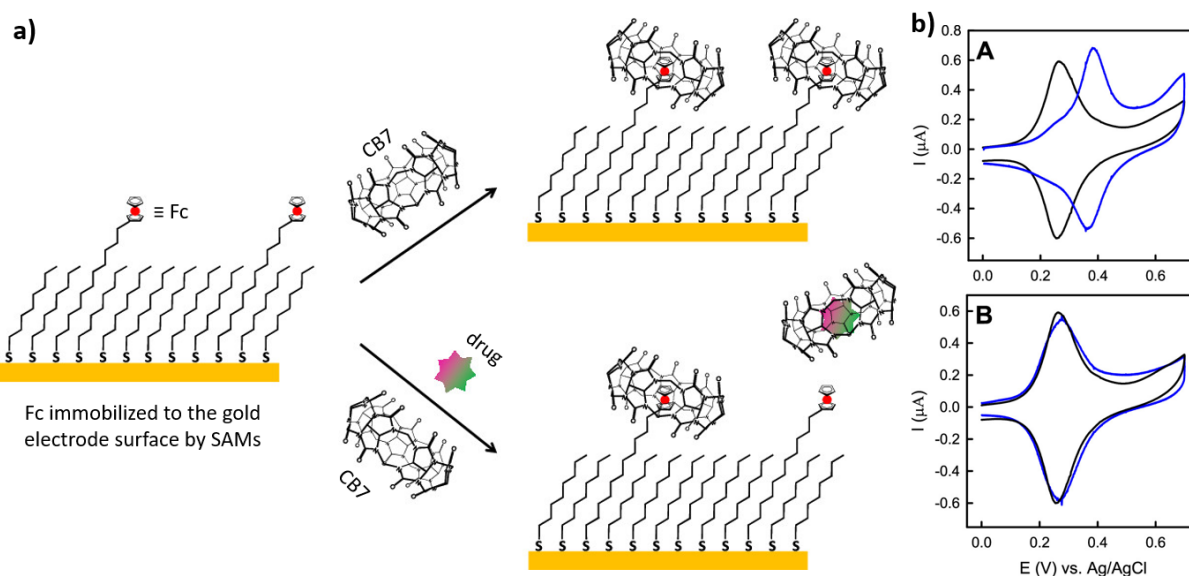
Figure 3.18 (a) Schematic representation of the host-guest complex formation between CB7 and Fc that is immobilized to the gold electrode surface in the absence and presence of redox-inactive drug. (b) The corresponding CV responses are shown, where graph A shows the potential shift upon CB7⊃Fc formation and graph B shows the potential shift back to the original potential of unbound Fc in the presence of the drug. The black curve represents the CV curve of Fc and the blue curve represents the CV curve of CB7⊃Fc. Reprinted (adapted) with permission from ref.[158] Copyright 2019 American Chemical Society.

Although the detection of redox-inactive analytes is possible, the need for highly organized alkanethiolate self-assembled monolayers (SAMs) on the gold electrode surface for the immobilization of Fc is a major drawback. This is because of the cumbersome processes involved in the preparation of SAMs, the limited electrochemical stability of SAMs in aqueous solutions, and the non-specific adsorption of analytes.[158, 159]

In the present thesis, novel electrochemical chemosensors based on host-guest type that do not require immobilization processes on the electrode surface have been investigated for the detection of redox-inactive analytes. The first research project discusses the design and development of a CB7-based electrochemical chemosensor using a platinum(II) complex as the redox indicator.

3.3. Cucurbit[*n*]urils

Cucurbit[*n*]urils (CB*n*) are a family of macrocyclic host molecules that are composed of methylene-bridged glycoluril units (Figure 3.19a), where '*n*' denotes the number of glycoluril units.[160, 161] The name 'cucurbituril' was proposed due to its structural resemblance to a pumpkin (Cucurbitaceae family).[57] The synthesis of CB*n* involves the acid-catalyzed condensation reaction between glycoluril and formaldehyde (or paraformaldehyde) (Figure 3.19b).[162, 163] CB*n* is composed of two carbonyl-lined portals and a hydrophobic cavity without any functional groups or electron pairs (see Figure 3.19a and the space-filling models in Figure

a)

	CB5	CB6	CB7	CB8
n	5	6	7	8
outer diameter (Å)	13.1	14.4	16.0	17.5
portal diameter (Å)	2.4	3.9	5.4	6.9
cavity diameter (Å)	4.4	5.8	7.3	8.8
height (Å)	9.1	9.1	9.1	9.1
cavity volume (Å³)	82	164	279	479

b)

c)
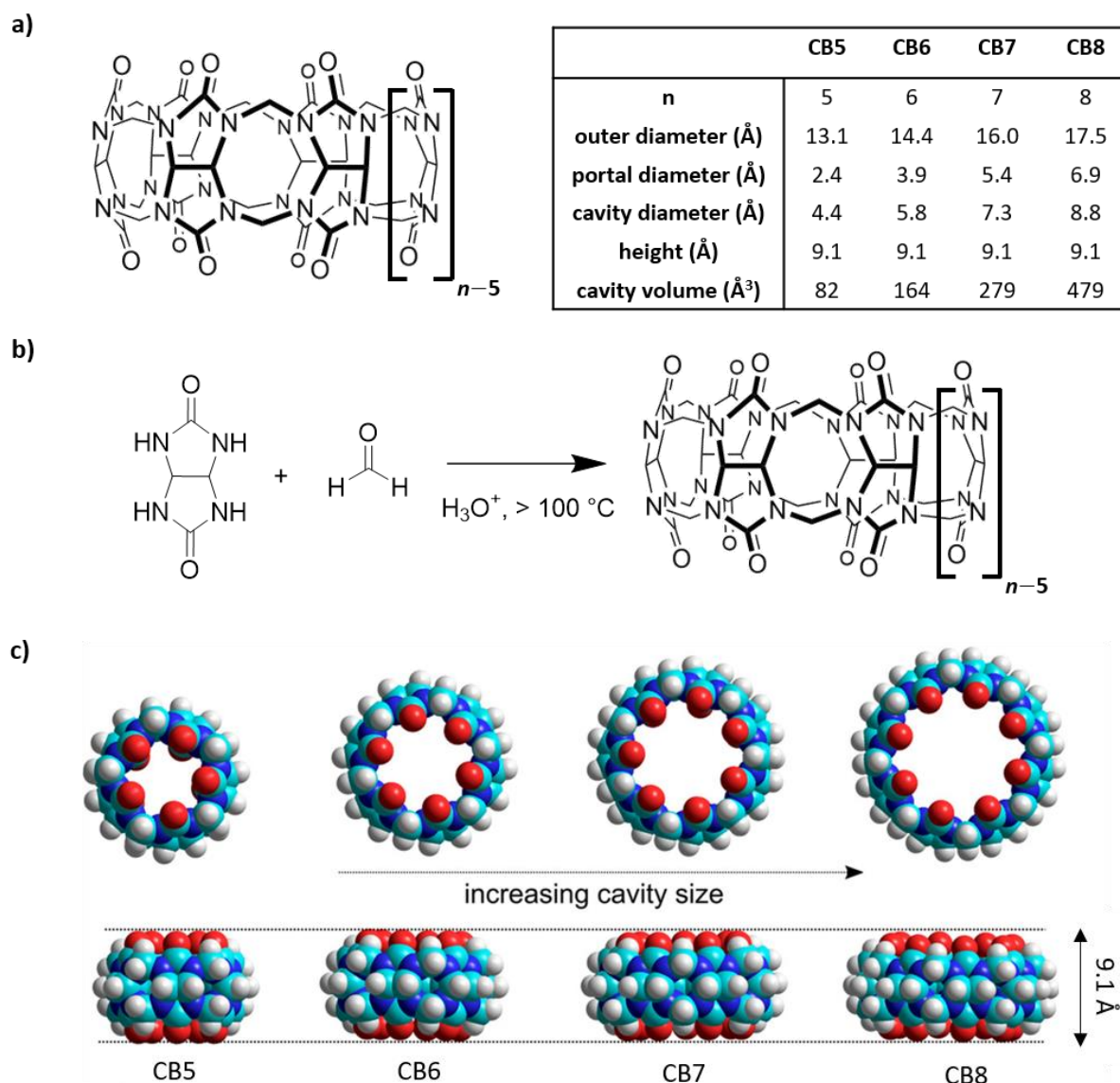
Figure 3.19 (a) Chemical structure of CB*n* and the structural parameters of CB5 to CB8. (b) CB*n* synthesis by acid-catalyzed condensation reaction between glycoluril and formaldehyde. (c) Space-filling models of CB5 – CB8, demonstrating the increasing cavity size with constant height. The red-coloured part represents the electronegative carbonyl-lined portals. Reprinted (adapted) with permission from ref.[160] Copyright 2015 American Chemical Society.

3.19c). The highly electronegative nature of CBn portals makes the portals highly attractive for cation binding and the hydrophobic cavity enables the encapsulation of hydrophobic molecules.[57] This combined feature provides CBn high affinity and selectivity for specific classes of guest molecules, including both neutral and positively charged guest molecules. The cavity and portal dimensions of CBn increase with the number of glycoluril units (see the table in Figure 3.19a and the space-filling models in Figure 3.19c), leading to different recognition properties for each CBn homologues with binding affinities in the range of $10^3 - 10^{17}$ M^{-1}.[74, 161, 164]
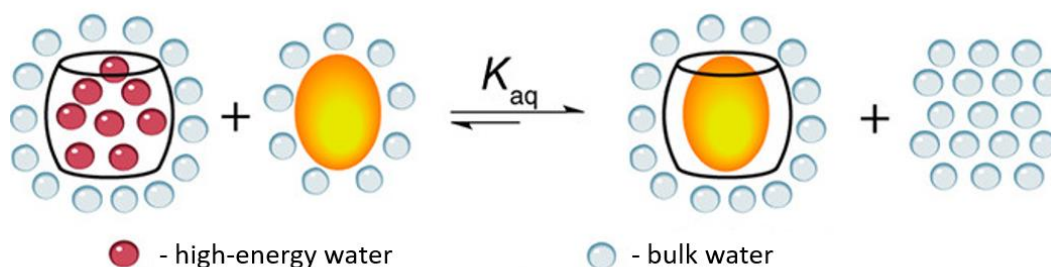

- high-energy water   - bulk water

Figure 3.20 Schematic representation of the release of high-energy water molecules upon guest binding. Reprinted (adapted) with permission from ref.[166] Copyright 2012 American Chemical Society.

In addition to these features, the strong enthalpic gain caused by the release of high-energy water molecules confined within the hydrophobic cavity of CBn upon guest binding contributes significantly to the strong binding affinity shown by CBn in aqueous solutions.[165, 166] The released water molecules further engage in stronger H-bonding networks within the aqueous bulk (Figure 3.20). The smaller homologues, such as CB5 and CB6, have a limited number of high-energy water releases due to their smaller cavity volume, whereas CB8 having a larger cavity volume allows for a more stable H-bonding network among cavity water molecules. Therefore, CB7 exhibits higher binding affinities due to the maximal high-energy water release compared to other CBn homologues.[166]

CB5 and its derivatives are reported to bind with gases (noble gases, methane, ethane) and solvent molecules (methanol and acetonitrile).[167-169] CB6 is known to bind alkyl ammonium ions and small aromatic hydrocarbons.[74] CB7 can bind a wider range of guests than CB6 or CB5, including adamantane, naphthalene, viologen, and ferrocene derivatives.[161, 170] CB8 is unique in its ability to form 1:2 or 1:1:1 ternary complexes with two identical or different guest molecules.[74, 170] CB8 binds various steroid hormones and drugs,[171] terpenes,[172] metal complexes (ferrocene),[173] and adamantane derivatives such as memantine.[160]

The solubility of CBn homologues is low (<10^{-5} M) in common solvents, whereas CB5 and CB7 have moderate solubility in water (20 – 30 mM).[170, 174] CBn homologues are soluble in acidic water and aqueous alkali metal ion solution.[170] To overcome the water solubility challenge, researchers investigated the introduction of functional groups onto CBn. A few established functionalization strategies include direct condensation with functionalized glycoluril,[175] building block approach with a template,[176] or *via* a direct method.[177] Among these strategies, the direct hydroxylation of CBn is widely employed as the primary step for functionalizing CBn.[178]

3.3.1. CBn-based chemosensors

Many biologically relevant analytes, such as drugs, hormones, amino acids, peptides, neurotransmitters, and toxins, generally exist in the concentration range of millimolar (mM) to nanomolar (nM) in aqueous environment.[6] Therefore, macrocyclic hosts with binding affinities greater than 10^3 M^{-1} are often suggested for the design of chemosensors.[74] Compared to other synthetic macrocyclic hosts, CBn offers high binding affinities in the range of $10^3 – 10^{17}$ M^{-1} towards the aforementioned analytes.[74, 161, 164, 179]

Furthermore, the size-selective binding of CBn enables the design of selective chemosensors.[74] According to the Mecozzi-Rebek rule, a packing coefficient (PC, ratio between the volume of the guest and the volume of the host cavity) of around 55% is associated with host-guest complexes having high binding affinity.[180] Nau and co-workers reported that the PC for representative sets of known guests with hydrophobic binding motifs showed average values of 47% for CB5, 58% for CB6, 52% for CB7, and 53% for CB8.[181, 182] These values closely align with the ideal PC (55% solution). In addition to these features, other characteristic properties of CBn, including chemical inertness, redox inactivity, non-toxic nature, photochemical inertness, and biocompatibility, enable CBn to be a promising candidate for developing chemosensors.[74, 183-185]

Since CBn are non-emissive and redox-inactive, previously mentioned sensing strategies (see section 3.1.3.) have been coupled to CBn to develop CBn-based chemosensors. Particularly, when employed in competitive binding assays like IDA, CBn have shown promising results in the detection of various biologically important analytes.[74, 186]

The complexation of chromophoric or emissive molecules with CBn can result in detectable photophysical changes due to the transfer of the molecule into a more hydrophobic and solvent-
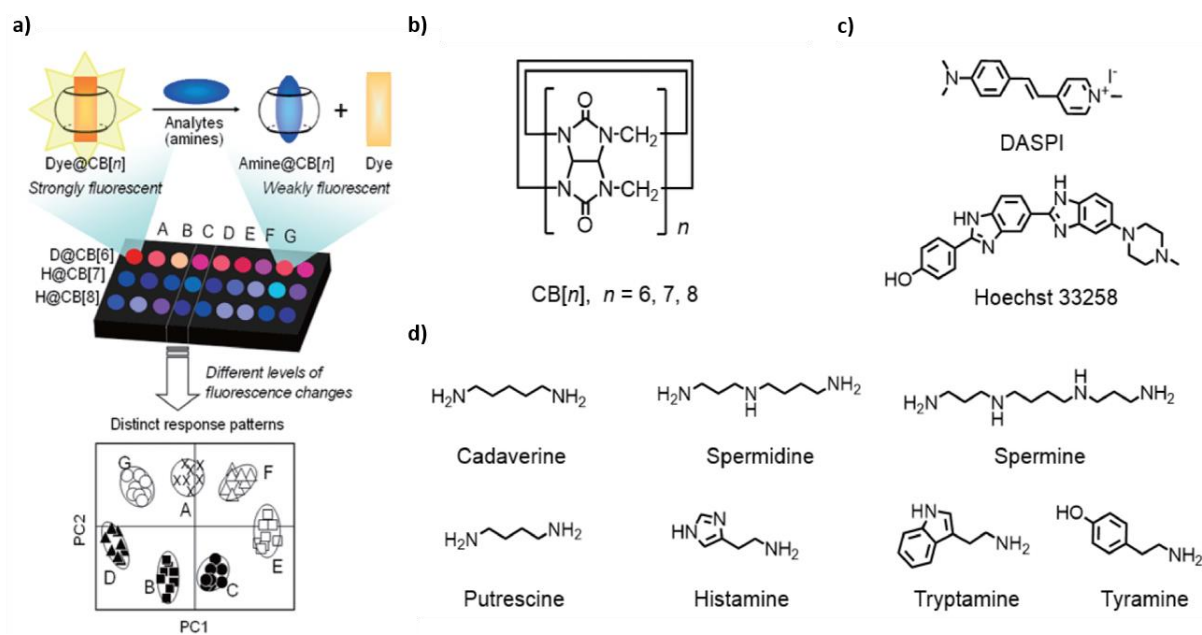
Figure 3.21 (a) Schematic representation of an IDA approach using CB*n*-based fluorescent dye complexes for the discrimination of biogenic amines. Chemical structures of (b) CB*n*, (c) dyes, and (d) polyamines. Reprinted (adapted) with permission from ref.[188] Copyright 2017, 2018 The Chemical Society of Japan.

protected environment of the CB*n* cavity.[74] Likewise, the redox properties of redox-active molecules are modulated upon complexation with CB*n* due to the changes in the microenvironment around these molecules.[187]

Numerous CB*n*-based chemosensors have been developed for the detection of various biologically relevant molecules. Some representative examples are discussed here. Nau and co-workers reported a CB*n*-based fluorescent chemosensor for the detection of steroids by utilizing an IDA approach.[171] They used berberine chloride (BC) and methylene blue (MB) as the fluorescent indicators for CB7, whereas BC and the perylene bis(diimide) derivative dye (PDI-OH) for CB8. The presence of steroids with high binding affinity for CB*n* caused the displacement of the dye from the CB*n* cavity, which is accompanied by a fluorescence turn-off response in aqueous media. Notably, the detection of steroids at low micromolar concentrations was possible. Moreover, each steroid showed a distinct fluorescence response to each reporter pair. Hence, they explored the potential for differential sensing in a microplate format. Employing principal component analysis (PCA) enabled the successful differentiation of 10 of the 12 steroids tested.

The detection of biogenic amines by utilizing an array of CB*n*-based fluorescent dye complexes was reported by Kim and co-workers (Figure 3.21).[188] In this IDA approach, fluorescent dyes such as (*trans*-4-[4-(dimethylamino)-styryl]-1-methylpyridinium iodide (DASPI) and
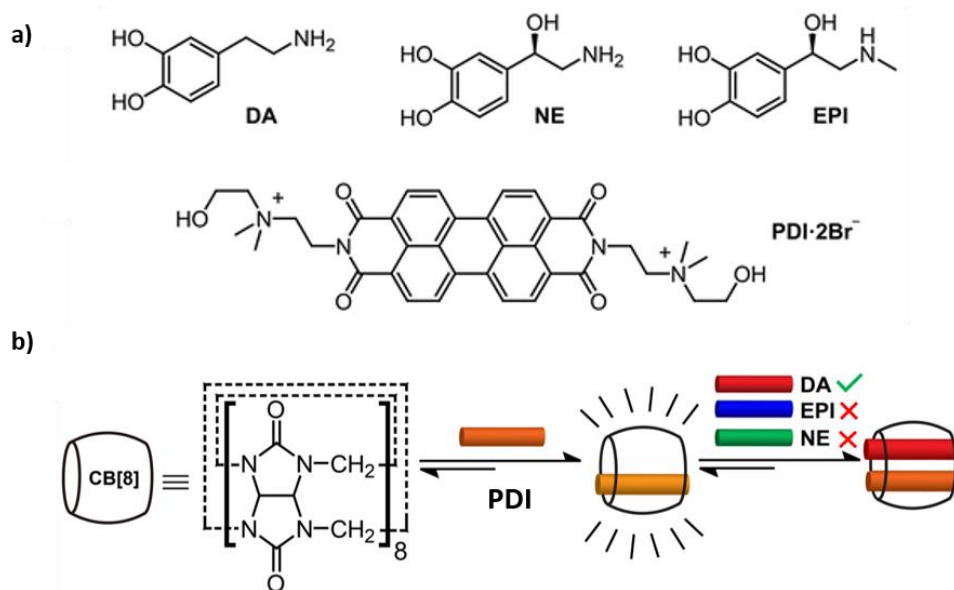
Figure 3.22 (a) Chemical structures of the neurotransmitters and PDI dye. (b) Schematic representation of the selectivity of CB8⊃PDI complex towards dopamine in the presence of neurotransmitters such as epinephrine and norepinephrine. Reprinted (adapted) with permission from ref.[192] Copyright 2013 Taylor & Francis.

bisbenzimide (Hoechst 33258) and three CB*n* homologues such as CB6, CB7, and CB8 were used. As mentioned earlier, fluorescence enhancement was observed upon complexation between CB*n* and dye, whereas fluorescence decreased in the presence of biogenic amines due to the displacement of dye from the CB*n* cavity. The fluorescence response was different for each amine, hence, the ability of the CB*n* sensors for pattern recognition of these amines was successfully investigated by PCA analysis.

Urbach and co-workers showed that the CB8⊃methyl viologen complex can selectively recognize peptides with N-terminal tryptophan compared to C-terminal or internal tryptophan residues through the formation of a 1:1:1 ternary complex.[189] Additionally, they demonstrated the detection of human insulin and human growth hormone by using a CB7⊃acridine orange chemosensor in an IDA format.[190, 191] In this case, the binding occurs at the N-terminal phenylalanine.

Scherman and co-workers reported a fluorescent-based ABA using CB8 as the host and PDI as the reporter dye (Figure 3.22a) for the detection of the neurotransmitter dopamine (DA) in water and low salt buffers.[192] They successfully showed that the detection of DA was possible even in the presence of known interferents, including ascorbic acid and other neurotransmitters such as epinephrine (EPI) and norepinephrine (NE) (Figure 3.22b), with a detection limit of below 2×10^{-5} M in water. The CB8⊃PDI complex formation results in fluorescence
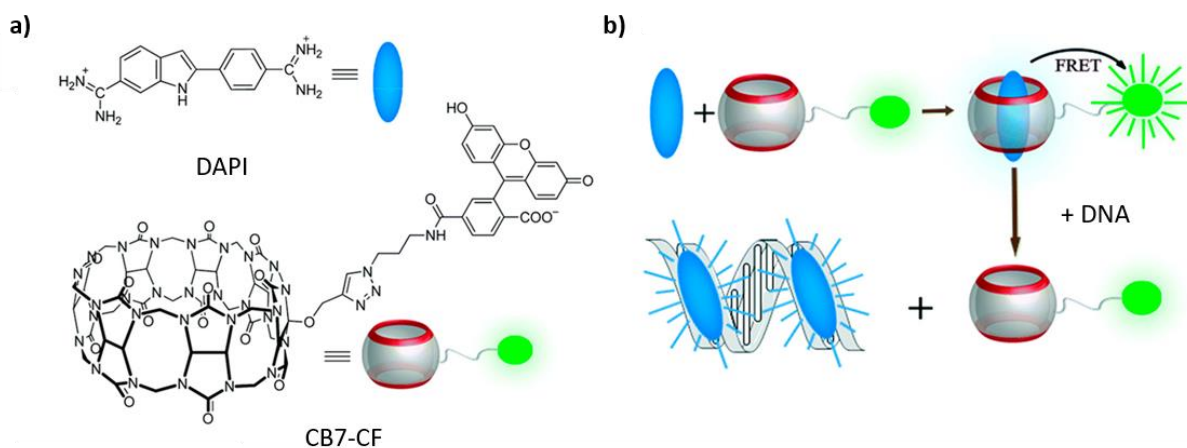
Figure 3.23 (a) Chemical structures of the dye DAPI and CB7-CF. (b) Schematic representation of the FRET-based chemosensor for DNA sensing. Reprinted (adapted) with permission from ref.[193] Copyright 2019 The Royal Society of Chemistry.

enhancement of the dye due to the breaking of the PDI π-stacks. Subsequently, the binding of the second guest (DA) quenches the fluorescence emission of the dye.

Nau and co-workers developed a supramolecular host-guest fluorescence resonance energy transfer (FRET) pair for the quantitative detection of DNA, employing carboxyfluorescein labelled CB7 (CB7-CF) as the acceptor and the nucleic stain 4',6-diamidino-2-phenylindole (DAPI) as the donor (Figure 3.23a).[193] In this approach, DAPI dissociates from the CB7 cavity in the presence of DNA due to the stronger binding affinity of DAPI for the minor grooves of DNA. This dissociation leads to a significant reduction in the FRET signal from the CB7-CF and the emergence of a new fluorescence emission band from the DNA-bound DAPI (Figure 3.23b).

In addition to employing fluorescence-based detection, Biedermann and co-workers reported CBn-based chemosensors accompanied by circular dichroism (CD) and fluorescence-detected circular dichroism (FDCD) for the detection of amino acids, proteins, steroids, terpenes, and drugs.[194, 195]

Earlier in section 3.2.3. , a few representative examples of electrochemical chemosensors based on CBn were discussed. In addition, the groups of Kaifer and Kim have showcased many other examples utilizing redox-based detection where CBn⊃guest complex formation induces a change in the reduction potential of redox-active guests.[196-202] For example, the half-wave potential ($E_{1/2}$) for the first and second reduction process of the herbicide paraquat (divalent cation) shifted to more negative potentials upon CB7 complexation.[198] In contrast, for the herbicide diquat (divalent cation), the addition of CB7 shifted the $E_{1/2}$ to less negative potential

for the first reduction process, whereas the second reduction process shifted to more negative values.[198] Hence, these analyte-dependent potential variations can offer characteristic fingerprints for redox-based analyte differentiation.

Li and co-workers presented a protein assay using a CB8⊃methyl viologen reporter pair-based electrochemical sensor.[203] They demonstrated the binding of CB8⊃methyl viologen complexes (MV@CB[8] as shown in Figure 3.24a) to aromatic amino acid side chains on surface-immobilized peptides. These peptides compete with the target protein, which leads to the binding of CB8⊃methyl viologen complexes with protein-free peptides (Figure 3.24b). Consequently, this produced an electrochemical signal readout inversely proportional to the amount of the target protein.
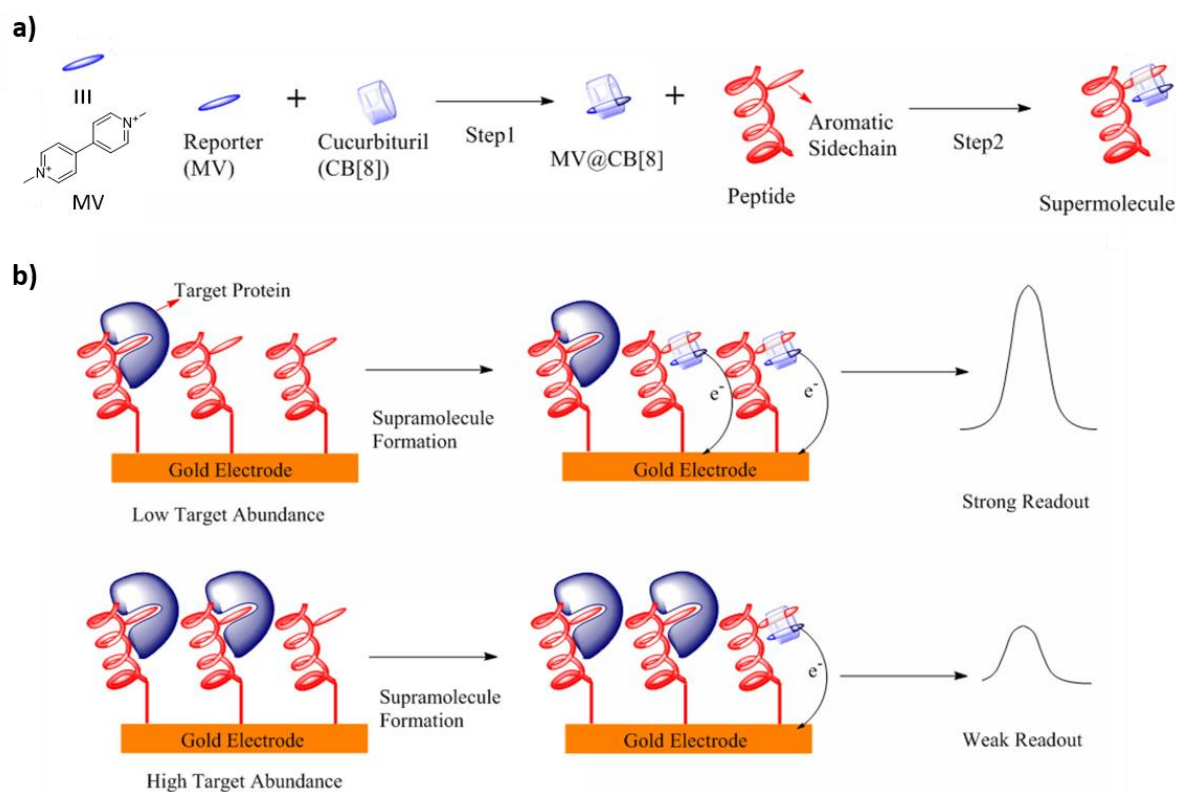

Figure 3.24 Schematic representation of an electrochemical sensor for the detection of proteins by using CB8 as the macrocyclic host and methyl viologen as the reporter. (a) Coupling of the protein-binding peptide with the reporter pair *via* host-guest complexation. (b) Functioning principle and the corresponding expected electrochemical signal readout of the protein assay. Reprinted (adapted) with permission from ref.[203] Copyright 2012 American Chemical Society.

3.3.2. CB*n*-based supramolecular tandem enzyme assays

Monitoring enzyme processes based on the molecular recognition of unlabelled enzymatic substrates or products by macrocyclic hosts in combination with IDA strategy is termed supramolecular tandem enzyme assays.[204] Nau and co-workers first introduced this concept by monitoring decarboxylase activity in a label-free continuous enzyme assay based on fluorescence response.[205] They demonstrated a product-selective tandem assay where the products of decarboxylase catalyzed reactions have strong binding affinity for the macrocyclic host (Figure 3.25 shows the schematic representation of a product-selective tandem assay[206]). For instance, CB7 binds weakly with a substrate (lysine, K_a = 870 M^{-1}) and strongly binds with the respective enzymatic product (cadaverine, K_a = 1.4 × 10^7 M^{-1}). Subsequently, the fluorescent dye gets displaced from the CB7 cavity upon product formation, resulting in a fluorescence switch-off response.
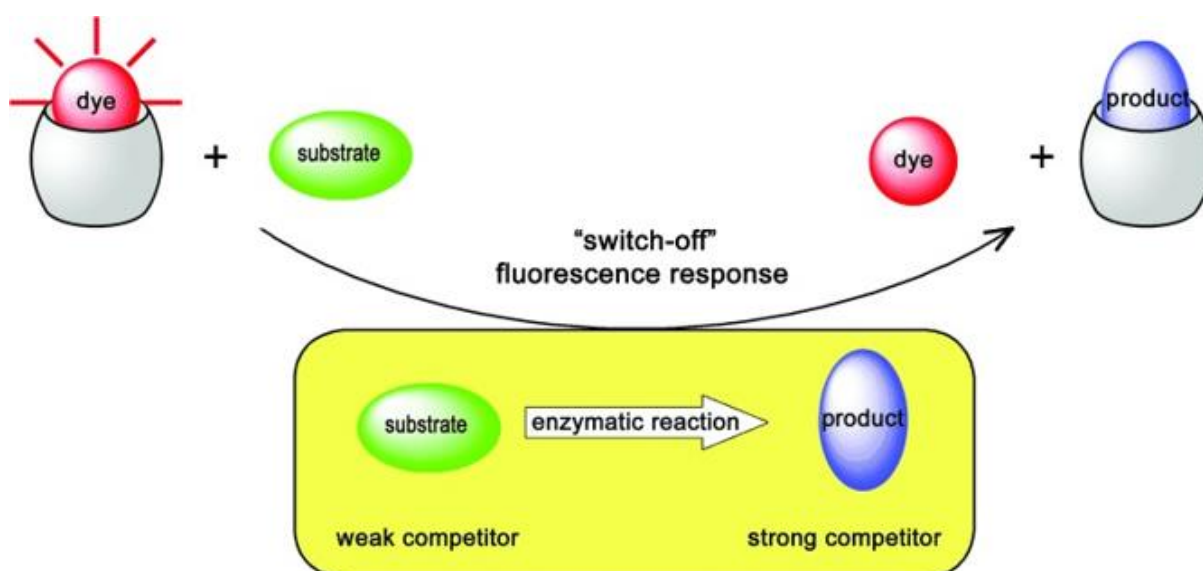

Figure 3.25 Schematic representation of product-selective tandem assay. Reprinted (adapted) with permission from ref.[206] Copyright 2008 WILEY-VCH Verlag GmbH & Co. KGaA, Weinheim.

In another work from Nau and co-workers, they reported the continuous monitoring of protease enzyme activity on unlabelled peptides by employing a CB7⊃acridine orange (CB7⊃AO) reporter pair (Figure 3.26).[207] CB7 binds selectively to the N-terminal phenylalanine residues formed during the enzymatic cleavage of enkephalin-type peptides by the metalloendopeptidase thermolysin. Hence, the products of the enzymatic reaction displace AO from the CB7 cavity, leading to a fluorescence switch-off response. In addition to monitoring enzyme activity, they also investigated the thermolysin inhibition process using the product-selective tandem assay.
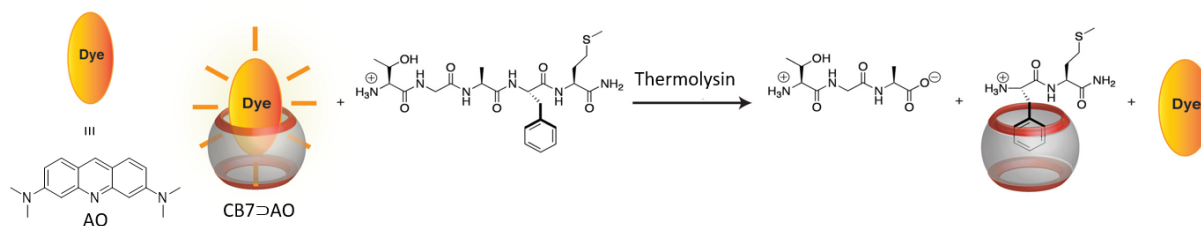
Figure 3.26 Example of product-selective tandem assay for monitoring the hydrolysis of Thr-Gly-Ala-Phe-Met-NH$_2$ peptide by protease enzyme thermolysin using CB7 and AO as the reporter pair. Reprinted (adapted) with permission from ref.[207] Copyright 2011 American Chemical Society.

Similarly, Nau and co-workers developed a substrate-selective tandem assay, which can be realized in cases where the host binds more strongly to the substrate rather than to the enzymatic product.[204, 208] For example, they investigated the oxidation of cadaverine to 5-aminopentanal by diamine oxidase enzyme, in which cadaverine has a stronger affinity to CB7 than the 5-aminopentanal (Figure 3.27). During the enzymatic reaction, the weak competitor 5-aminopentanal is formed, allowing the fluorescent dye AO to bind with CB7, which in turn produces a fluorescence switch-on response.
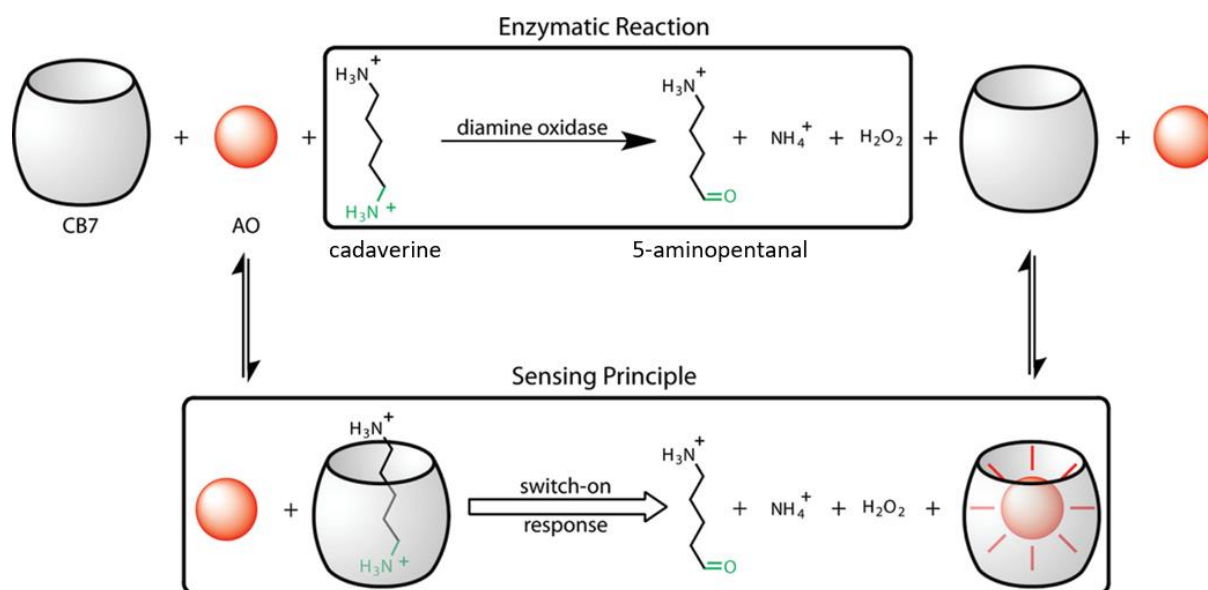

Figure 3.27 Schematic representation of substrate-selective tandem assay for monitoring the oxidation of cadaverine to 5-aminopentanal by diamine oxidase enzyme using CB7 and AO as the reporter pair. Reprinted (adapted) with permission from ref.[208] Copyright 2009 American Chemical Society.

3.3.3. CB*n*-based supramolecular tandem membrane assays

Monitoring the translocation of analytes across the phospholipid bilayer membrane of vesicles by utilizing membrane-impermeable reporter pairs that are encapsulated inside the vesicle lumen is termed supramolecular tandem membrane assays.[84, 209] Nau and co-workers first reported this concept for screening various analytes *via* IDA format.[209] They have shown a CB7⊃BC reporter pair loaded liposome for the real-time fluorescence monitoring of analyte translocation through the lipid bilayer (Figure 3.28). In the presence of membrane-permeable analytes, BC is displaced from the CB7 host cavity, resulting in a fluorescence response. This CB7⊃BC loaded liposome allowed the monitoring of Alzheimer's drug amantadine.

In another work by Biedermann and Nau, a fluorescent artificial receptor membrane assay (FARMA) based on liposome encapsulated CB8⊃dicationic dye reporter pair was introduced that follows an ABA format.[210] The FARMA enabled real-time monitoring of more than 100 analytes across the lipid bilayer within the biologically relevant concentration range (nM–μM).

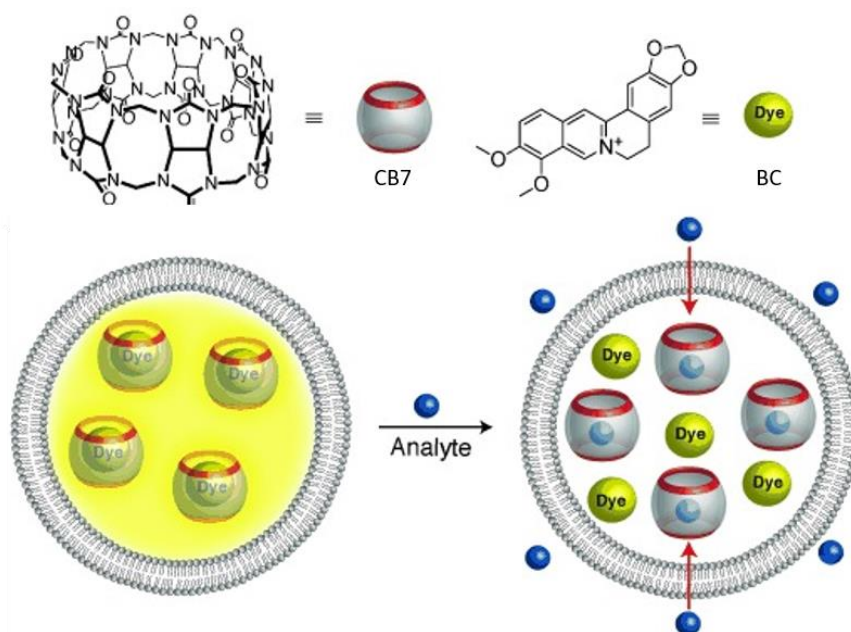**Figure 3.28** Schematic representation of CB*n*-based supramolecular tandem membrane assays using CB7⊃BC reporter pair encapsulated liposome for the real-time fluorescence monitoring of analyte translocation. Reprinted by permission from ref.[209] Copyright 2014 WILEY-VCH Verlag GmbH & Co. KGaA, Weinheim.

4. Aim of the thesis

Chemosensors based on supramolecular host-guest chemistry have received increasing attention due to the wide range of possibilities for practical sensing applications. Developing chemosensors comprised of artificial receptors as recognition elements and a signal transduction unit for reporting the binding of target analytes provides a robust, low-cost, fast-responding sensing approach with real-time monitoring and thus, offers numerous diagnostic opportunities. Among the several artificial receptors known to bind with small organic molecules, cucurbit[n]urils (CBn) are promising recognition elements for developing chemosensors due to their water solubility, chemical stability, non-toxic nature, low-cost synthesis pathway, and exceptional binding affinities for various analytes, including drugs and biomolecules. Most of the reported CBn-based chemosensors utilize fluorescence-based detection methods. However, fluorescent chemosensors rely on an external light source to activate the emissive species for producing fluorescence signals, which may lead to major issues such as autofluorescence, light source instability, and light scattering. These challenges can adversely affect the performance of the sensing assay, thereby reducing the signal-to-noise ratio. In this regard, chemiluminescence- and electrochemical-based detection methods can be utilized as alternative signal transduction methods for developing CBn-based chemosensors.

Chemiluminescent chemosensors operate without the need for an external light source, as chemiluminescence is produced from chemical reactions and thus can potentially overcome the drawbacks of fluorescent chemosensors. Due to its superior signal-to-noise ratio, the chemiluminescence-based signal readout is widely adapted in various areas of research ranging from clinical diagnostic to pharmaceutical research.

Another upsurging area of research is the development of electrochemical chemosensors that produce electrical signals in response to analyte recognition. These sensors have emerged as a potential sensing platform due to their exceptional sensitivity, affordability, and compact design.

The main aim of my thesis was to design and develop novel signal transduction methods for use in CBn-based chemosensors by investigating chemiluminescence- and electrochemical-based detection methods and establishing proof-of-concept solutions for molecular diagnostics.

The present thesis describes different approaches for developing novel CB*n*-based chemosensors utilizing chemiluminescence- or electrochemical-based signal readout and their potential sensing applications in biofluids.

Chemiluminescent chemosensors based on host-guest chemistry have been reported for hydrogen peroxide detection in water and for imaging reactive oxygen species *in vitro* and *in vivo*. However, no chemiluminescent chemosensors have been reported based on host-guest chemistry for sensing small bioactive organic molecules in biofluids.

The first research project aims to design and develop a novel chemiluminescent chemosensor using CB*n* as the macrocyclic host and phenoxy 1,2-dioxetane as the chemiluminescent indicator to detect biologically relevant organic analytes in biofluids. Additionally, this project aims to establish the potential of CB*n* to enhance the chemiluminescence emission of phenoxy 1,2-dioxetanes that have found practical uses in enzyme-coupled chemiluminescence assays, thus providing a non-toxic and cost-effective alternative to existing surfactant chemiluminescence enhancers. Moreover, I intend to combine phenoxy 1,2-dioxetanes with CB*n*-dye conjugates to develop a chemosensor based on chemiluminescence resonance energy transfer (CRET)-based detection strategy. The main objective of this project is to investigate chemosensor designs that circumvent the challenges of the existing fluorescent chemosensors, thereby providing enhanced sensitivity for molecular diagnostic applications.

Macrocyclic hosts play a vital role in developing electrochemical sensors due to their analyte recognition properties. Nevertheless, the current design principles of electrochemical chemosensors based on supramolecular host-guest chemistry necessitate an immobilization method on the electrode surface. However, major challenges are associated with these sensors as the immobilization process is not straightforward, has limited stability, and leads to non-specific adsorption of analytes. Therefore, investigating a new design strategy for electrochemical sensors is demanding to overcome these problems.

The second research project aims to develop a novel design principle for an electrochemical chemosensor based on an indicator displacement assay that utilizes CB*n* as the macrocyclic host and an electrochemically active compound as the redox indicator. This chemosensor aims to detect redox-inactive analytes, specifically targeting the biologically relevant analytes in aqueous solutions and biofluids. Unlike the existing electrochemical chemosensor designs, this approach aims to eliminate the need for immobilization processes on the electrode surface and to use commercially available screen-printed electrodes, which require minimal sample

volumes. Ultimately, this project intends to develop miniaturized, disposable, cost-effective, and portable electrochemical sensors with high sensitivity. Thus, this approach could offer a promising alternative to fluorescent chemosensors, especially in emergency on-site applications.

5. Chemiluminescent cucurbit[*n*]uril-based chemosensor for the detection of drugs in biofluids
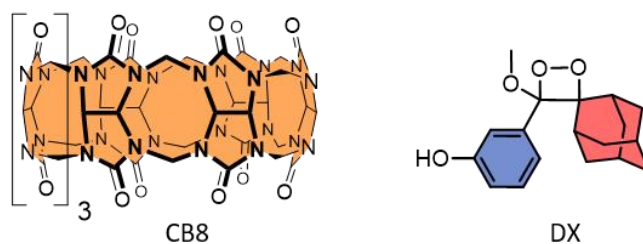
The results described in this chapter have been published as "Chemiluminescent cucurbit[n]uril-based chemosensor for the detection of drugs in biofluids" in ACS Sensors, 2022.[211] The synthesis, experimental data collection, and analysis were carried out by me under the supervision of Dr. Pierre Picchetti and Priv.-Doz. Dr. Frank Biedermann. The manuscript was written with the contributions of all authors. The co-authors contributed by providing valuable discussions, synthesizing material (CB7-CF: Dr. Changming Hu), and reviewing the article draft. Sections in this chapter have been reproduced from the published work[211] with permission from the American Chemical Society.

5.1. Introduction

Chemosensors based on macrocyclic hosts as recognition elements generate a detectable signal, such as spectroscopic readout, upon binding with the target analytes.[6, 212] Among numerous macrocyclic hosts,[213-216] CB*n* are prime candidates for developing chemosensors due to their chemical stability,[162] exceptional binding affinity for a variety of analytes, such as drugs in aqueous environments ($K_a > 10^3$ M^{-1}),[74, 217, 218] biocompatibility,[183] and cost-effective synthesis.[219, 220] There are many literature examples of CB*n*-based chemosensors utilizing fluorescence as signal readout.[74, 221, 222] Fluorescent chemosensors require an external light source to excite the fluorescent species, and thus, the signal-to-noise ratio is often suboptimal due to light interference resulting from excitation and autofluorescence of other fluorescent compounds in the sample.[223]

Employing CL-based detection methods in chemosensors would be an alternative design strategy for overcoming the challenges associated with fluorescent chemosensors, as an external light source is not required to activate the chemiluminescent species and thus, provide high sensitivity for sensing applications. CL-based detection methods have been broadly applied in many fields, such as developing chemiluminescent hydrogels,[224] light-on/light-off switches,[225] self-reporting polymers,[226] and agents for photodynamic therapy.[94] There are even ready-to-use chemiluminescent detection reagents available for enzymes such as horseradish peroxidase, alkaline phosphatase, and β-galactosidase.[100, 227] Notably, CL-based readout is
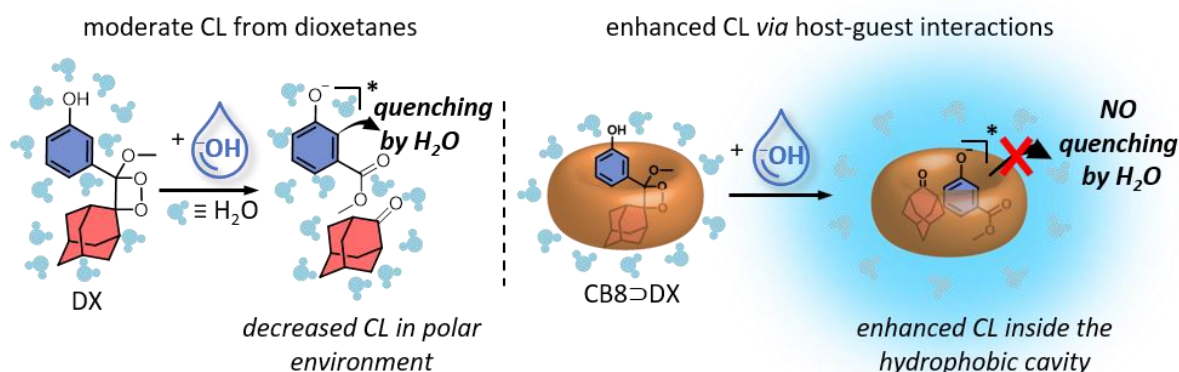
Figure 5.1 (a) Chemical structures of CB8 and chemiluminescent DX. (b) Schematic representation of CB8-induced modulation of CL of DX.

extensively utilized in immunoassays for clinical diagnostics and pharmaceutical studies.[100, 228, 229] Shabat and co-workers have reported the design of a β-CD-based host-guest inclusion complex using CL as signal output for *in vitro* and *in vivo* imaging.[128]

Given the high sensitivity and potential applications of CL-based sensing systems, developing a chemiluminescent host-guest-based chemosensor for sensing biologically relevant organic molecules, such as drugs, in biofluids would be a promising approach for molecular diagnostics.

Choosing an appropriate chemiluminescent probe is crucial when designing a chemiluminescent chemosensor. Phenoxy 1,2-dioxetanes (PDOs) are interesting candidates as they can be specifically triggered by analytes or enzymes to emit light and are widely employed in CL-based assays.[113, 116, 118, 230, 231] Due to the solvent-induced quenching, PDOs exhibit relatively lower CL quantum yields in an aqueous environment.[97, 123] Therefore, performance enhancers such as surfactant-dye adducts can be used to enhance the CL intensity of PDOs by providing an apolar environment.[110] Nevertheless, when applied to live cells, these performance enhancers can be chemically unstable and toxic.[232] Thus, employing a non-surfactant-based performance enhancer for PDOs is particularly interesting.

In my investigations, I developed a chemiluminescence-based chemosensor (CCS) assay utilizing CB8 as the macrocyclic host and a structurally simple PDO, 3-(4-methoxyspiro[1,2-dioxetane-3,2′-tricyclo[3.3.1.1^{3,7}]decan]-4-yl)phenol (DX) (Figure 5.1a) as the chemiluminescent indicator to achieve the detection of drugs in biofluids at low micromolar concentrations. In addition, an alternative approach to enhance the CL of PDOs by using biocompatible CB8 as a non-surfactant CL performance enhancer (Figure 5.1b) is demonstrated. Furthermore, the possibility of developing chemiluminescence resonance energy transfer (CRET)-based assays to detect analytes is described.

This chapter first focuses on the development of the CCS assay and its ability to detect drugs in biofluids such as human urine and human serum. The following sections discuss CB8 as a non-surfactant-based performance enhancer for PDOs and the design of a CRET-based sensing assay.

5.2. Results and discussion

5.2.1. Chemiluminescent properties of DX

DX was synthesized by following reported procedures (see section 5.4.3. in experimental details for the synthesis and characterization of DX).[96, 233]

In an acidic aqueous solution (pH 6.0), DX was observed to be stable for approximately 1 h (Figure 5.2a) whereas a blue CL emission ($\lambda_{em, max}$ = 471 nm) was observed when the pH increased to basic condition (pH 9.6) (Figure 5.2c-d). This is due to the formation of an electronically excited phenoxy methyl ester intermediate (E*) after deprotonation of the phenol group of DX (pK_a ≈ 9.0) (Figure 5.2e).

The conversion of DX to its degradation products at pH 9.6 was confirmed by UV-Vis absorption spectroscopy (Figure 5.2b), as the absorption band at λ_{max} = 282 nm corresponding to the π-π* transition in DX decreases and two intense bands at λ_{max} = 305 nm and λ_{max} = 315 nm emerge corresponding to the new π-π* and n-π* transition in the 3-hydroxybenzoic acid methyl ester (E).

5.2.2. Host-guest inclusion complex of DX with CB8

Given the strong binding of 1-adamantanol to CB7 (log K_a = 10.4) and CB8 (log K_a = 6.8) in water,[234] I expected efficient complex formation between PDOs and CB*n* (*n* = 7 and 8) within

the micromolar concentration range. As anticipated, it was observed that DX forms a strong host-guest inclusion complex with CB8 (log $K_{a,CB8 \supset DX}$ = 6.2), which was determined by an IDA in 10 mM PBS at pH 6.0 (see section 5.4.5. in experimental details and Figure 5.32 in supplementary data). Furthermore, the formation of the CB8⊃DX inclusion complex was also confirmed by mass spectrometry (see Figure 5.33 in supplementary data).
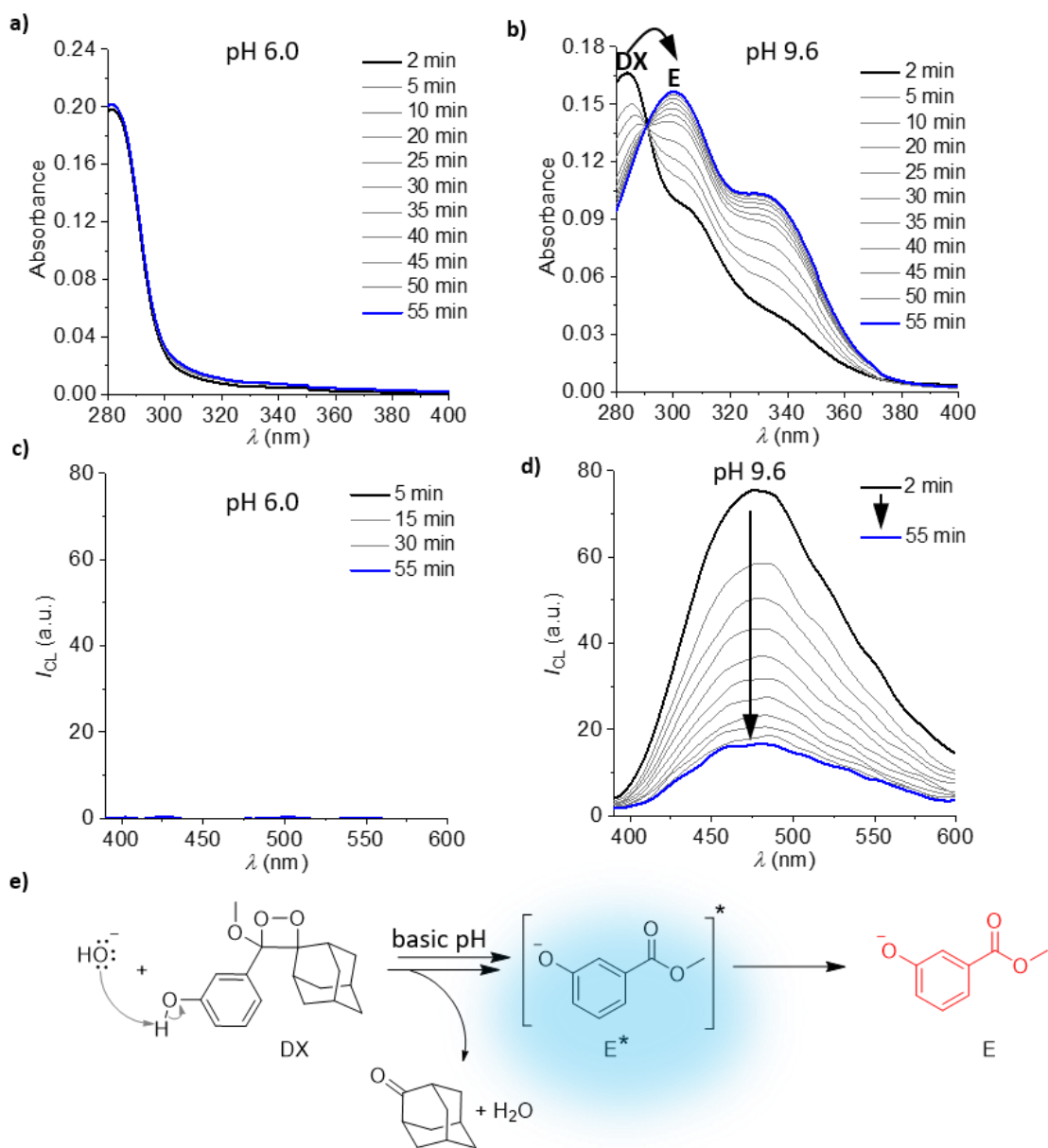

Figure 5.2 (a) UV-Vis absorption spectra of DX with time at pH 6.0. (b) Change in the UV-Vis absorption spectra of DX with time at pH 9.6. (c) CL profiles of DX with time at pH 6.0. (d) CL profiles of DX with time at pH 9.6. (e) Schematic representation of the base-triggered chemiexcitation of DX. All these measurements were performed using 60 µM DX in 10 mM PBS containing 2.5 vol% DMSO.

5.2.3. Chemiluminescent properties of DX in its inclusion complex with CB8

To investigate the chemiluminescent properties of the CB8⊃DX inclusion complex, the CL reaction of DX was triggered by the addition of NaOH solution to adjust the pH of the solution to basic (pH 9.6). Interestingly, a 4.5-fold enhancement of CL intensity for CB8⊃DX complex (λ_{max} = 455 nm) was observed compared to the free DX (λ_{max} = 471 nm) at pH 9.6 in 10 mM PBS (Figure 5.3). This enhancement in CL intensity can be explained as follows: CB8 encapsulates both the electronically excited state of the phenoxy derivative (E*) and the adamantanone, protecting the excited state from deactivation. In terms of mechanism, the chromophore generated upon base addition, *i.e.*, E*, is confined within the hydrophobic cavity of CB8, thus shielding it from the surrounding water molecules (Figure 5.1b). Notably, the CB8⊃DX complex exhibits a hypsochromic shift (Δ = 16 nm, see Figure 5.34a in supplementary data) in the emission wavelength maximum when compared to free DX. This observation further confirms the host-guest complex formation according to the inclusion complex hypothesis.[63, 235] The reproducibility of the CL enhancement was validated by six replica measurements, resulting in a promising relative standard deviation (RSD) of 4% (see Figure 5.34b in supplementary data).
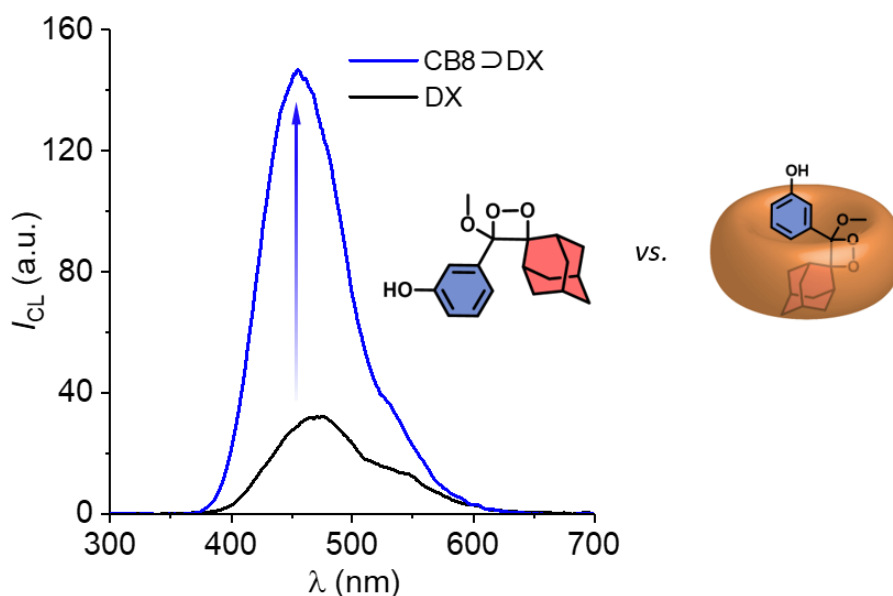

Figure 5.3 CL spectra of CB8⊃DX (30 μM) and DX (30 μM) in 10 mM PBS containing 2.5 vol% DMSO at pH 9.6.
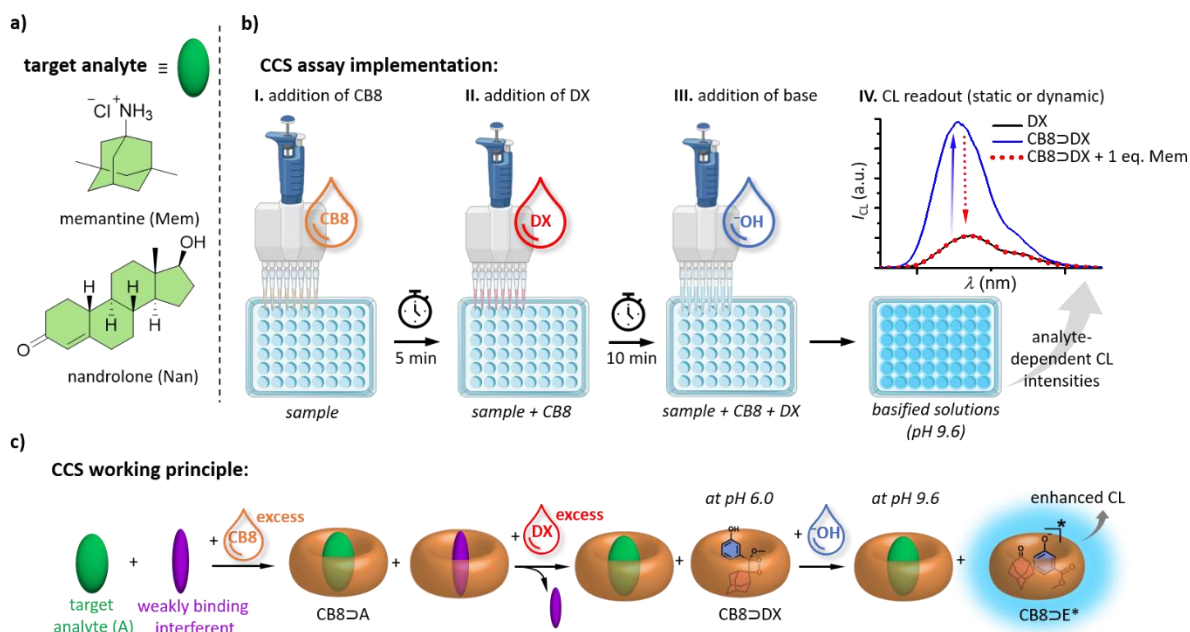
Figure 5.4 (a) Chemical structures of the analytes. (b) Schematic representation of the CCS assay implementation. The graph shows the Mem-dependent decrease in the CL intensity (Mem = 30 µM, CB8 = 30 µM, and DX = 30 µM in 10 mM PBS at pH 9.6). (c) Schematic representation of the working principle of CCS assay.

There are reports of methylated β-CD derivatives being used as non-surfactant additives for CL enhancement of 1,2-dioxetanes.[128, 236] Nevertheless, a much higher concentration of methylated β-CD derivatives is required to achieve a sufficient level of dioxetane complexation, which affects the efficiency of the chemosensor for micromolar detection of target analytes. Furthermore, it has been shown that non-methylated CDs act as CL quenchers.[128]

5.2.4. Chemiluminescent detection of analytes

Next, I investigated the possibility of developing a CCS assay by using CB8 as the macrocyclic host due to its high affinity for various analytes and its observed CL enhancement effect on DX. CB8 has a high binding affinity for hydrophobic drugs such as memantine (Mem, log K_a = 12.9),[237] a medication for the treatment of Alzheimer's disease,[238] and nandrolone (Nan, log K_a = 7.3),[171] an anabolic steroid (Figure 5.4a).[239] Thus, the detection of these high-affinity drugs by CCS assay was analysed as these drugs can effectively displace the chemiluminescent reporter DX from the CB8 cavity, thereby reducing the CL signal intensity.

The schematic representation of the CCS assay implementation is shown in Figure 5.4b (see section 5.4.6. in experimental details for the CCS assay procedure). First, CB8 (30 µM) was added to an aqueous solution of the analyte (A) at pH 6.0, resulting in a spectroscopically silent
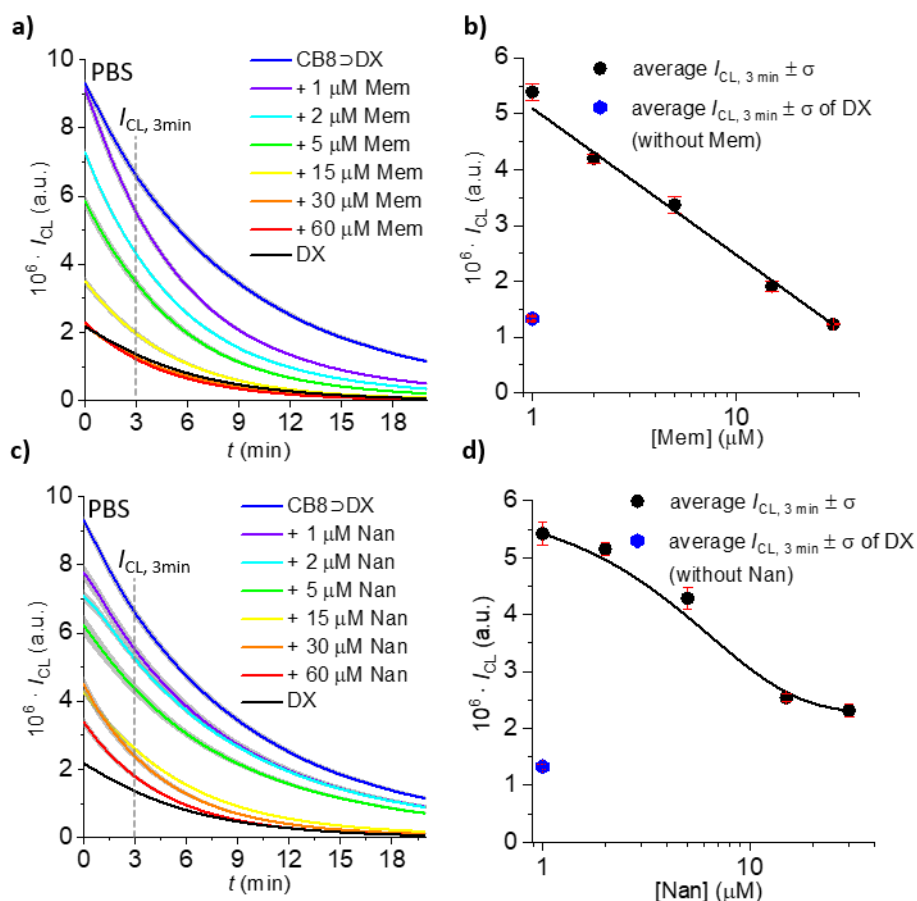
Figure 5.5 (a) Time-dependent CL response of CCS (30 μM CB8 and 30 μM DX) in Mem-spiked (0 – 60 μM) PBS samples and (b) semi-log plot of corresponding I_{CL} plotted at 3 min. (c) Time-dependent CL response of CCS (30 μM CB8 and 30 μM DX) in Nan-spiked (0 – 60 μM) PBS samples and (d) semi-log plot of corresponding I_{CL} plotted at 3 min. All measurements were performed in PBS (10 mM, containing 2.5 vol% DMSO, pH 9.6). The average I_{CL} and the corresponding standard deviation (σ) were calculated from six replica measurements.

CB8⊃A complex (Figure 5.4c). Then, after an equilibration time of about 5 min, an equimolar amount of DX (30 μM) was added, which caused the sequestering of the residual unoccupied CB8 forming the CB8⊃DX complex (Figure 5.4c). Finally, the CL emission was triggered by the addition of NaOH$_{aq}$, and the CL kinetic profiles were recorded by collecting light range from 320 – 740 nm. The higher binding affinities of CB8 with Mem or Nan compared to DX ensure that no analyte is displaced from the CB8⊃A complex. Meanwhile, weaker CB8-binding interferents in the media, such as metabolites, get displaced from the CB8 cavity upon DX addition (Figure 5.4c).

As expected, a gradual decrease in CL intensity was observed with increasing analyte concentration (0 – 60 μM) when the CCS assay was performed in analyte-spiked (Mem or Nan) PBS samples (10 mM, pH 6.0) (Figure 5.5). Thus, no CL enhancement was observed for samples with equimolar analyte concentration (graph in Figure 5.4b, IV, red curve).
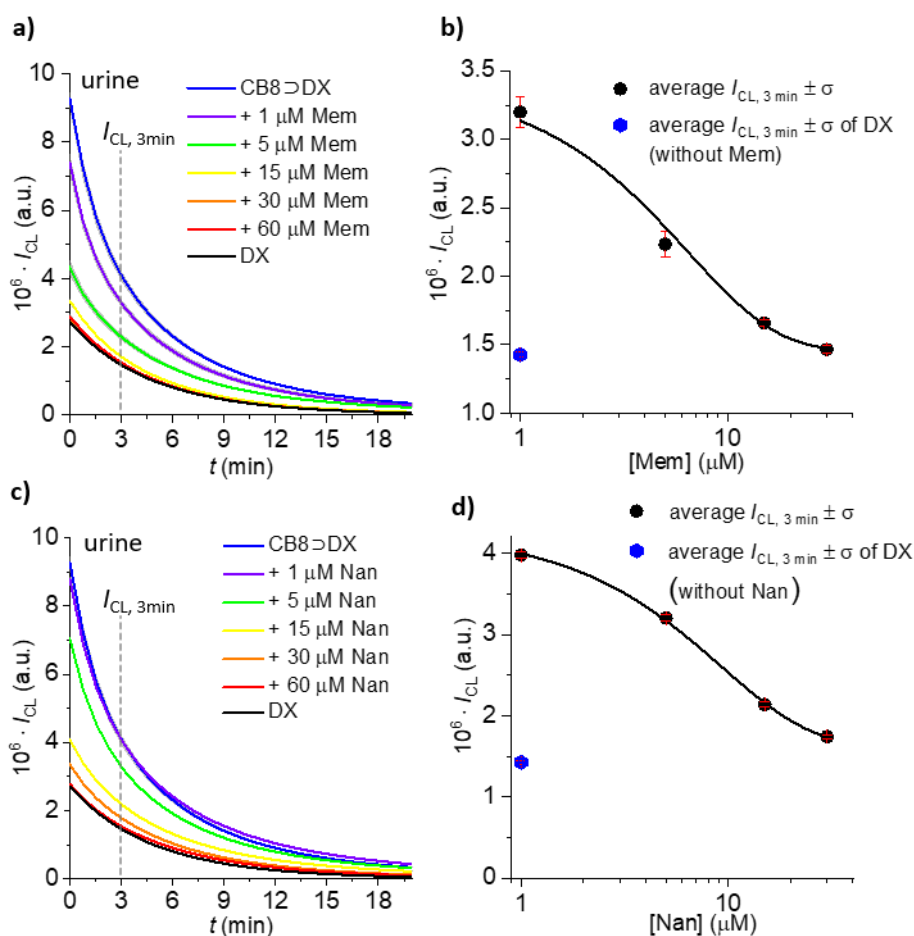
Figure 5.6 (a) Time-dependent CL response of CCS (30 µM CB8 and 30 µM DX) in Mem-spiked (0 – 60 µM) urine samples and (b) semi-log plot of corresponding I_{CL} plotted at 3 min. (c) Time-dependent CL response of CCS (30 µM CB8 and 30 µM DX) in Nan-spiked (0 – 60 µM) urine samples and (d) semi-log plot of corresponding I_{CL} plotted at 3 min. All measurements were performed in urine (1:1 diluted with 10 mM PBS containing 2.5 vol% DMSO, pH 9.6). The average I_{CL} and the corresponding standard deviation (σ) were calculated from six replica measurements.

Based on these findings, the CCS assay was next applied in biofluids (human urine and deproteinized human serum). Notably, the detection of analytes (Mem and Nan) was also possible in corresponding analyte-spiked (0 – 60 µM) human urine (1:1 diluted with 10 mM PBS at pH 6.0) (Figure 5.6) and analyte-spiked (0 – 60 µM) deproteinized human serum (1:3 diluted with 10 mM PBS at pH 6.0) (Figure 5.7). In addition, a control experiment was conducted using DX alone, without CB8, for the detection of analytes (see Figure 5.35 in supplementary data). In this case, detecting Mem and Nan was impossible, which supports the proposed mechanism of the CCS assay.

In contrast to antibody-based assays that require long equilibration times,[240] CCS assay can be conducted rapidly. Furthermore, investigations into the equilibration period (between 5 and
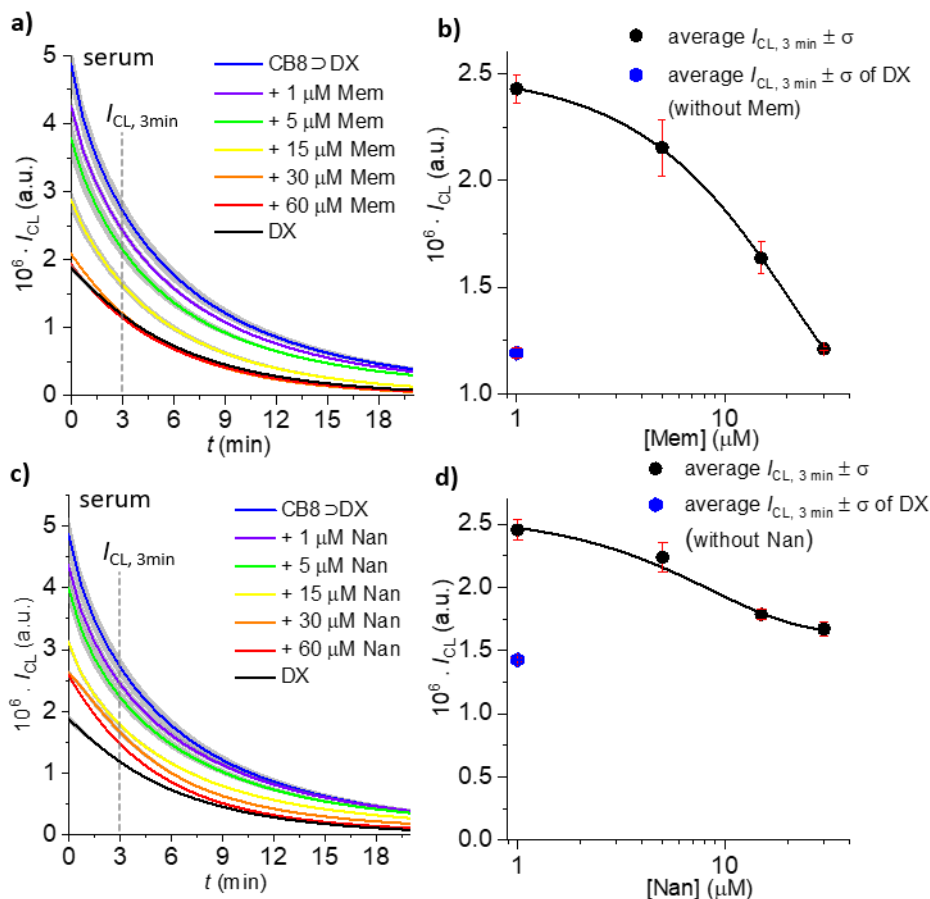
Figure 5.7 (a) Time-dependent CL response of CCS (30 µM CB8 and 30 µM DX) in Mem-spiked (0 – 60 µM) serum samples and (b) semi-log plot of corresponding I_{CL} plotted at 3 min. (c) Time-dependent CL response of CCS (30 µM CB8 and 30 µM DX) in Nan-spiked (0 – 60 µM) serum samples and (d) semi-log plot of corresponding I_{CL} plotted at 3 min. All measurements were performed in deproteinized serum (1:3 diluted with 10 mM PBS containing 2.5 vol% DMSO, pH 9.6). The average I_{CL} and the corresponding standard deviation (σ) were calculated from six replica measurements.

20 min) for premixing Mem with CB8 showed no notable effect on the resulting CL intensity (see Figure 5.36 in supplementary data).

The obtained results show that the CCS assay can detect Mem at concentrations as low as 1 µM. Since the therapeutic range of Mem in plasma lies between 0.50 – 0.83 µM and toxicity level at 1.67 µM,[241] there is potential to further refine the CCS assay to detect Mem overdosing and abnormal drug intake in patients having Alzheimer's disease.[242] Additionally, anti-doping agencies in sports competitions closely monitor Nan levels, and this enables the detection of drug abuse when intake levels increase to 7 nM for female athletes and 18 nM for male athletes.[243] Even though the developed CCS assay lacks a nanomolar detection range, it operates effectively in the micromolar range. Therefore, this assay may find potential use for on-site detection of Nan in unauthorized preparations used by athletes during sports competitions.

5.2.5. CB8 as CL enhancer for the commercially available CDP-Star dioxetane

Next, I explored the potential of CB8 as a CL enhancer for the commercially available CDP-Star dioxetane (Figure 5.8a), which undergoes alkaline phosphatase (ALP)-catalyzed dephosphorylation to generate CL emission and is widely utilized in enzyme-linked immunosorbent assays.[98, 123] Interestingly, a 15-fold increase in the CL intensity was observed upon adding an equimolar concentration of CB8 (30 µM) to a solution of enhancer-free CDP-Star (30 µM) in TRIS buffer (10 mM, containing 1 mM $MgSO_4$, pH 9.0), followed by the addition of 3 U mL^{-1} of ALP at 37 °C (Figure 5.8b). Notably, when a premix of CB8 with an equimolar amount of Mem (30 µM) was added to CDP-Star, there was no CL intensity enhancement due to the aforementioned reasons (Figure 5.8b). Moreover, the addition of β-CD to CDP-Star led to significant quenching of the CL signal (see Figure 5.37 in supplementary data). This further highlights the role of CB8 as a CL performance enhancer for dioxetanes.
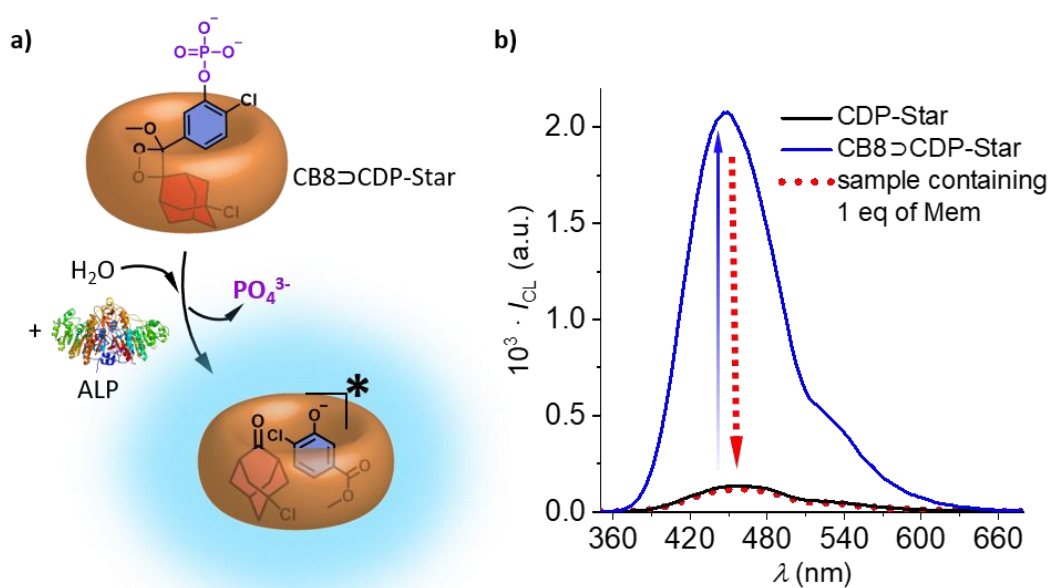

Figure 5.8 (a) Schematic representation of the ALP-catalyzed dephosphorylation of CDP-Star, resulting in an enhanced CL signal due to the complexation of CDP-Star with CB8. (b) CL emission spectra of CDP-Star (30 µM) in the presence and absence of CB8 (30 µM) in 10 mM TRIS buffer containing 1 mM $MgSO_4$ and 3 U mL^{-1} of ALP at 37 °C (pH 9.0). Also shown is the CL emission when 1 eq. of Mem was added to CDP-Star prior to CB8 and ALP addition.

5.2.6. Investigation of CRET between DX and CB7-CF

During the binding affinity studies of DX, I found out that DX also forms a relatively strong inclusion complex with CB7 (log $K_{a,CB7 \supset DX}$ = 7.2 in water at pH 6.0), which was determined by an IDA (see section 5.4.5. in experimental details and Figure 5.38 in supplementary data). When the CL response of DX with the addition of CB7 was evaluated, no CL enhancement was observed for the CB7⊃DX complex in basic media (Figure 5.9a). A plausible mechanistic interpretation is as follows: The smaller cavity of CB7 compared to CB8 can only accommodate the adamantane moiety but not the chromophore of DX, and thus, the chromophore is exposed to the surrounding water molecules (Figure 5.9b), causing the deactivation process. However, CRET[128] can be achieved by using a CB7-dye conjugate as a suitable host for sensing applications.
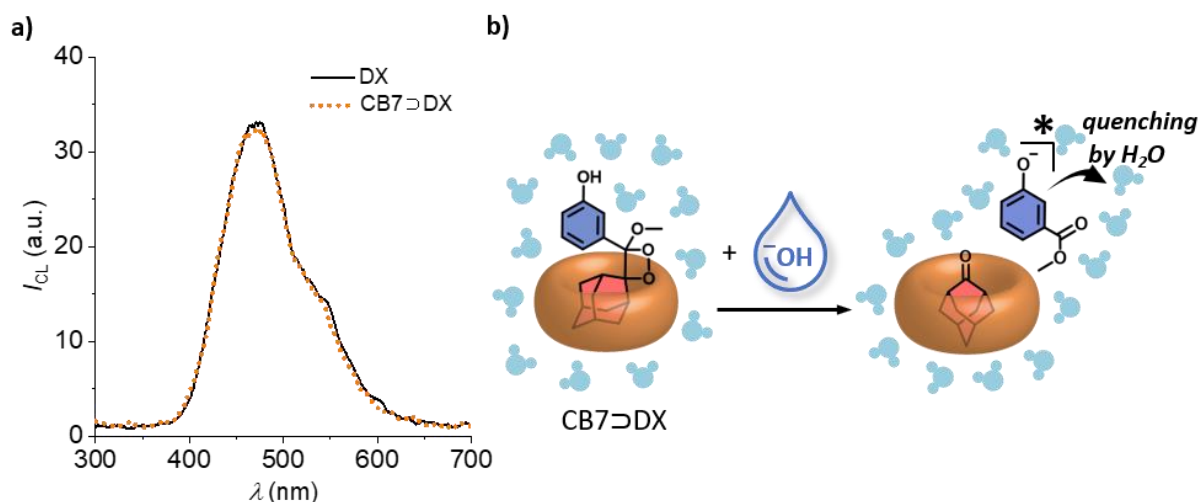

Figure 5.9 (a) CL spectra of DX (30 µM) and CB7⊃DX (30 µM) in water containing 2.5 vol% DMSO, pH 9.6. (b) Schematic representation of the binding mode of DX to CB7.

The CRET experiments were performed using carboxyfluorescein azide (CF-N$_3$) as the CRET acceptor, which was covalently attached to CB7 (CB7-CF, Figure 5.10a). CB7-CF was synthesized by following literature procedures (see section 5.4.4. in experimental details for the synthesis and characterization of CB7-CF).[193] The absorbance profile of CF-N$_3$ showed significant spectral overlap with the emission profile of DX (CRET-donor, Figure 5.10b).

The schematic representation of the CRET is depicted in Figure 5.10c, I. To a solution of CB7-CF (0 – 15 µM) in water (pH 6.0), 10 µM of DX was added. CL was subsequently triggered by adding NaOH$_{aq}$. Luminescence intensities were recorded in the wavelength range 450 – 470 nm and 540 – 560 nm, corresponding to DX and CB7-CF, respectively. CRET was observed as indicated by the CB7-CF-dependent emission, whereas a reduction in CL intensity
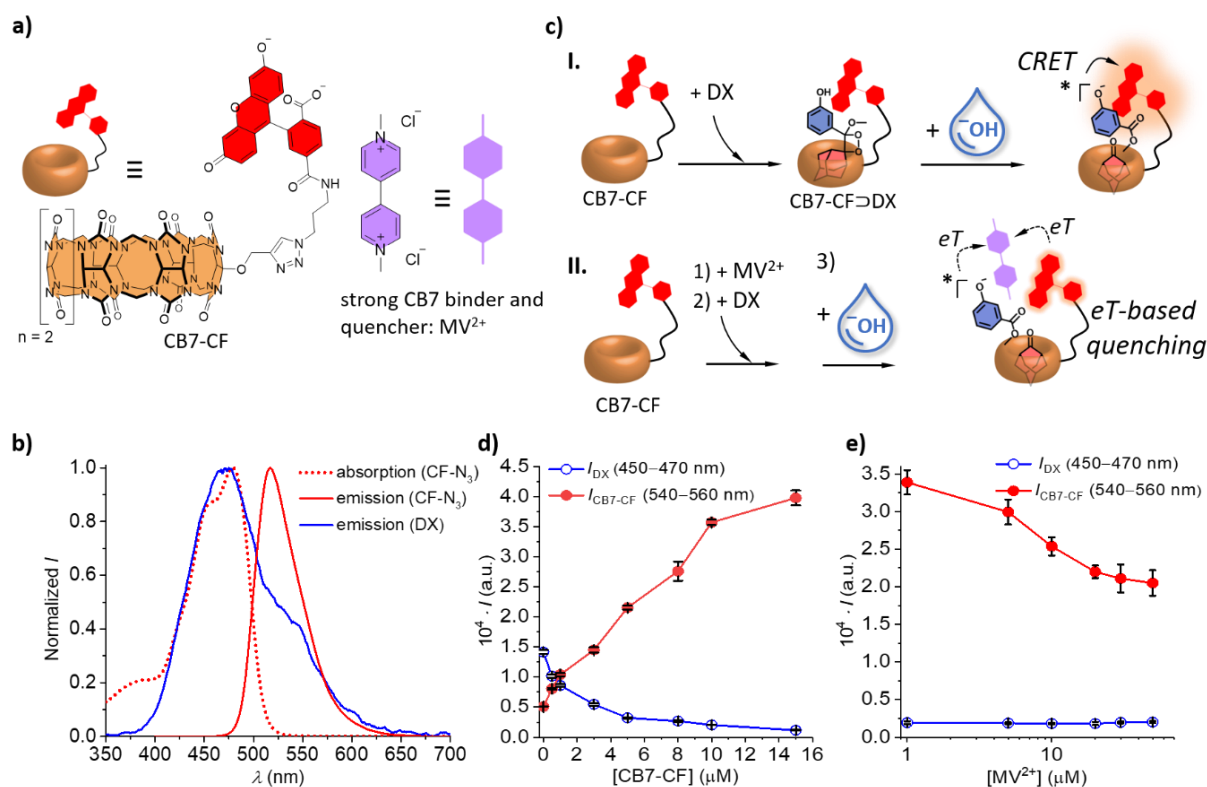
Figure 5.10 (a) Chemical structures of CB7-CF and MV^{2+}. (b) Normalized absorption ($\lambda_{abs,max}$ = 477 nm) and emission profiles of the acceptor dye CF-N$_3$ (λ_{ex} = 477 nm, $\lambda_{em,max}$ = 520 nm) in water. The normalized CL spectrum of DX at pH 9.6 in water is also shown. (c) Schematic representation of the binding mechanism and CRET process between DX and CB7-CF in the absence and presence of MV^{2+}. (d) CB7-CF-dependent CRET luminescence intensities with DX (10 μM in water containing 2.8 vol% DMSO, pH 9.6). (e) CRET luminescence intensities (DX = 10 μM and CB7-CF = 10 μM in water containing 2.8 vol% DMSO, pH 9.6) at different MV^{2+} concentrations. The average emission intensities and the corresponding standard deviation (σ) were calculated from five replica measurements.

of DX was also seen (Figure 5.10d). The importance of CB7-CF as an anchor point for the binding of DX was further confirmed by the control experiment in which the dye CF-N$_3$ and DX were investigated for CRET (the same protocol was followed) and a lower CRET intensity of 50% was observed compared to the CB7-CF study (see Figure 5.39a in supplementary data).

5.2.7. CRET-based detection of methyl viologen

Next, I studied the potential of the developed CRET process to detect methyl viologen (MV^{2+}, log $K_{a,CB7}$ = 7.4 in water, Figure 5.10a),[178] a herbicide known to cause Parkinson's disease.[244] The CRET experiments were conducted in MV^{2+}-spiked water samples (pH 6.0) (see 5.4.6. in experimental details for the CRET assay procedure). Notably, it was observed that the increasing concentrations of MV^{2+} (0 – 50 μM) resulted in quenching of the CRET signal (Figure 5.10e). Therefore, micromolar detection of MV^{2+} is possible in aqueous solutions using the developed CRET-based chemosensor. In this case, MV^{2+} likely functions as an electron

transfer (eT) quencher for DX and CB7-CF (Figure 5.10c, II).[245, 246] Evidence for eT quenching of DX by MV^{2+} was investigated by adding MV^{2+} to a premix of DX and CF-N$_3$ solution in water (pH 9.6), which resulted in a partially quenched CL (see Figure 5.39b in supplementary data). In addition, this control experiment suggests that the detection of MV^{2+} was not possible with DX and CF-N$_3$. Another control test was carried out, where a strongly binding CB7 guest amantadine (log $K_{a,CB7}$ = 12.6)[247] was added to a CB7-CF⊃DX containing solution. Here, amantadine is not expected to play a role in eT quenching. In this case, it was observed that the CL signal of DX was not quenched (see Figure 5.40 in supplementary data), although DX is displaced by amantadine from the CB7 cavity. The observed CRET in this case is due to the formation of aggregates between CB7-CF and DX. These formed aggregates are similar to the case observed when CF-N$_3$ and DX were analyzed. These results also support the electron transfer quenching property of MV^{2+}.

5.2.8. Current limitations and performance of the CCS assay

The limit of detection (LOD) of Mem and Nan in PBS, human urine, and deproteinized human serum was calculated from the linear-response range of the obtained CCS calibration curve (see section 5.4.7. in experimental details and Figures 5.41 and 5.42 in supplementary data). The determined LOD values are provided in Table 5.1. Other studies, such as fluorescent-based CB*n* chemosensors reported the detection of Nan (0 – 43.2 µM) in PBS[248] and Mem (0 – 2 µM) in spiked human serum.[237] Using CCS assay, Mem and Nan can be detected in the micromolar concentration range. At present, the developed CCS assay is restricted to detecting drugs like Mem and Nan that have high binding affinities for CB8.

Table 5.1 LODs for the detection of Mem and Nan in PBS, urine, and serum samples.

	Mem (µM)	Nan (µM)
PBS	0.4	0.8
urine	0.6	3.9
serum	3.2	11

To reduce the effect of autofluorescence background signal in the case of fluorescent chemosensors, experiments require a sensitive fluorimeter and 3 mL cuvettes. Notably, a microplate reader can be utilized to execute the CCS assay in a high-throughput and low-volume format, even in human urine and human serum, due to the efficient autofluorescence background elimination.

In addition, I performed recovery studies using Mem-spiked urine samples from three healthy voluntary donors to understand the CCS assay under the impact of the matrix-to-matrix effect (see section 5.4.7. in experimental details). The CCS assay showed good recoveries (>80%) in all the tested samples (Table 5.2).

For the validation of the CCS assay, an IDA reported for Mem in biofluids was employed (see section 5.4.7. in experimental details).[237] The validation results (Table 5.3) yielded comparable analyte concentration values to those obtained in IDA (see Figure 5.43 in supplementary data for corresponding calibration curves of IDA and CCS).

Table 5.2 Calculated recoveries for urine-spiked samples from different donors using the CCS assay.

spiked conc. [µM]	observed conc. [µM]	recovery
urine donor 1		
1.0	1.3 ± 0.1	130%
2.0	1.7 ± 0.1	85%
4.0	3.9 ± 0.4	97%
5.0	4.7 ± 0.1	94%
7.0	7.2 ± 0.2	103%
urine donor 2		
1.0	0.9 ± 0.1	90%
2.0	2.2 ± 0.2	110%
4.0	3.7 ± 0.7	92%
5.0	5.5 ± 0.6	110%
7.0	6.2 ± 0.1	88%
urine donor 3		
1.0	1.1 ± 0.4	110%
2.0	2.7 ± 0.2	135%
4.0	3.3 ± 0.2	82%
5.0	4.9 ± 0.5	98%
7.0	7.4 ± 0.3	106%

Table 5.3 Results of the validation of the CCS assay with the previously reported IDA assay.

spiked conc. [μM]	observed conc. [μM]		recovery	
	IDA	CCS	IDA	CCS
1.0	0.8 ± 0.1	1.3 ± 0.1	80%	130%
2.0	1.7 ± 0.1	1.7 ± 0.1	85%	85%
4.0	3.8 ± 0.1	3.9 ± 0.3	95%	97%
7.0	6.9 ± 0.2	7.2 ± 0.2	98%	103%

5.3. Conclusion

In conclusion, a novel chemiluminescent cucurbit[*n*]uril-based chemosensor was successfully developed and applied for the detection of analytes in saline media and biofluids. Specifically, the chemosensor was able to detect the Alzheimer's drug memantine and the anabolic steroid nandrolone in biofluids such as human urine and human serum at a low micromolar concentration regime. Moreover, the potential of cucurbit[8]uril to function as a non-surfactant chemiluminescent enhancer of phenoxy 1,2-dioxetanes was described. These findings can be adapted to existing dioxetane-based chemiluminescent assays to enhance the performance of the assay. In addition, combining dioxetane with cucurbit[7]uril-dye conjugate enabled the design of a chemiluminescence resonance energy transfer-based assay, which was confirmed by the detection of methyl viologen, a known herbicide responsible for causing Parkinson's disease. The herein-developed chemiluminescent assay circumvents the problems associated with other optical chemosensors which require an excitation light source for sample irradiation. It appears promising that this proposed sensing approach may find applications in diagnostic laboratories or point-of-care use.

5.4. Experimental details

5.4.1. Materials and methods

All purchased chemicals and solvents were used as received from suppliers without any further purification. DCM was collected following standard protocols for solvent drying and was stored over molecular sieves (3 Å) to ensure aridity over long periods. 2,7-dimethyldiazapyrenium diiodide (MDAP)[249] and *N*-methyl-4-pyridinylium[2.2]paracyclophane (MPCP)[237] were synthesized according to established literature methods. The 10 mM PBS buffer (137 mM NaCl, 2.7 mM KCl, 10 mM Na_2HPO_4 and 1.8 mM KH_2PO_4) was prepared from Gibco PBS tablets and Milli-Q water. The pH of the PBS solution was adjusted to pH 6.0 by adding diluted HCl. All experiments with CDP-Star and ALP were performed in a 10 mM TRIS buffer solution containing $MgSO_4$ (1 mM) at pH 9.0.

Urine samples were provided by three healthy volunteers and were used within 3 – 4 days after excretion (the urine was stored in the fridge at 4 °C). The collected urine was further diluted (1:1) with 10 mM PBS (pH 6.0) and the pH value was adjusted to pH 6.0 by adding diluted HCl for CL measurements.

Human serum normal (chemicon) was purchased from Merck and used in a deproteinized form. The deproteinization was performed according to a reported perchloric acid-based protein precipitation procedure.[250] The CL measurements were performed in 1:3 dilutions of the deproteinized human serum with 10 mM PBS (after perchloric acid-based deproteinization, the pH of the serum sample was adjusted to pH 6.0).

CB7[251] and CB8[163] were prepared by following reported literature examples and also purchased from Strem or Sigma. Stock solutions of CB8, CB7, and analytes (Mem, Nan) were prepared in Milli-Q water.

The concentration of MDAP, BC, MPCP, and Nan stock solutions was determined according to their molar absorption coefficients (MDAP: $\varepsilon = 7800 \ M^{-1}cm^{-1}$ at 393 nm, BC: $\varepsilon = 22300 \ M^{-1}cm^{-1}$ at 344 nm, MPCP: $\varepsilon = 7111 \ M^{-1}cm^{-1}$ at 335 nm, Nan: $\varepsilon = 15320 \ M^{-1}cm^{-1}$ at 248 nm)[237, 248] by UV-Vis absorption titration measurements in Milli-Q water. The concentration of CB8, CB7, Mem, and amantadine stock solutions were determined by fluorescence titration against a known concentration of MPCP dye (λ_{ex} = 368 nm and λ_{em} = 531 nm), MDAP dye (λ_{ex} = 339 nm and λ_{em} = 452 nm), CB8⊃BC$_2$ receptor complex (λ_{ex} = 462 nm and λ_{em} = 548 nm) and CB7⊃MDAP receptor complex (λ_{ex} = 339 nm and λ_{em} =

452 nm), respectively, in Milli-Q water. The stock solution of DX was prepared in DMSO due to its low solubility and chemical instability in water.

All the experiments involving human participants (urine sample collection from healthy voluntary donors) were in accordance with the formal statement of ethical principles published by the World Medical Association in the Declaration of Helsinki in 1964 and its later amendments or comparable ethical standards.[252, 253] Informed consent was obtained from all individual participants included in the study.[254, 255]

5.4.2. Instrumentation

Nuclear magnetic resonance (NMR) spectroscopy

^{1}H and ^{13}C NMR spectra were recorded in CDCl$_3$ or D$_2$O on a Bruker Advance 500 spectrometer at 25 °C. The chemical shifts (δ) are given in ppm and refer to residual protons on the corresponding deuterated solvent. For the characterization of symmetric signals, the median point of the signal was chosen and for multiplets, the signal range was used. The multiplicities of the signals were abbreviated as follows: s = singlet, d = doublet, t = triplet, m = multiplet. All coupling constants (J) are stated as modulus in Hertz (Hz).

Infrared (IR) spectroscopy

IR spectra were recorded on a Thermo Scientific Nicolet iS50 spectrometer. Samples were measured in the wavelength range from 4000 cm^{-1} to 400 cm^{-1} upon direct deposition of the pure compounds.

Electrospray ionization mass spectrometry (ESI-MS)

Mass spectra were recorded on a Bruker microOTOF-Q (208–320 Vac, 50/60 Hz, 1800 VA). A trace amount of the sample was dissolved into 1 mL MeOH or MeOH/EtOAc and then treated in an ultrasound bath for 30 s. All MS spectra were collected in the positive mode in the mass range m/z 100 – 2000. Optimized parameters are as follows: dry temperature: 100 °C, dry gas: 3.0 L/min, ion energy: 5.0 eV, collision energy: 10.0 eV, collision RF: 800 Vpp, transfer time: 120 μs, prepulse storage: 10 μs.

UV-Vis absorption spectroscopy

Absorbance spectra were measured at 25 °C in Milli-Q water on a Jasco V-730 double-beam UV-Vis spectrophotometer. For UV-Vis absorption experiments, PMMA cuvettes with a light

path of 10 mm and dimensions of 10 × 10 mm and a spectroscopic cut-off at 220 nm were utilized. In addition, the cuvettes were equipped with a magnetic stirrer, allowing rapid mixing.

Fluorescence spectroscopy

Steady-state emission spectra and time-resolved emission profiles for the titration experiments were recorded on a Jasco FP-8300 fluorescence spectrometer equipped with a 450 W Xenon arc lamp, double-grating excitation, and emission monochromators. Emission spectra were corrected for source intensity (lamp and grating) and the emission spectral response (detector and grating) by standard correction curves. All titration and kinetic experiments were carried out at 25 °C by using a water thermostatic cell holder STR-812, while the cuvettes were equipped with a magnetic stirrer, allowing rapid mixing. For fluorescence-based titration experiments and CRET measurements, PMMA cuvettes with a light path of 10 mm and dimensions of 10 × 10 mm from Brand with a spectroscopic cut-off at 300 nm were utilized.

Chemiluminescence spectroscopy

Time-resolved CL profiles were recorded on a CLARIOstar Plus microplate reader using the software-implemented luminescence method. No filter was used when collecting the CL spectra, and the gain was set to 4000. The measurement interval time was 1 s. Samples were prepared in a white Optiplate with 96 wells. The total volume of the sample in a well was 200 µL. All measurements were carried out at 25 °C.

5.4.3. Synthesis and characterization of DX

All reactions were carried out under a nitrogen (N$_2$) atmosphere. The round-bottom flasks used in the reactions were dried using a heat gun (250 °C) while purging with N$_2$ before use.
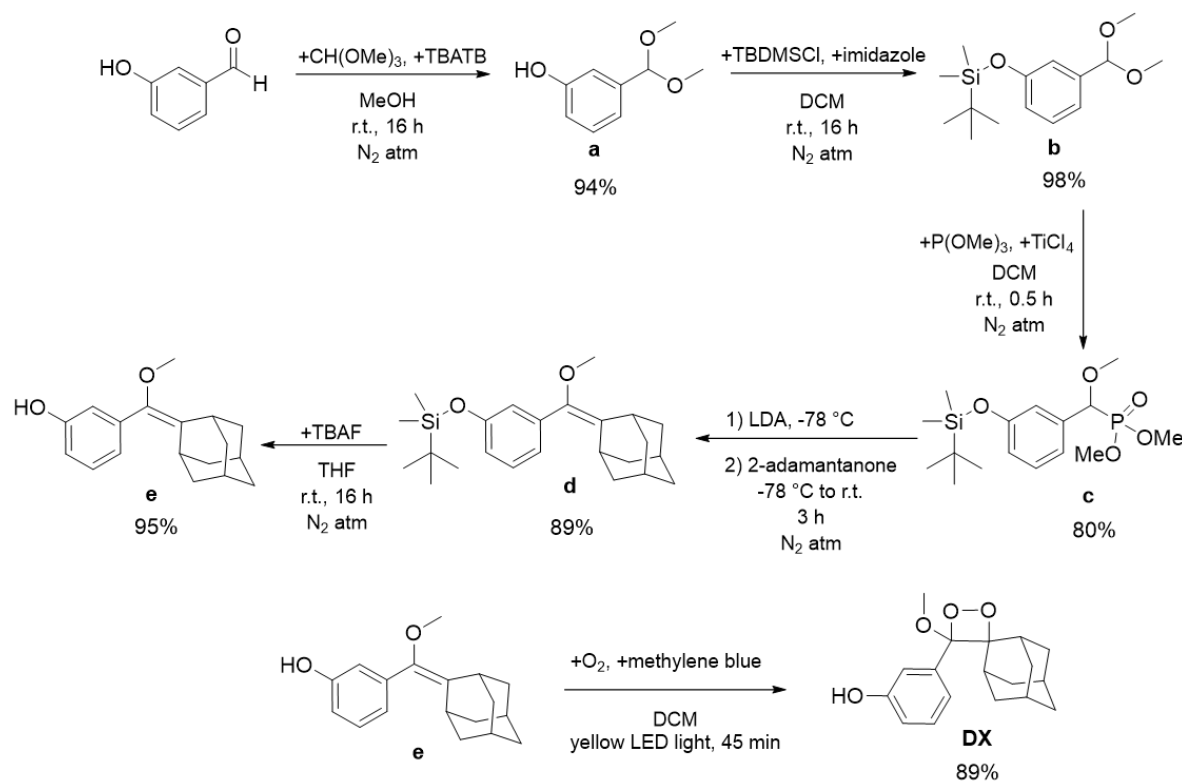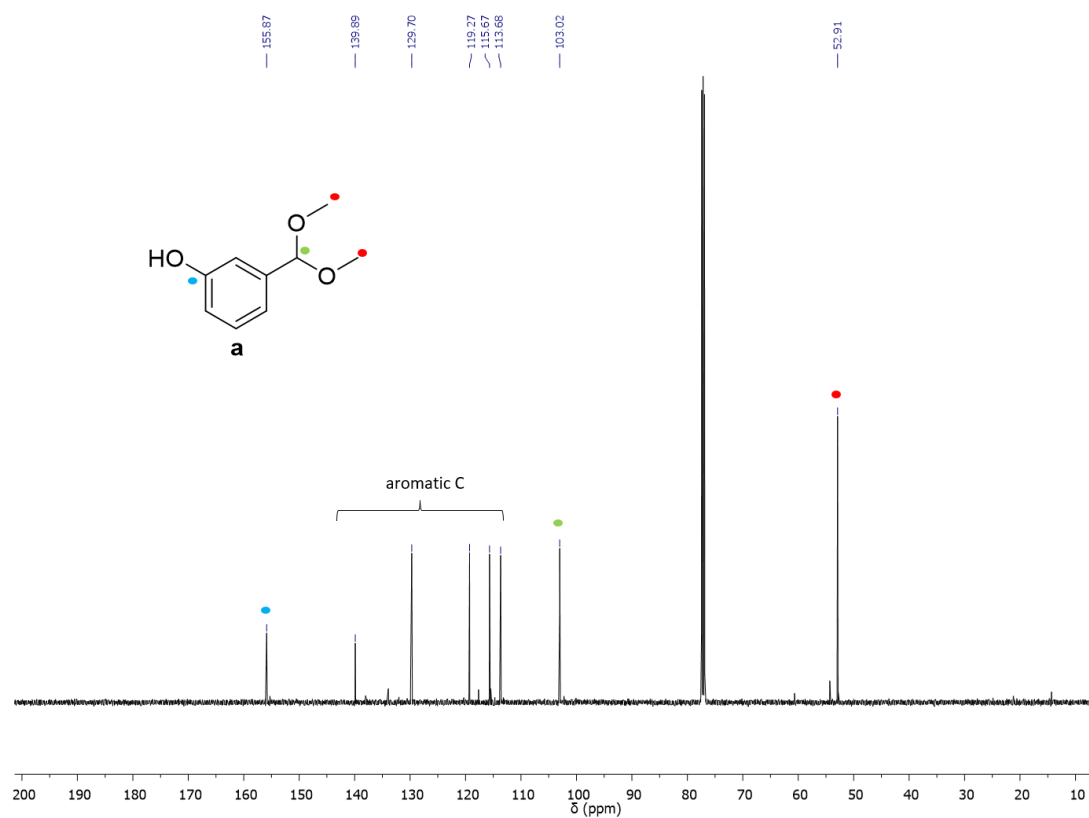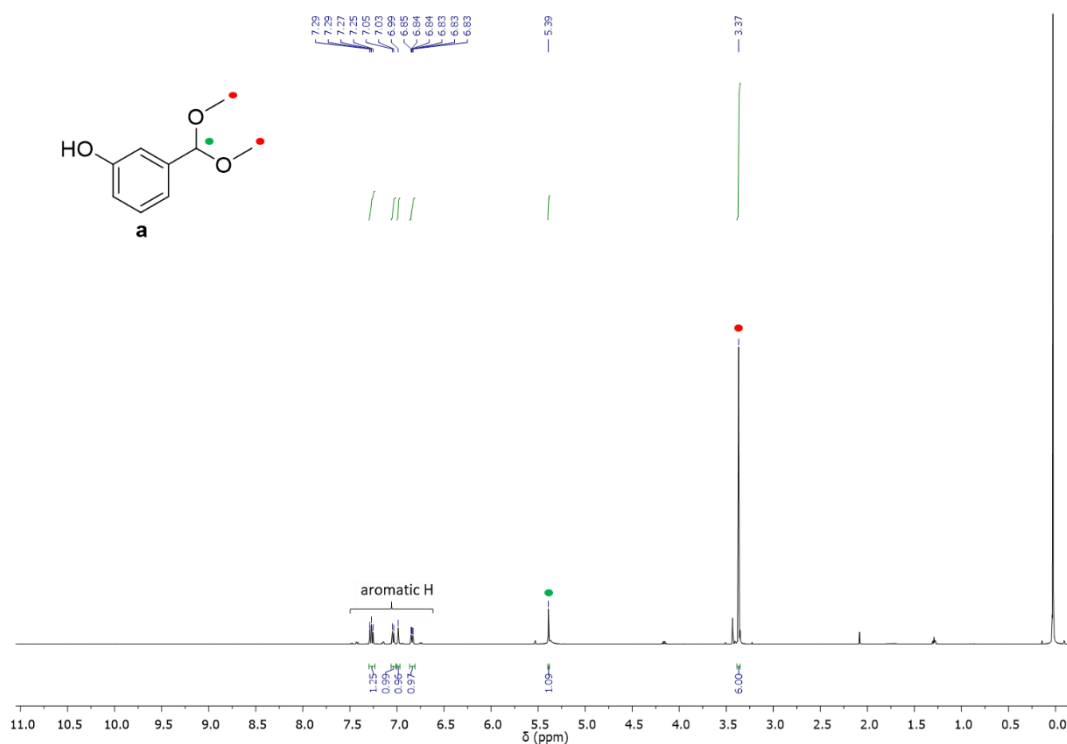

Figure 5.11 Reaction scheme for the synthesis of DX.

Synthesis of 3-(dimethoxymethyl)phenol (a). In a round-bottom flask equipped with a magnetic stirrer, 3-hydroxybenzaldehyde (1.00 g, 8.19 mmol) was dissolved in dry MeOH (10.0 mL). Subsequently, under stirring, trimethyl orthoformate (1.80 mL, 16.38 mmol) was added dropwise, followed by TBATB (0.20 g, 0.41 mmol) addition. The reaction mixture was allowed to stir for 16 h at room temperature. The organic solvent was removed under reduced pressure and the crude product was purified by column chromatography (silica gel, EtOAc/Hex 20:80 containing a few drops of TEA), yielding (**a**) as a colourless oil (1.3 g, yield = 94%). R$_f$ = 0.39.

^{1}**H NMR** (CDCl$_3$, 500 MHz) δ 7.29-7.25 (m, 1H), 7.04 (d, *J* = 10 Hz, 1H), 6.99 (s, 1H), 6.85-6.83 (m, 1H), 5.39 (s, 1H), 3.37 (s, 6H) ppm. ^{13}**C NMR** (126 MHz, CDCl$_3$) δ 155.87, 139.89, 129.70, 119.27, 115.67, 113.68, 103.02, 52.91 ppm. **IR** (ATR) *v* 3349 (-OH), 2940 (C-H in -

OCH$_3$), 2832 (aromatic C-H), 1592, 1454, 1267, 1192, 1168, 1155, 1100, 1037, 988, 865, 777, 697 cm^{-1}. **ESI-MS** m/z [M+Na]$^+$calcd for C$_9$H$_{12}$O$_3$Na 191.068; found 191.0668.

Figure 5.12 ^{1}H NMR spectrum (500 MHz) of **a** in CDCl$_3$.

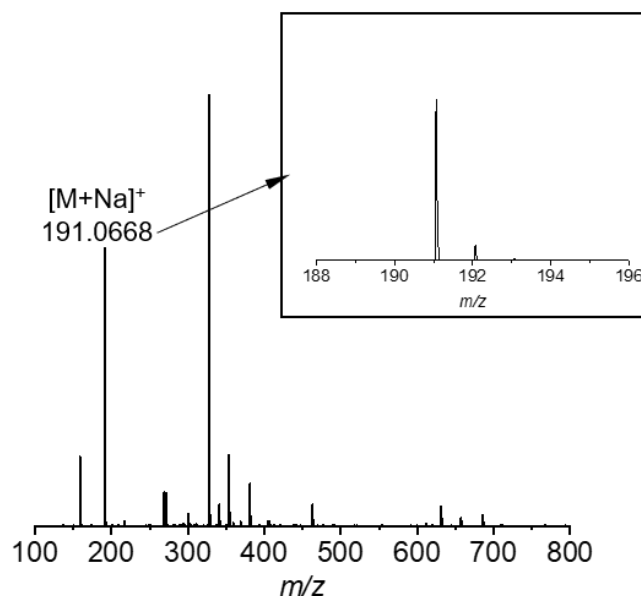**Figure 5.13** ^{13}C NMR spectrum (126 MHz) of **a** in CDCl$_3$.

Figure 5.14 ESI-MS spectrum of **a**.

Additional information on the synthesis and analysis is available in the Chemotion repository:

https://dx.doi.org/10.14272/reaction/SA-FUHFF-UHFFFADPSC-CJTUFUALQD-UHFFFADPSC-NUHFF-NUHFF-NUHFF-ZZZ

Synthesis of tert-butyl(3-(dimethoxymethyl)phenoxy)dimethylsilane (b). In a round-bottom flask equipped with a magnetic stirrer, (**a**) (2.00 g, 11.9 mmol) and imidazole (1.21 g, 17.8 mmol) were dissolved in dry DCM (20.0 mL). Subsequently, TBDMSCl (2.33 g, 15.5 mmol) was added, and the solution was stirred at room temperature for 16 h. The white precipitate formed was filtered off and the filtrate was concentrated under reduced pressure. The crude product was purified by column chromatography (silica gel, EtOAc/Hex 5:95), yielding (**b**) as a colourless oil (3.30 g, yield = 98%). R_f = 0.44.

1H NMR (CDCl$_3$, 500 MHz) δ 7.24-7.20 (m, 1H), 7.04 (d, *J* = 5 Hz, 1H), 6.94 (s, 1H), 6.80 (d, *J* = 10 Hz, 1H), 5.34 (s, 1H), 3.32 (s, 6H), 0.98 (s, 9H), 0.19 (s, 6H) ppm. **13C NMR** (CDCl$_3$, 126 MHz) δ 155.64, 139.63, 129.18, 120.10, 119.74, 118.48, 102.87, 52.65, 25.70, -4.41 ppm. **IR** (ATR) ν 2954 (C-H in -OCH$_3$), 2930, 2895, 2858, 2829, 1603, 1587, 1484, 1472, 1445, 1435, 1390, 1361, 1277, 1252, 1192, 1171, 1155, 1102, 1079, 1053, 1004, 976, 889, 857, 837, 808, 778, 741, 695, 679 cm^{-1}. **ESI-MS** m/z [M+Na]$^+$ calcd for C$_{15}$H$_{26}$O$_3$SiNa 305.1548; found 305.1500.
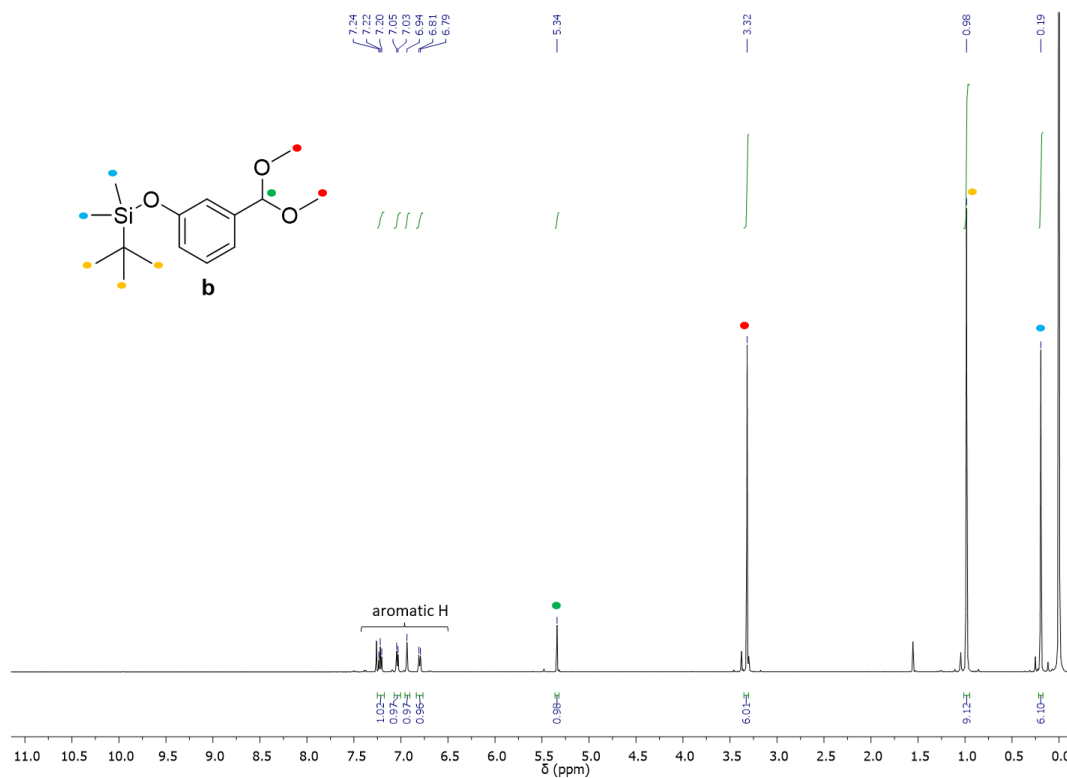
Figure 5.15 ^{1}H NMR spectrum (500 MHz) of **b** in CDCl$_3$.
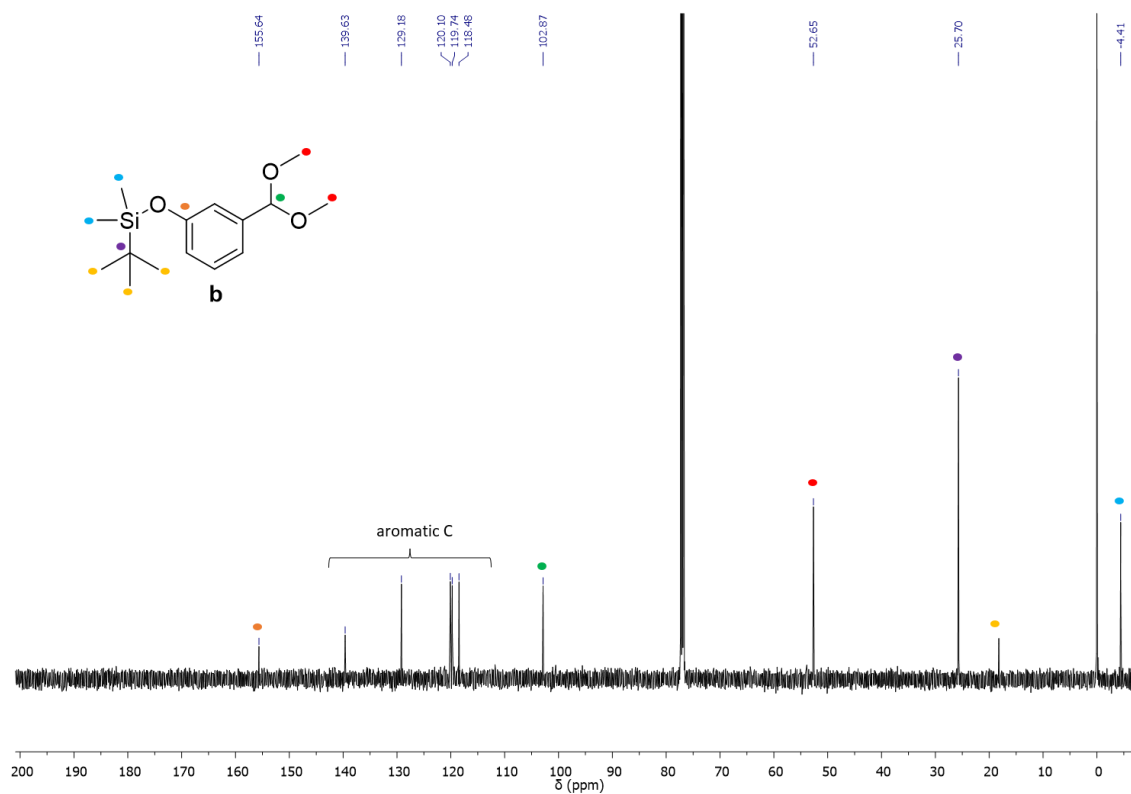

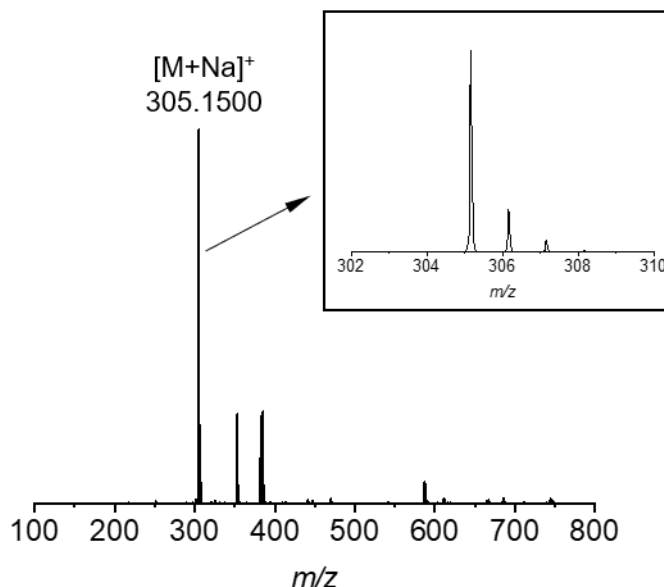**Figure 5.16** ^{13}C NMR spectrum (126 MHz) of **b** in CDCl$_3$.

Figure 5.17 ESI-MS spectrum of **b**.

Additional information on the synthesis and analysis is available in the Chemotion repository:

https://dx.doi.org/10.14272/reaction/SA-FUHFF-UHFFFADPSC-AOCDPIJDJV-UHFFFADPSC-NUHFF-NUHFF-NUHFF-ZZZ

Synthesis of dimethyl ((3-((tert-butyldimethylsilyl)oxy)phenyl)(methoxy)methyl)phosphonate (c). In a round-bottom flask equipped with a magnetic stirrer, (**b**) (1.00 g, 3.54 mmol) and trimethyl phosphite (0.63 mL, 5.31 mmol) were dissolved in dry DCM (20.0 mL). Subsequently, TiCl$_4$ (600 µL, 5.31 mmol) was added dropwise under stirring at 0 °C and further stirred after complete addition for 30 min at room temperature. Subsequently, the reaction mixture was poured into an ice-cold NaHCO$_3$ solution (15.0 mL, saturated). The aqueous mixture was extracted with DCM. The combined organic layers were dried over Na$_2$SO$_4$ and concentrated under reduced pressure. The crude product was purified by column chromatography (silica gel, EtOAc/Hex 70:30), yielding (**c**) as a colourless oil (1.02 g, yield = 80%). R$_f$ = 0.63.

^{1}H NMR (CDCl$_3$, 500 MHz) δ 7.25-7.22 (m, 1H), 7.01 (d, *J* = 5 Hz, 1H), 6.94 (s, 1H), 6.81 (d, *J* = 5 Hz, 1H), 4.48 (d, *J* = 15 Hz, 1H), 3.70 (d, *J* = 10 Hz, 3H), 3.66 (d, *J* = 10 Hz, 3H), 3.38 (s, 3H), 0.98 (s, 9H), 0.20 (s, 6H) ppm. **^{13}C NMR** (CDCl$_3$, 126 MHz) δ 155.88, 155.86, 135.59, 129.51, 129.49, 121.14, 121.09, 120.49, 120.46, 119.65, 119.60, 80.71, 58.66, 58.54, 53.68, 53.62, 25.69, 18.24, -4.45 ppm. **IR** (ATR) *v* 2945.78, 1276.64 (P-O), 1250.12, 1105.50, 984.48, 868.78 cm^{-1}. **ESI-MS** m/z [M+Na]$^+$calcd for C$_{16}$H$_{29}$O$_5$PSiNa 383.1419; found 383.1498
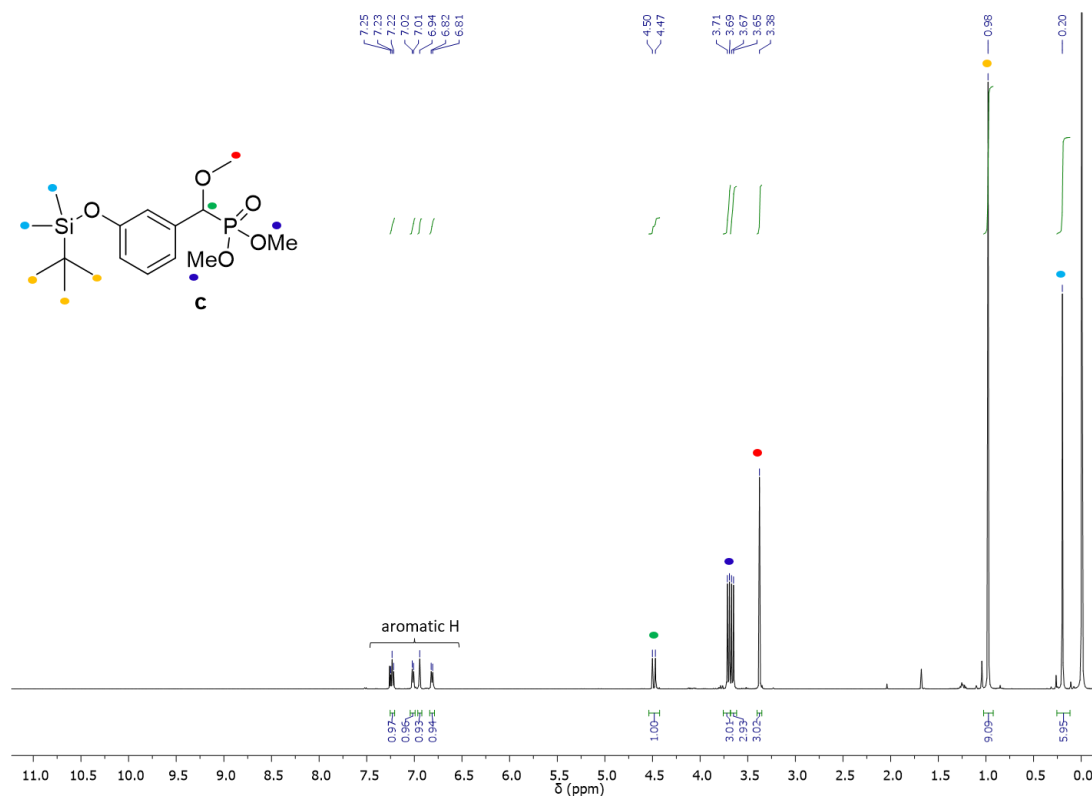
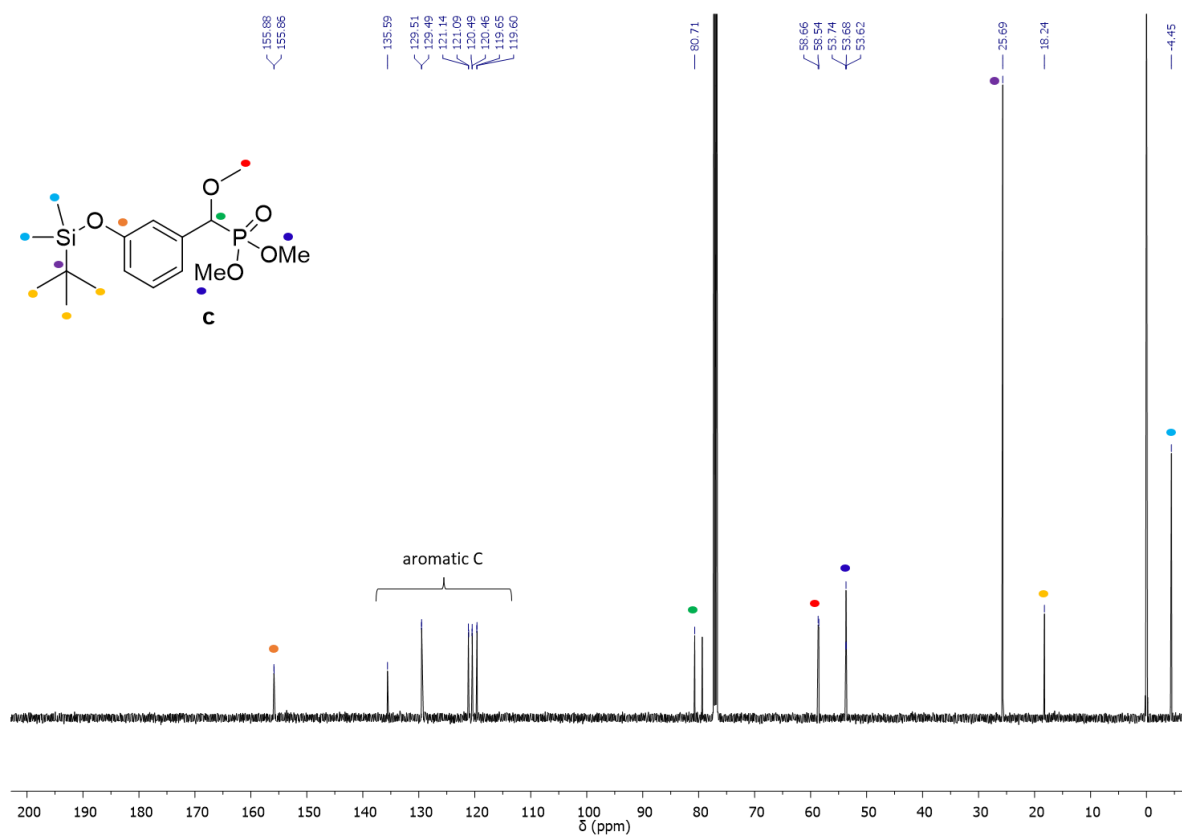**Figure 5.18** ^{1}H NMR spectrum (500 MHz) of **c** in CDCl$_3$.

Figure 5.19 ^{13}C NMR spectrum (126 MHz) of **c** in CDCl$_3$.
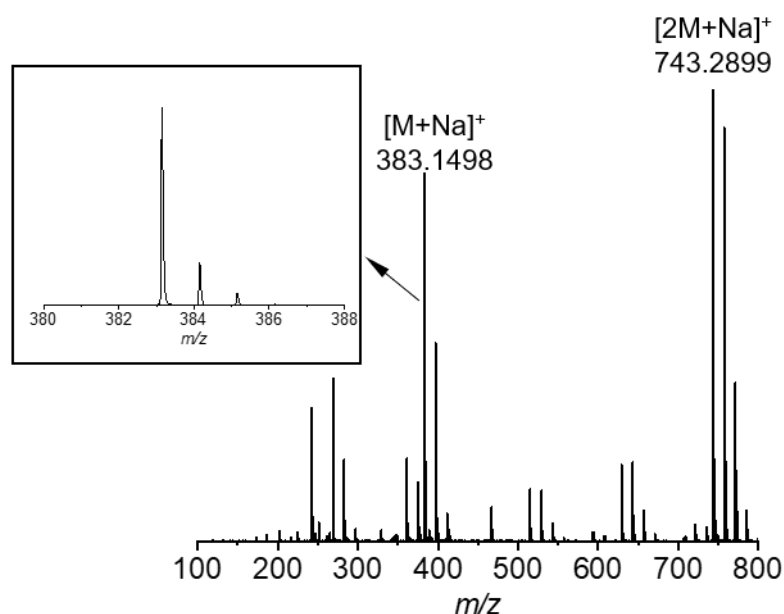
Figure 5.20 ESI-MS spectrum of **c**.

Additional information on the synthesis and analysis is available in the Chemotion repository:

https://dx.doi.org/10.14272/reaction/SA-FUHFF-UHFFFADPSC-KAJYJUIYDC-UHFFFADPSC-NUHFF-NUHFF-NUHFF-ZZZ

Synthesis of (3-((-adamantan-2-ylidene)(methoxy)methyl)phenoxy)(tert-butyl)dimethylsilane (d). In a round-bottom flask equipped with a magnetic stirrer, (**c**) (1.00 g, 2.77 mmol) was dissolved in dry THF (10.0 mL). LDA (2.00 M in THF, 2.00 mL, 14.74 mmol) was added dropwise at -78 °C under stirring and after complete addition, the reaction mixture was stirred for 30 min at -78 °C. Subsequently, 2-adamantanone (0.50 g, 3.33 mmol) dissolved in dry THF (10.0 mL) was added dropwise and the reaction mixture was further stirred for 30 min at - 78 °C and for an additional 3 h at 25 °C. The reaction mixture was poured into brine, and the aqueous mixture was extracted using EtOAc. The combined organic layer was dried over Na_2SO_4 and the organic solvent was evaporated under reduced pressure. The crude product was purified by silica gel column chromatography (EtOAc/Hex 5:95), yielding (**d**) as a colourless oil (0.95 g, yield = 89%). R_f = 0.64.

^{1}H NMR (CDCl$_3$, 500 MHz) δ 7.21-7.18 (m, 1H), 6.91 (d, J = 10 Hz, 1H), 6.80 (s, 1H), 6.80-6.76 (m, 1H), 3.29 (s, 3H), 3.24 (s, 1H), 2.63 (s, 1H), 1.97-1.78 (m, 12H), 0.98 (s, 9H), 0.20 (s, 6H) ppm. **^{13}C NMR** (CDCl$_3$, 126 MHz) δ 155.47, 143.49, 136.93, 131.40, 129.05, 122.68, 121.23, 119.48, 57.79, 39.34, 39.20, 37.37, 32.39, 30.47, 30.31, 28.50, 25.84, 18.38, -4.30 ppm. **IR** (ATR) v 2945.78, 1276.64, 1105.50, 868.78 cm^{-1}. **ESI-MS** m/z [M+Na]$^+$calcd for $C_{24}H_{36}O_2SiNa$ 407.2382; found 407.2371.
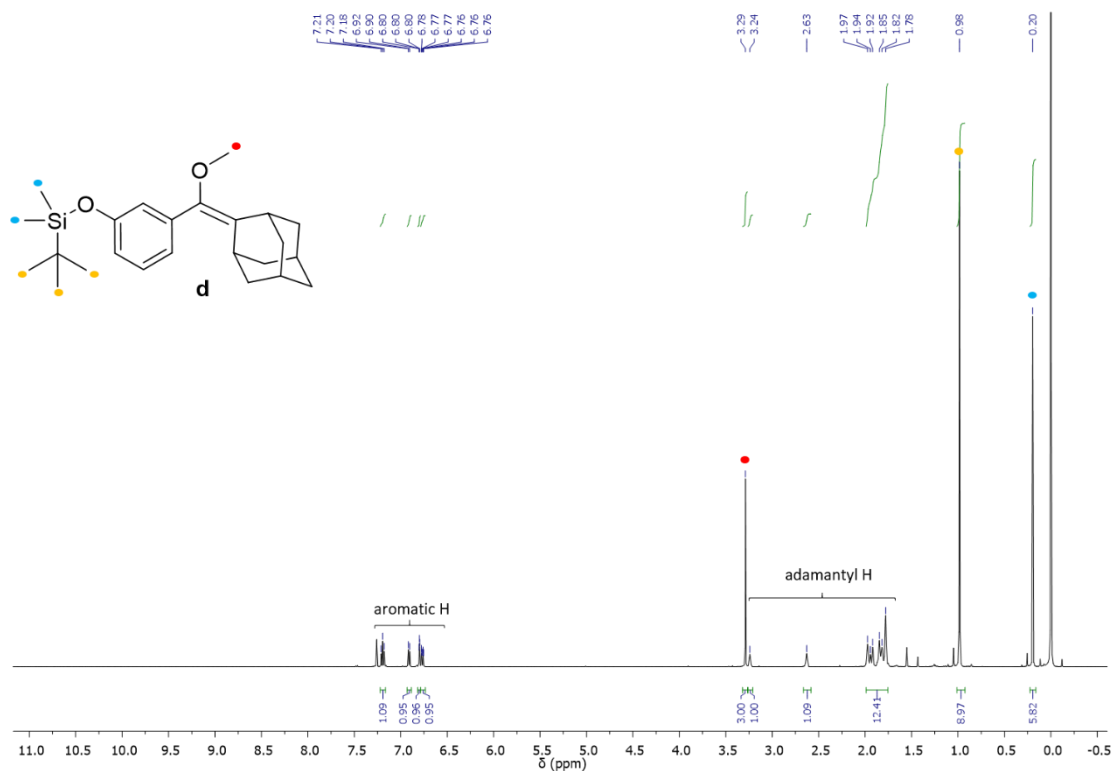
Figure 5.21 ^{1}H NMR spectrum (500 MHz) of **d** in CDCl$_3$.
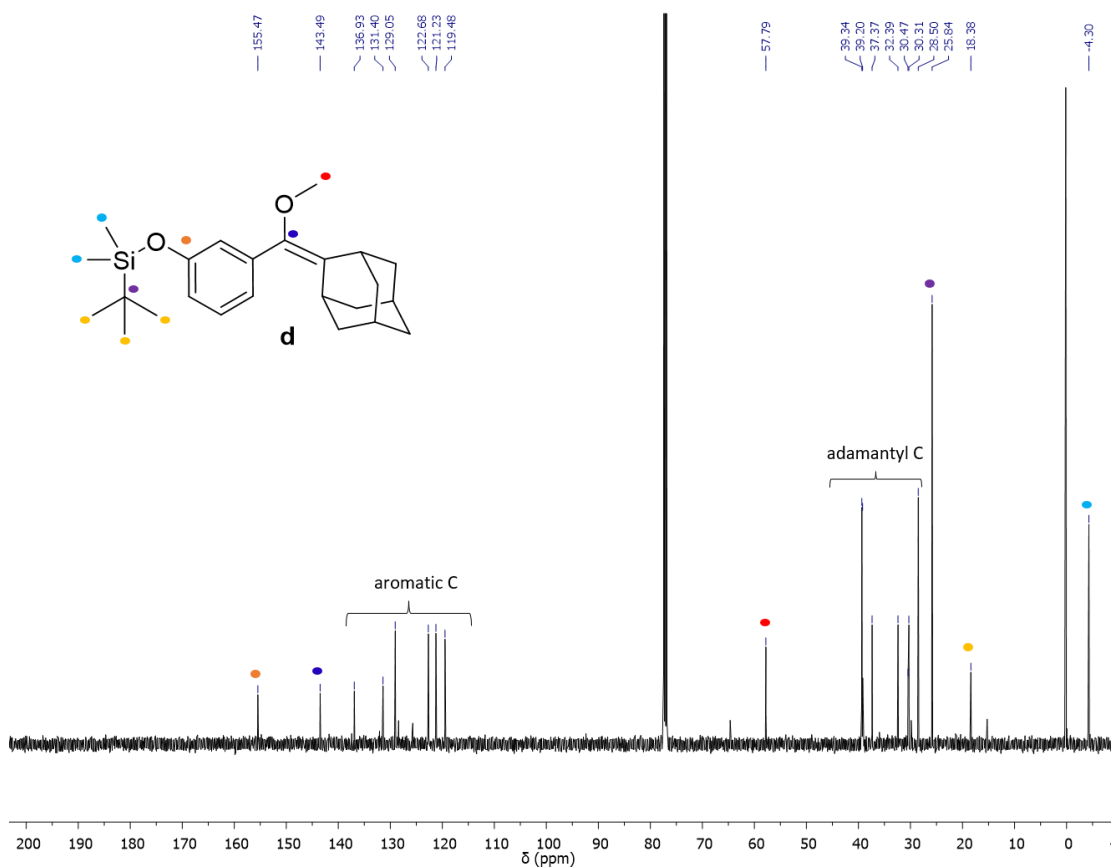

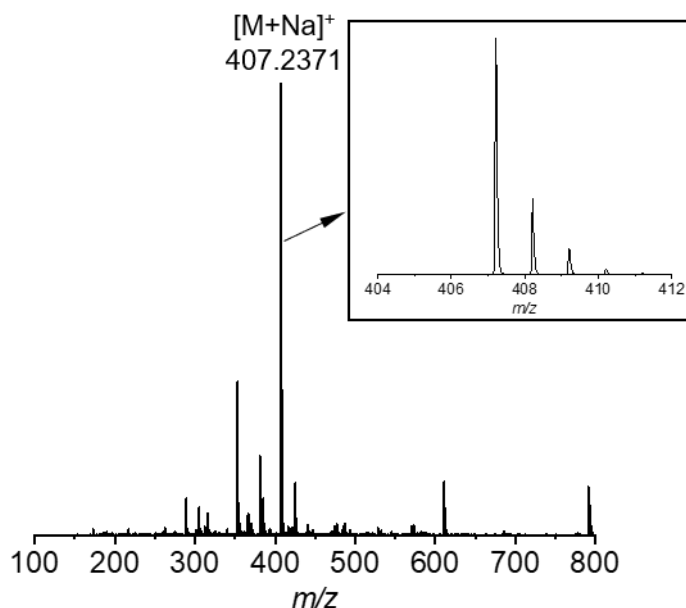**Figure 5.22** ^{13}C NMR spectrum (126 MHz) of **d** in CDCl$_3$.

Figure 5.23 ESI-MS spectrum of **d**.

Additional information on the synthesis and analysis is available in the Chemotion repository:
https://dx.doi.org/10.14272/reaction/SA-FUHFF-UHFFFADPSC-SVZAUCYKJS-UHFFFADPSC-NUHFF-NWIFF-NUHFF-ZZZ

Synthesis of 3-(adamantan-2-ylidene(methoxy)methyl)phenol (e). In a round-bottom flask, (**d**) (1.50 g, 3.90 mmol) and TBAF (1.00 M in THF, 4.50 mL, 4.50 mmol) were dissolved in dry THF (10.0 mL) and stirred for 16 h at room temperature. The organic solvents were evaporated under reduced pressure and the crude product was purified by column chromatography (EtOAc/Hex 15:85), yielding (**e**) as a white solid (1.00 g, yield = 95%). $R_f = 0.50$.

^{1}H NMR (CDCl$_3$, 500 MHz) δ 7.23-7.20 (m, 1H), 6.89 (d, J = 10 Hz, 1H), 6.81 (s, 1H), 6.77-6.75 (m, 1H), 4.87 (s,1H), 3.30 (s, 3H), 3.24 (s, 1H), 2.65 (s, 1H), 1.97-1.79 (m, 12H) ppm. **^{13}C NMR** (CDCl$_3$, 126 MHz) δ 155.34, 143.06, 137.17, 131.95, 129.16, 122.11, 116.02, 114.41, 57.78, 39.22, 39.08, 37.19, 32.23, 30.23, 28.32 ppm. **IR** (ATR) v 3344.49 (-OH), 2945.78, 1276.64, 1105.50, 868.78 cm^{-1}. **ESI-MS** m/z [M+Na]$^+$ calcd for C$_{18}$H$_{22}$O$_2$Na 293.1517; found 293.1461.
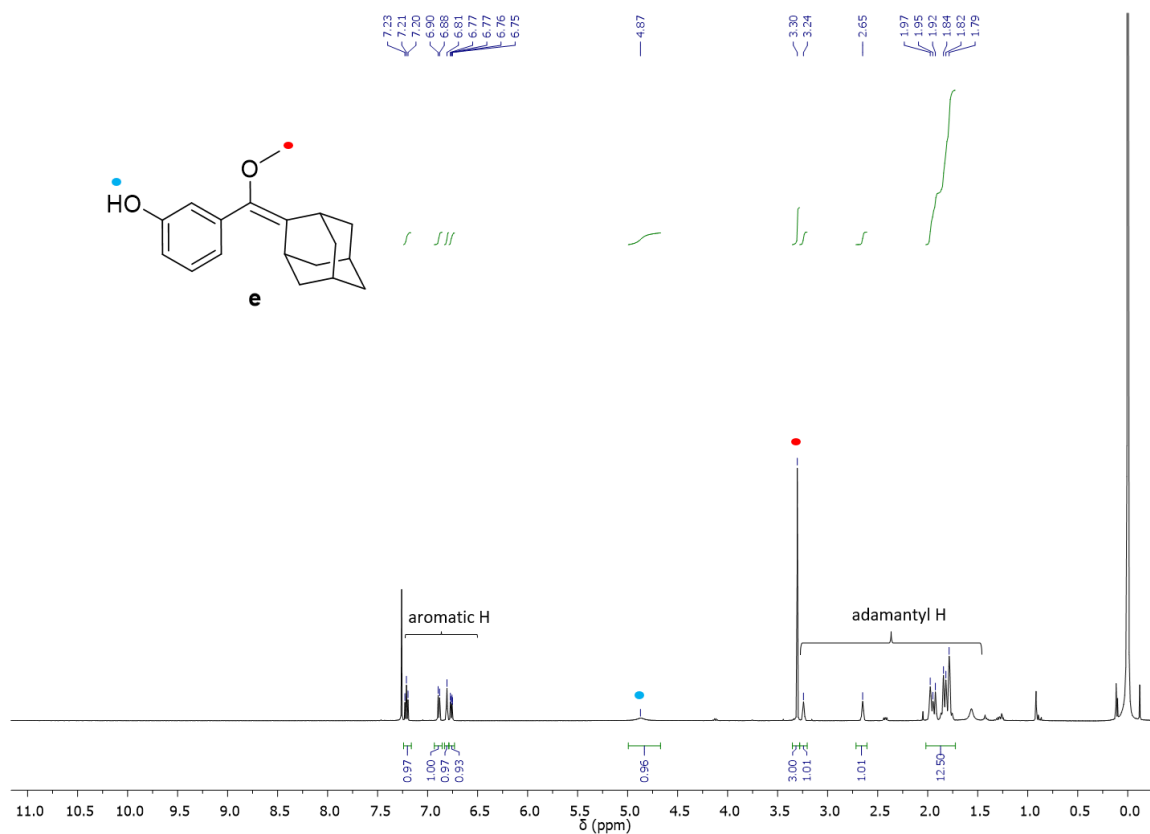
Figure 5.24 ^{1}H NMR spectrum (500 MHz) of **e** in CDCl$_3$.
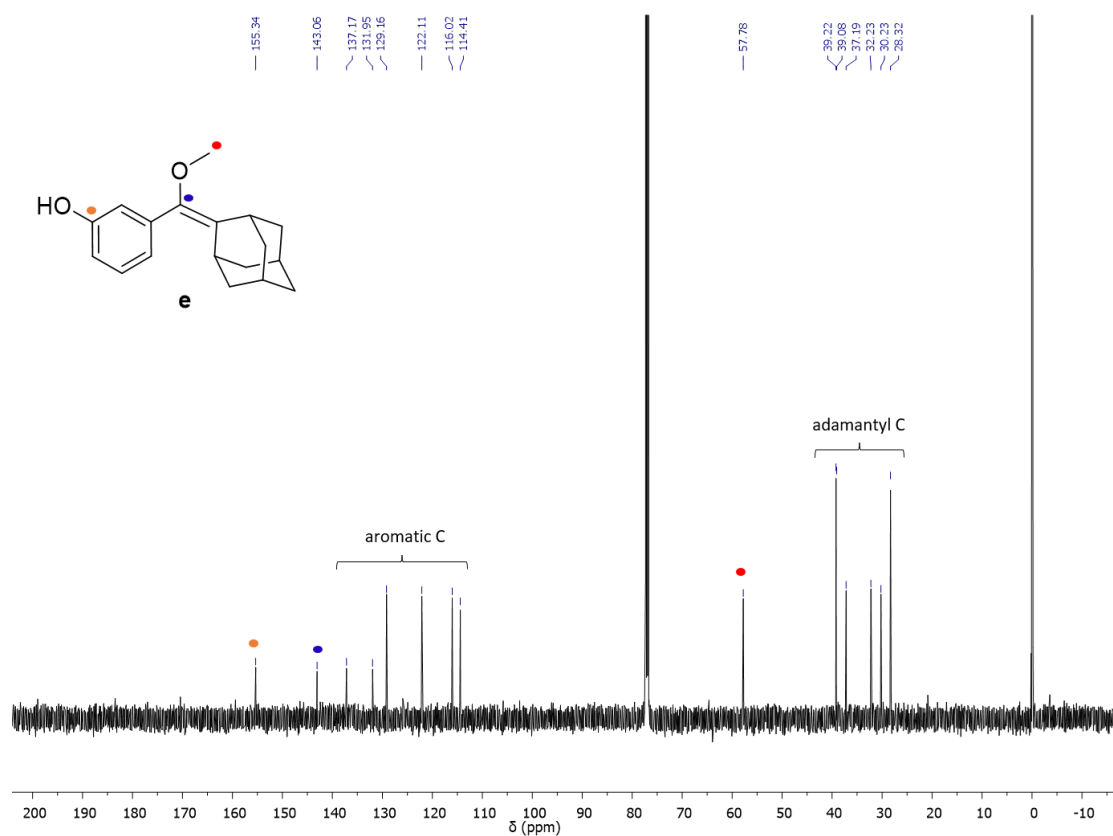

Figure 5.25 ^{13}C NMR spectrum (126 MHz) of **e** in CDCl$_3$.

Figure 5.26 ESI-MS spectrum of **e**.

Additional information on the synthesis and analysis is available in the Chemotion repository:

https://dx.doi.org/10.14272/reaction/SA-FUHFF-UHFFFADPSC-UOQZATKCYB-UHFFFADPSC-NUHFF-NYHMH-NUHFF-ZZZ

Synthesis of DX. In a round bottom flask, methylene blue (120 µL, 0.41 µM in dry DCM) was added to a solution of (**e**) (20.0 mg, 0.074 mmol) in dry DCM (5.00 mL). The reaction mixture was stirred and illuminated for 45 min using a 17 W LED lamp (2700 K) while pure O_2 was bubbled through the reaction mixture at room temperature. Subsequently, the reaction mixture was filtered through a minimal amount of silica to remove residual methylene blue, yielding a colourless filtrate. The organic solvent was removed under reduced pressure and the final product was obtained as a white solid (20.0 mg, yield = 89%). Compound **DX** is stored at - 20 °C under an inert atmosphere and in the dark to prevent its decomposition.

^{1}H NMR (CDCl$_3$, 500 MHz) δ 7.31-7.28 (m, 1H), 7.22-7.19 (m, 1H), 6.91-6.86 (m, 1H), 6.79-6.77 (m, 1H), 5.47 (s, 1H), 3.23 (s, 3H), 3.04 (s, 1H), 2.65 (s, 1H), 1.96-1.60 (m, 12H) ppm. **^{13}C NMR** (CDCl$_3$, 126 MHz) δ 155.86, 136.58, 129.67, 116.53, 112.11, 95.81, 50.11, 36.56, 34.87, 33.13, 32.49, 31.82, 31.70, 26.18, 26.05 ppm. **IR** (ATR) v 3408, 2912, 2857, 993 cm^{-1}. **ESI-MS** m/z [M+Na]$^+$ calcd for $C_{18}H_{22}O_4Na$ 325.1415; found 325.1403.
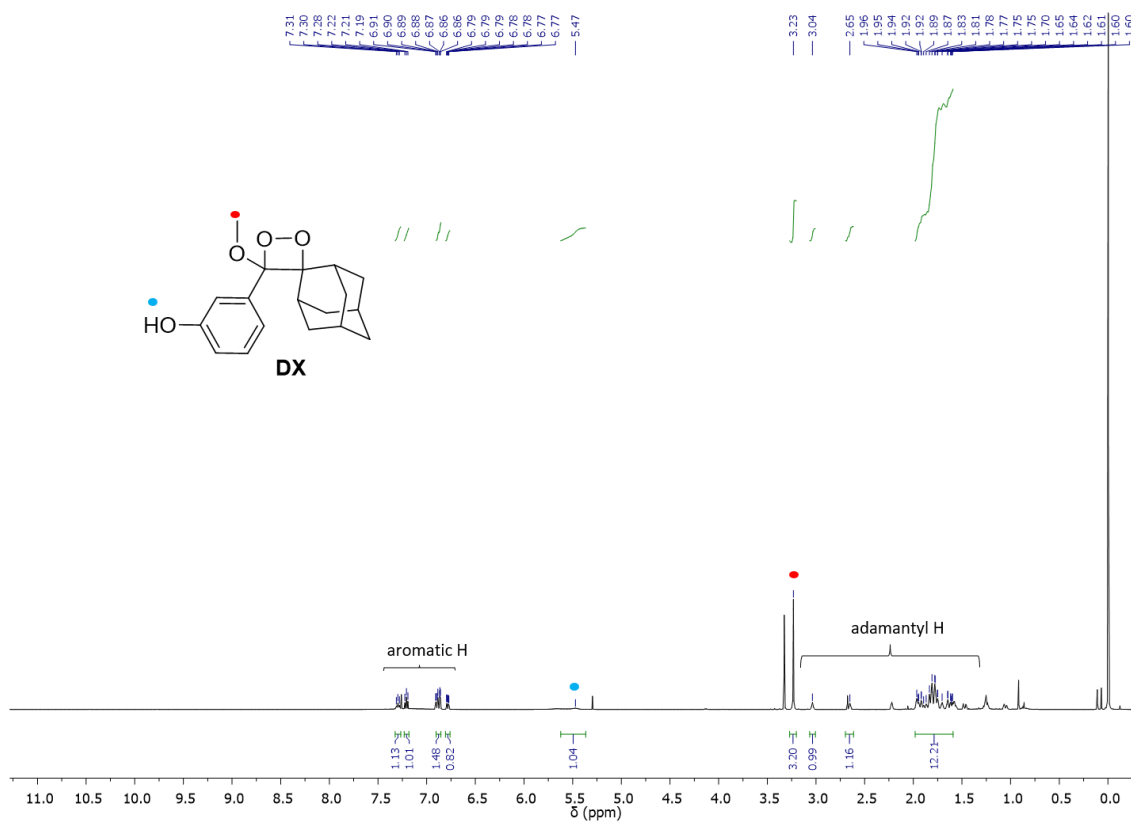
Figure 5.27 ^{1}H NMR spectrum (500 MHz) of **DX** in CDCl$_3$.

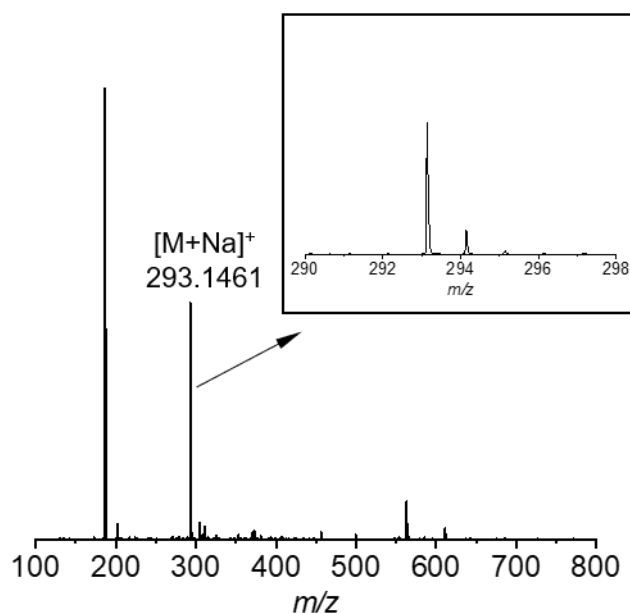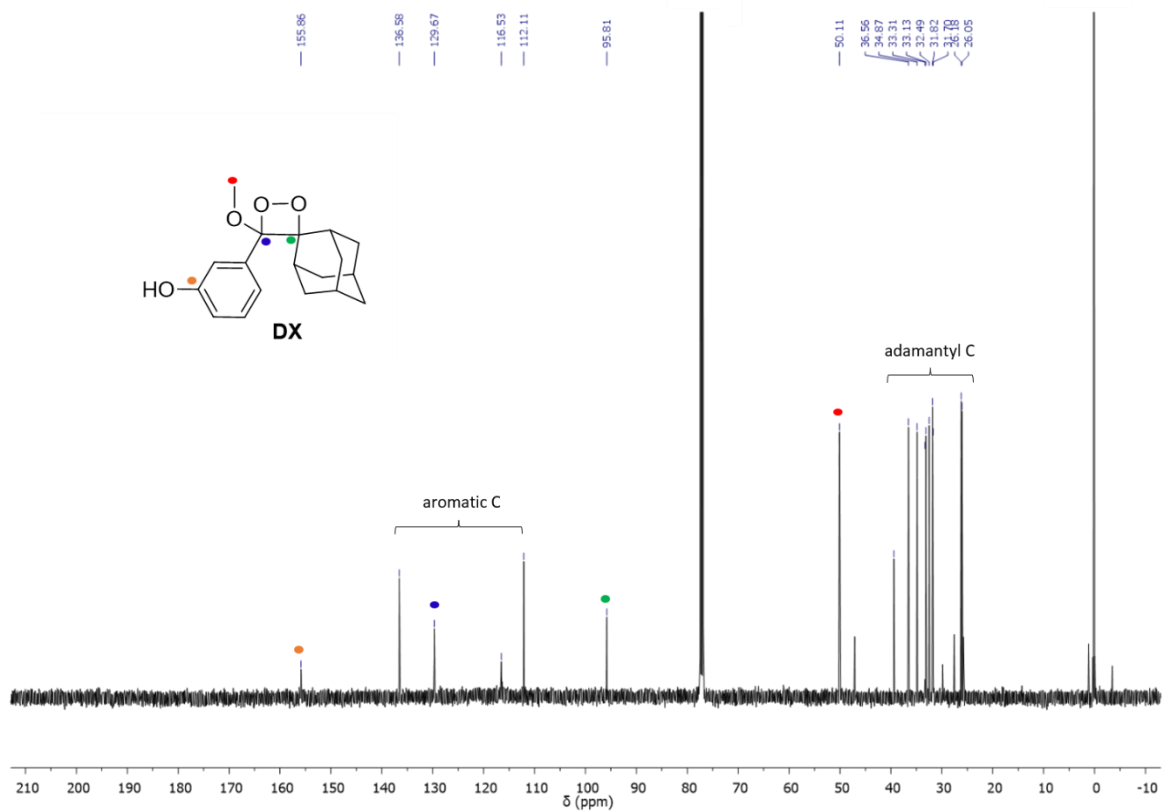**Figure 5.28** ^{13}C NMR spectrum (126 MHz) of **DX** in CDCl$_3$.
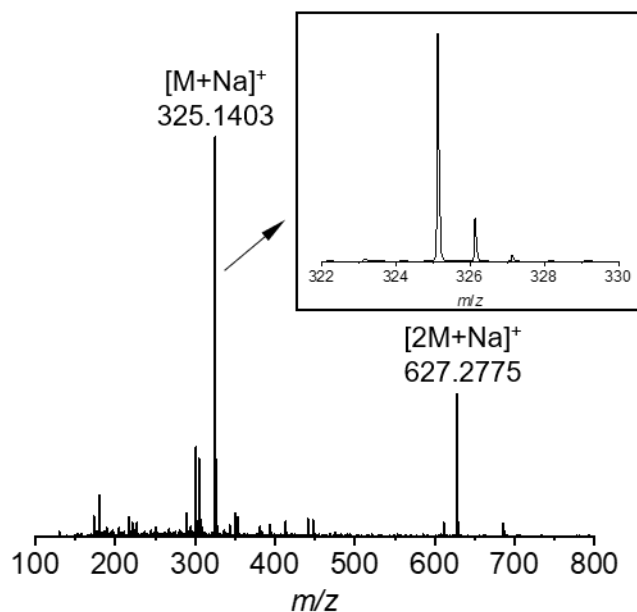
Figure 5.29 ESI-MS spectrum of **DX**.

Additional information on the synthesis and analysis is available in the Chemotion repository:

https://dx.doi.org/10.14272/reaction/SA-FUHFF-UHFFFADPSC-RVRTXMFVLY-
UHFFFADPSC-NUHFF-NUHFF-NUHFF-ZZZ

Figure 5.30 Overlapped IR spectra of **DX** (grey) and **e** (red) showing the characteristic peroxide band of **DX** at 950-1000 cm^{-1}

5.4.4. Synthesis and characterization of CB7-CF

Dr. Changming Hu carried out the synthesis of CB7-CF.

CB7-CF was prepared according to a previously reported procedure by Nau and co-workers.[193] The formation of CB7-CF was c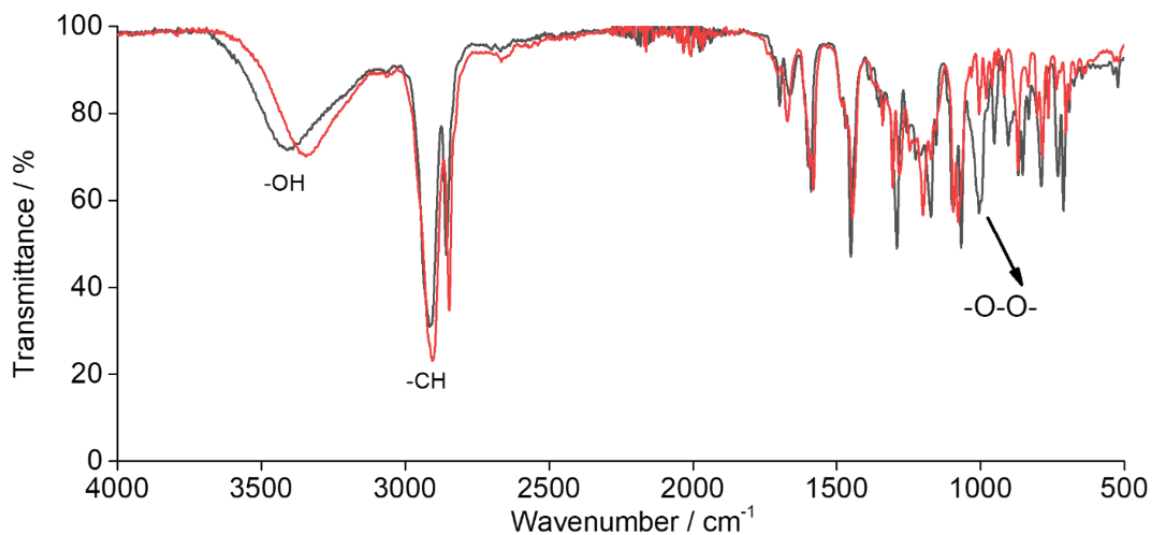onfirmed by mass spectrometry of its imidazole (C$_8$mim)[256] complex, CB7-CF⊃C$_8$mim (1:1): ESI-MS m/z [CB7-CF⊃C$_8$mim]$^{2+}$ calcd. for C$_{85}$H$_{90}$N$_{36}$O$_{21}$ 975.3540; found 975.7440.
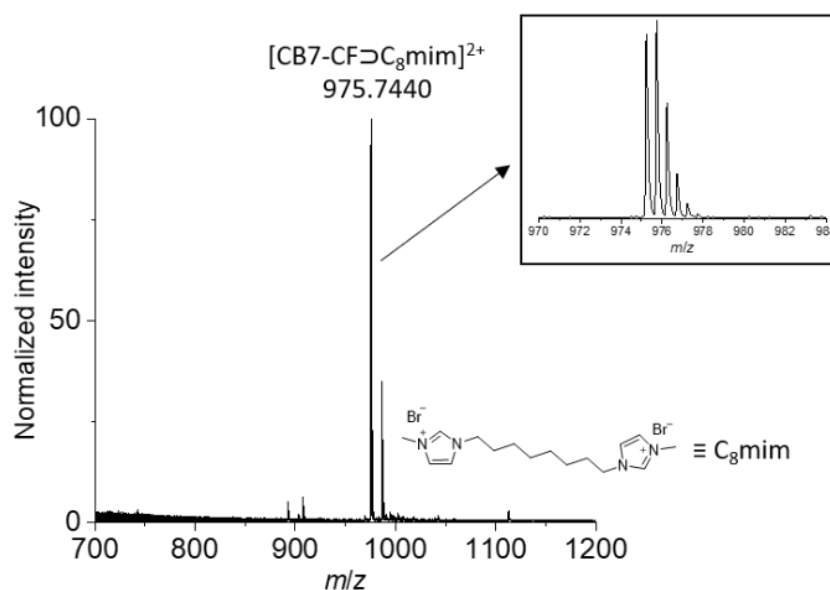
Figure 5.31 ESI-MS spectrum of CB7-CF⊃C$_8$mim (1:1).

5.4.5. Binding affinity studies

CB7⊃DX binding constant determination by IDA

The binding constant for CB7⊃DX was determined by IDA, following a reported procedure.[75] The binding isotherm is obtained by titrating a known concentration of DX stock solution to the CB7⊃BC complex (CB7 = 2.07 µM, BC = 4.0 µM) in water at 25 °C (λ_{ex} = 421 nm, λ_{em} = 542 nm) (see Figure 5.38 in supplementary data).

$$H + G \leftrightharpoons HG \qquad H + D \leftrightharpoons HD \tag{Eq. 1}$$

$$I_{em} = \alpha_{HD} \cdot [HD] + \alpha_D \cdot [D] \tag{Eq. 2}$$

$$K_a (HG) = [HG] / [H] \cdot [G]; \qquad K_a (HD) = [HD] / [H] \cdot [D] \tag{Eq. 3}$$

$$[G]_0 = [G] + [HG]; \qquad [D]_0 = [D] + [HD]; \tag{Eq. 4}$$

$$[H]_0 = [H] + [HD] + [HG] \qquad \text{Eq. 5}$$

The obtained binding isotherm was fitted to a binding model derived from Eq. 1–5 to obtain the binding constant ($K_{a, \text{CB7}}$). All numerical solutions were determined by using the Wolfram Mathematica software (https://github.com/ASDSE/thermosimfit).

CB8⊃DX binding constant determination by IDA

The binding constant was determined by an IDA using BC as the indicator in PBS (10 mM, pH 6.0), following a reported procedure.[237] The binding constant of CB8⊃BC$_2$ in PBS (pH 6.0) was determined by DBA with a binding model obtained from Eq. 6–10. In DBA, fluorescent titration of BC (2 µM) with increasing concentration of CB8 stock solution in PBS (10 mM, pH 6.0) at 25 °C ($\lambda_{\text{ex}} = 355$ nm, $\lambda_{\text{em}} = 536$ nm) was performed. The binding constant for CB8⊃DX was determined by titrating a known concentration of DX stock solution to the CB8⊃BC$_2$ complex (CB8 = 1.06 µM, BC = 6.01 µM) in PBS (10 mM, pH 6.0) at 25 °C ($\lambda_{\text{ex}} = 355$ nm, $\lambda_{\text{em}} = 536$ nm). See Figure 5.32 in supplementary data.

$$H + G \leftrightharpoons HG \quad\quad H + D \leftrightharpoons HD \quad\quad HD + D \leftrightharpoons HDD \qquad \text{Eq. 6}$$

$$I_{em} = \alpha_{HD} \cdot [HD] + \alpha_{HDD} \cdot [HDD] + \alpha_D \cdot [D] \qquad \text{Eq. 7}$$

$$K_a\,(HG) = [HG] / [H] \cdot [G]; \;\; K_a\,(HD) = [HD] / [H] \cdot [D]; \;\; K_a\,(HDD) = [HDD] / [HD] \cdot [D] \quad \text{Eq. 8}$$

$$[G]_0 = [G] + [HG]; \;\; [D]_0 = [D] + [HD] + 2[HDD]; \qquad \text{Eq. 9}$$

$$[H]_0 = [H] + [HD] + [HDD] + [HG] \qquad \text{Eq. 10}$$

The binding isotherm was fitted to a binding model derived from Eq. 7–10 to obtain the binding constant ($K_{a, \text{CB8}}$). All the numerical solutions were determined by using the Wolfram Mathematica software (https://github.com/ASDSE/thermosimfit).

5.4.6. Chemiluminescence experiments

CCS assay procedure

Analyte spiked (0 – 60 µM) PBS or human urine (1:1 diluted with 10 mM PBS, pH 6.0) or deproteinized human serum (1:3 diluted with 10 mM PBS, pH 6.0) was added to the wells of a 96-well white Optiplate. Followed by the addition of CB8 stock solution (30 µM), the mixture was left at room temperature for 5 min. Then, DX stock solution was added (30 µM) and the mixture was left at room temperature for another 10 min after mixing. The CL was induced by the addition of $NaOH_{aq}$ (10 mM, 10 µL) *via* the plate reader injector. The Optiplate was briefly shaken for 20 s using a plate reader built-in shaker. The total volume in each well was 200 µL and contained 2.5 vol% DMSO (from DX stock solution). The CL intensity (whole wavelength range) was recorded immediately after shaking.

CRET assay between DX and CB7-CF

To a solution of CB7-CF (0 – 15 µM in Milli-Q water, pH 6.0) filled in a 96-well white Optiplate, 10 µM of DX was added. The CL was triggered by adding $NaOH_{aq}$ (10 mM, 10 µL). After shaking for 20 s using a plate reader built-in shaker, luminescence intensities in the wavelength range of 450 – 470 nm (DX) and 540 – 560 nm (CB7-CF) were recorded. The total volume in each well was 200 µL and contained 2.8 vol% DMSO (from DX stock solution). The same procedure was followed for $CF-N_3$ and DX.

CRET assay in the presence of MV^{2+}

To MV^{2+}-spiked solutions (0 – 50 µM in Milli-Q water, pH 6.0) filled in a 96-well white Optiplate, 10 µM of CB7-CF stock solutions was added. The mixture was left at room temperature for 2 – 3 min. To this, 10 µM DX was added and the mixture was mixed well. The CL was triggered by adding $NaOH_{aq}$ (10 mM, 10 µL) *via* the plate reader injector. After shaking for 20 s using a plate reader built-in shaker, luminescence intensities in the wavelength range of 450 – 470 nm (DX) and 540 – 560 nm (CB7-CF) were recorded. The total volume in each well was 200 µL and contained 2.8 vol% DMSO (from DX stock solution). The same procedure was followed for $CF-N_3$ and DX.

5.4.7. Performance studies of CCS

Determination of the LOD values

Calibration curves (Figures 5.41 and 5.42 in supplementary data) were obtained by plotting the I_{CL} at 3 min for PBS (10 mM, pH 6.0), deproteinized human serum (diluted 1:3 with 10 mM PBS, pH 6.0), or diluted human urine (diluted 1:1 with 10 mM PBS, pH 6.0) spiked with either Mem or Nan (0 – 60 μM). The linear range of the calibration curves was fitted with a linear regression curve. The LOD was calculated using the following equation:

$$LOD = 3.3 \cdot \left(\frac{\sigma_{average \ I_{CL} \ of \ CB8 \supset DX}}{|\ slope \ of \ linear \ fit\ |} \right)$$

Validation and recovery studies

The CCS validation studies were performed using Mem-spiked urine samples (diluted 1:1 with 10 mM PBS, pH 6.0), determined by an IDA using BC as the indicator and CB8 as the macrocyclic host.[237] The IDA calibration curve was obtained by the titration of a known concentration of Mem stock solution to CB8⊃BC$_2$ complex (CB8 = 20.2 μM, BC = 120 μM) in urine (1:1 diluted with 10 mM PBS, pH 6.0) at 25 °C (λ_{ex} = 462 nm; λ_{em} = 548 nm) (see Figure 5.43a in supplementary data). For the validation studies, the obtained IDA calibration curve was used to determine the Mem concentration of unknown samples. The same unknown samples were determined with the CCS calibration curve (Figure 5.43b in supplementary data). The recoveries were calculated from the following equation.

$$\% \ recovery = \frac{[Mem]observed - [Mem]before \ spiking}{[Mem]expected} \times 100$$
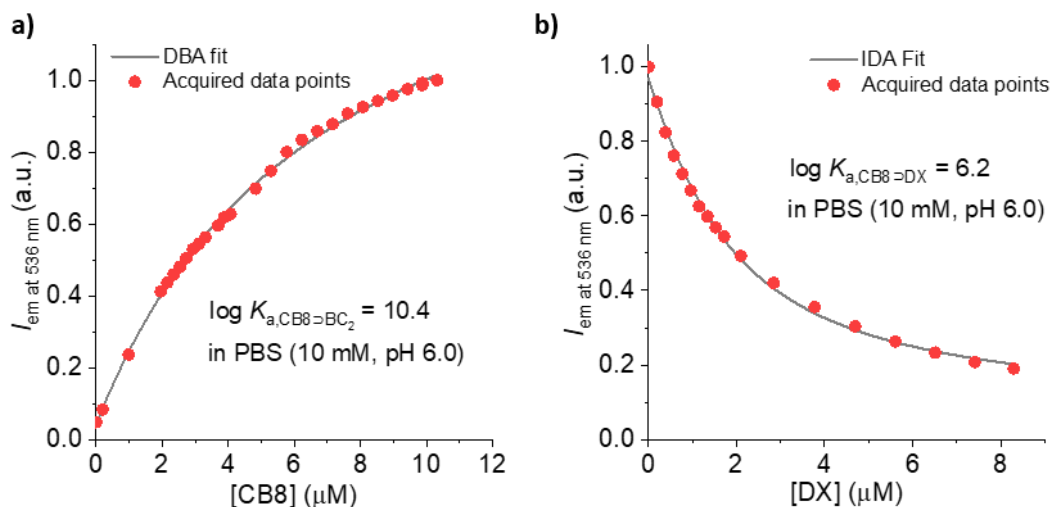
5.5. Supplementary data

Figure 5.32 (a) Representative DBA binding isotherm determined by the fluorescent titration experiment of BC (2 µM) with increasing concentration of CB8 in PBS (10 mM, pH 6.0) at 25 °C (λ_{ex} = 355 nm, λ_{em} = 536 nm). The estimated fitting error in log K_a is 0.01. (b) Representative IDA binding isotherm determined by the fluorescent titration experiment of CB8⊃BC$_2$ (CB8 = 1.06 µM, BC = 6.01 µM) with increasing concentration of DX in PBS (10 mM, pH 6.0) at 25 °C (λ_{ex} = 355 nm, λ_{em} = 536 nm). The estimated fitting error in log K_a is 0.04.
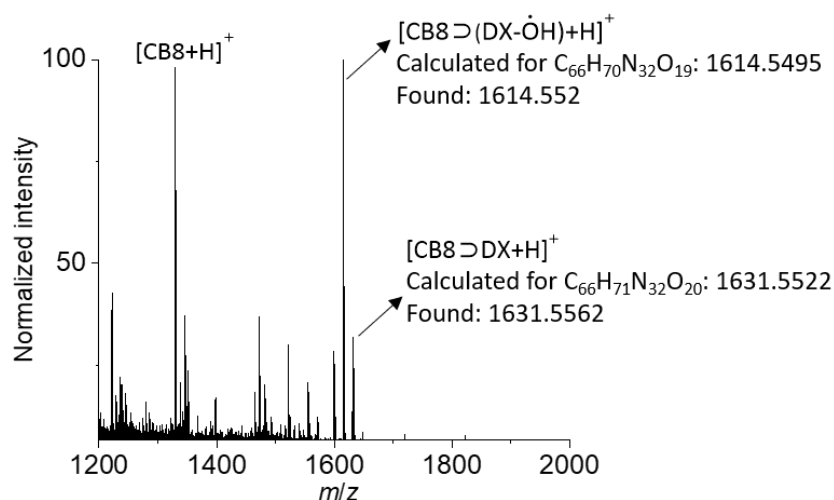
Figure 5.33 ESI-MS spectrum of CB8⊃DX complex in positive ion mode.
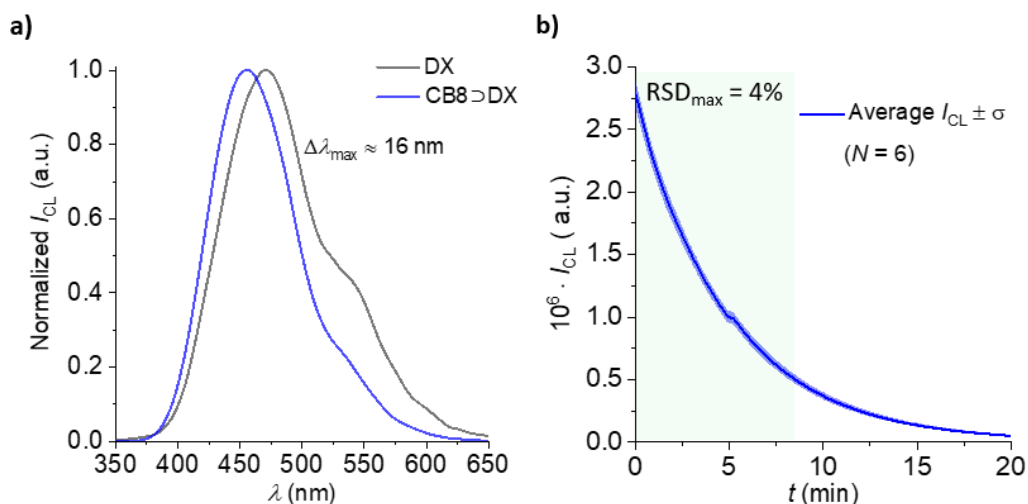
Figure 5.34 (a) Normalized CL spectra of CB8⊃DX (30 µM) and DX (30 µM) in 10 mM PBS containing 2.5 vol% DMSO, pH 9.6. (b) Reproducibility of the CL enhancement in 10 mM PBS containing 2.5 vol% DMSO, pH 9.6 (marked green area is where the error is never larger than 4%). The average I_{CL} and the relative standard deviation (σ) were calculated from six replica measurements.
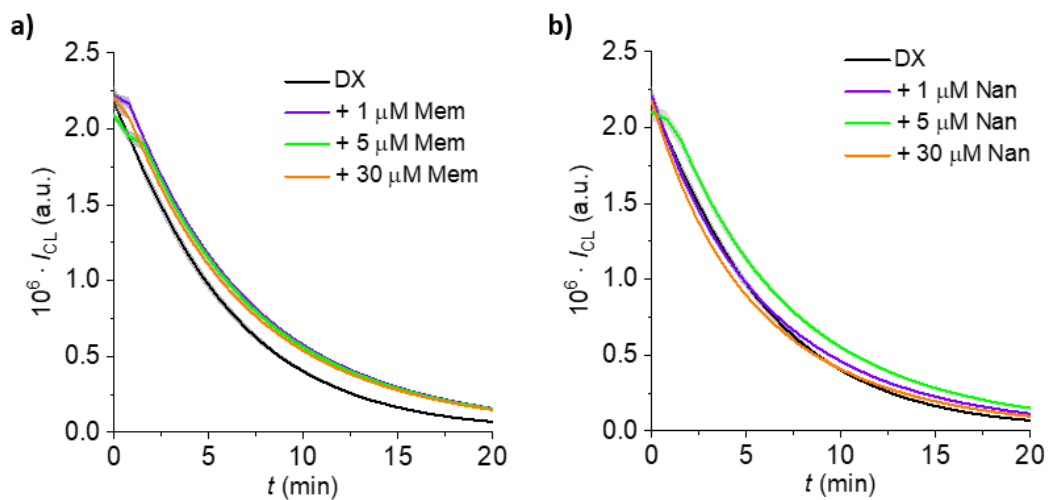
Figure 5.35 Time-dependent CL response of DX (30 µM) in (a) Mem-spiked (0 – 30 µM) and (b) Nan-spiked (0 – 30 µM) PBS samples (10 mM, containing 2.5 vol% DMSO, pH 9.6). The average I_{CL} and the corresponding standard deviation (σ) were calculated from six replica measurements.
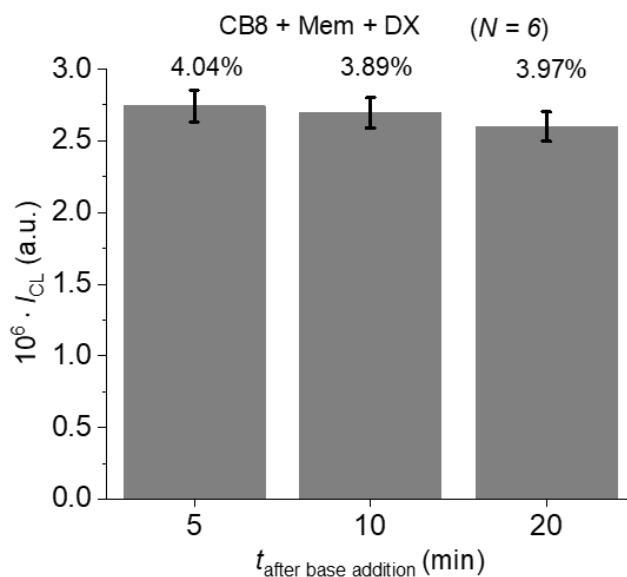
Figure 5.36 Effect of the time of premixing CB8 (30 µM) with Mem (30 µM) on the final CL after the addition of DX (30 µM) in 10 mM PBS (containing 2.5 vol% DMSO, pH 9.6). RSD was calculated from six replica experiments.
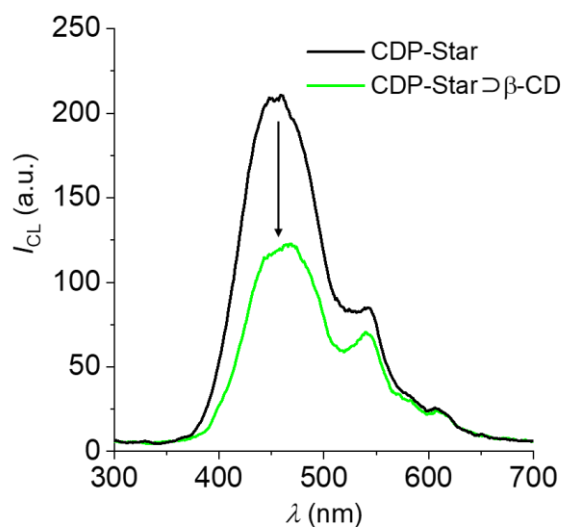
Figure 5.37 CL spectra of CDP-Star (30 µM) in the presence and absence of β-CD (30 µM) in TRIS buffer (10 mM containing 1 mM MgSO$_4$, pH 9.0). The CL spectrum was measured immediately after the addition of ALP, 3 U·mL^{-1} at 37 °C.
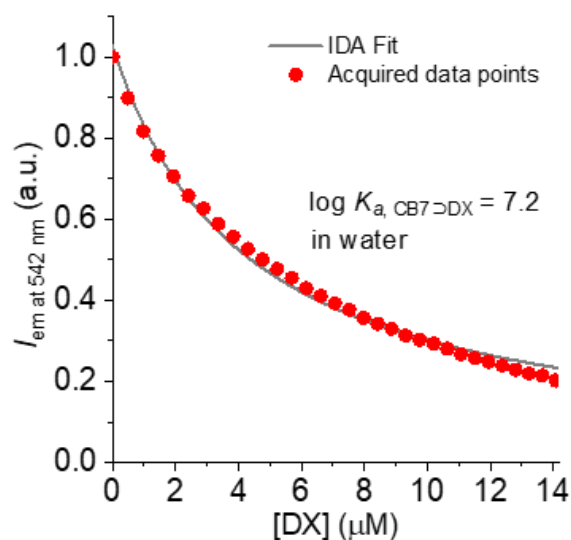
Figure 5.38 Representative IDA binding isotherm determined by fluorescent titration experiment of CB7⊃BC (log K_a = 7.23 from ref[75], CB7 = 2.07 µM, BC = 4.0 µM) with increasing concentration of DX in deionised water at 25 °C (λ_{ex} = 421 nm, λ_{em} = 542 nm). The estimated fitting error in log K_a is 0.01.
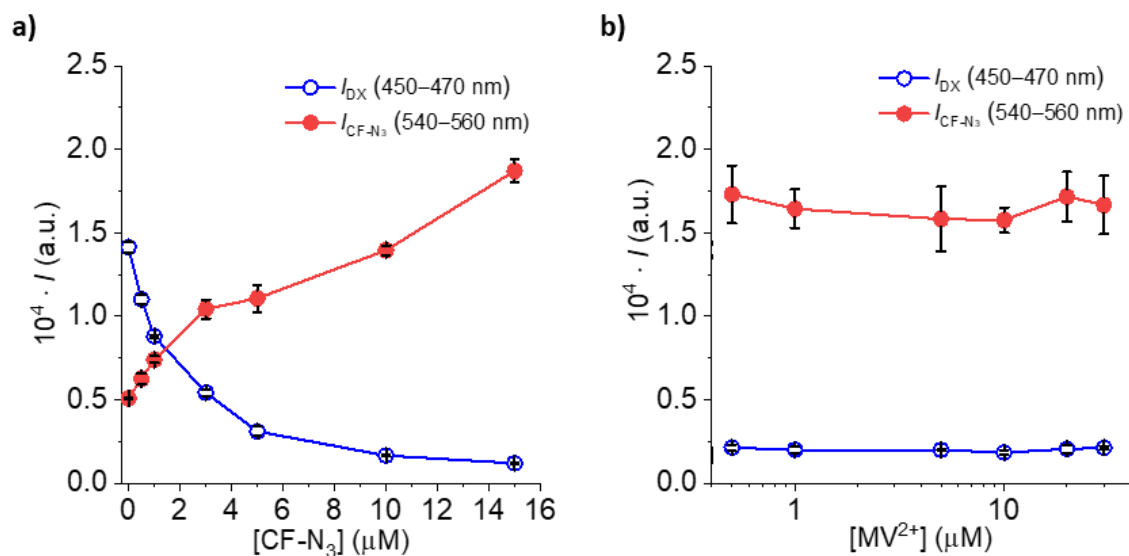
Figure 5.39 (a) CF-N₃-dependent CRET luminescence intensities with DX (10 µM in water containing 2.8 vol% DMSO, pH 9.6). (b) MV²⁺-dependent CRET luminescence intensities between DX and CF- N₃ (10 µM in water containing 2.8 vol% DMSO, pH 9.6). The average emission intensities and the corresponding standard deviation (σ) were calculated from five replica measurements.
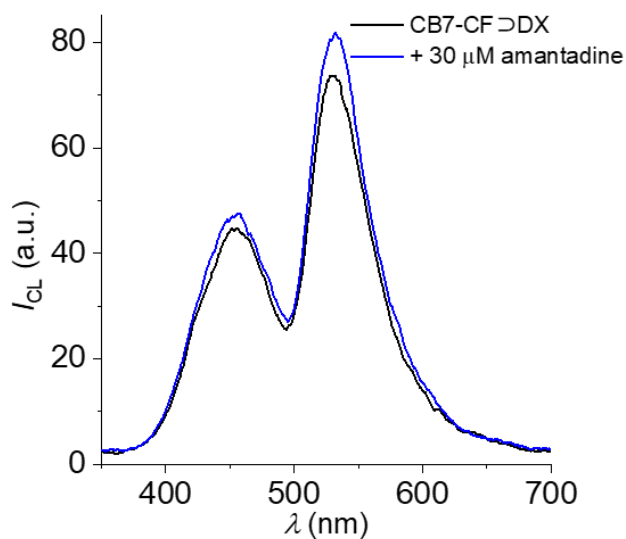
Figure 5.40 CRET intensities were recorded in the presence and absence of amantadine (30 µM) in water containing 2.8 vol% DMSO, pH 9.6 (CB7-CF = 10 µM, DX = 30 µM).

linear fit for Mem in PBS:

$$I_{CL} = -1.15012 \cdot 10^6 \cdot [\text{Mem}] + 6.50823 \cdot 10^6$$

LOD = 0.4 µM

linear fit for Mem in urine:

$$I_{CL} = -0.193608 \cdot 10^6 \cdot [\text{Mem}] + 2.70364 \cdot 10^6$$

LOD = 0.6 µM

linear fit for Mem in serum:

$$I_{CL} = -0.171543 \cdot 10^6 \cdot [\text{Mem}] + 2.63165 \cdot 10^6$$

LOD = 3.2 µM
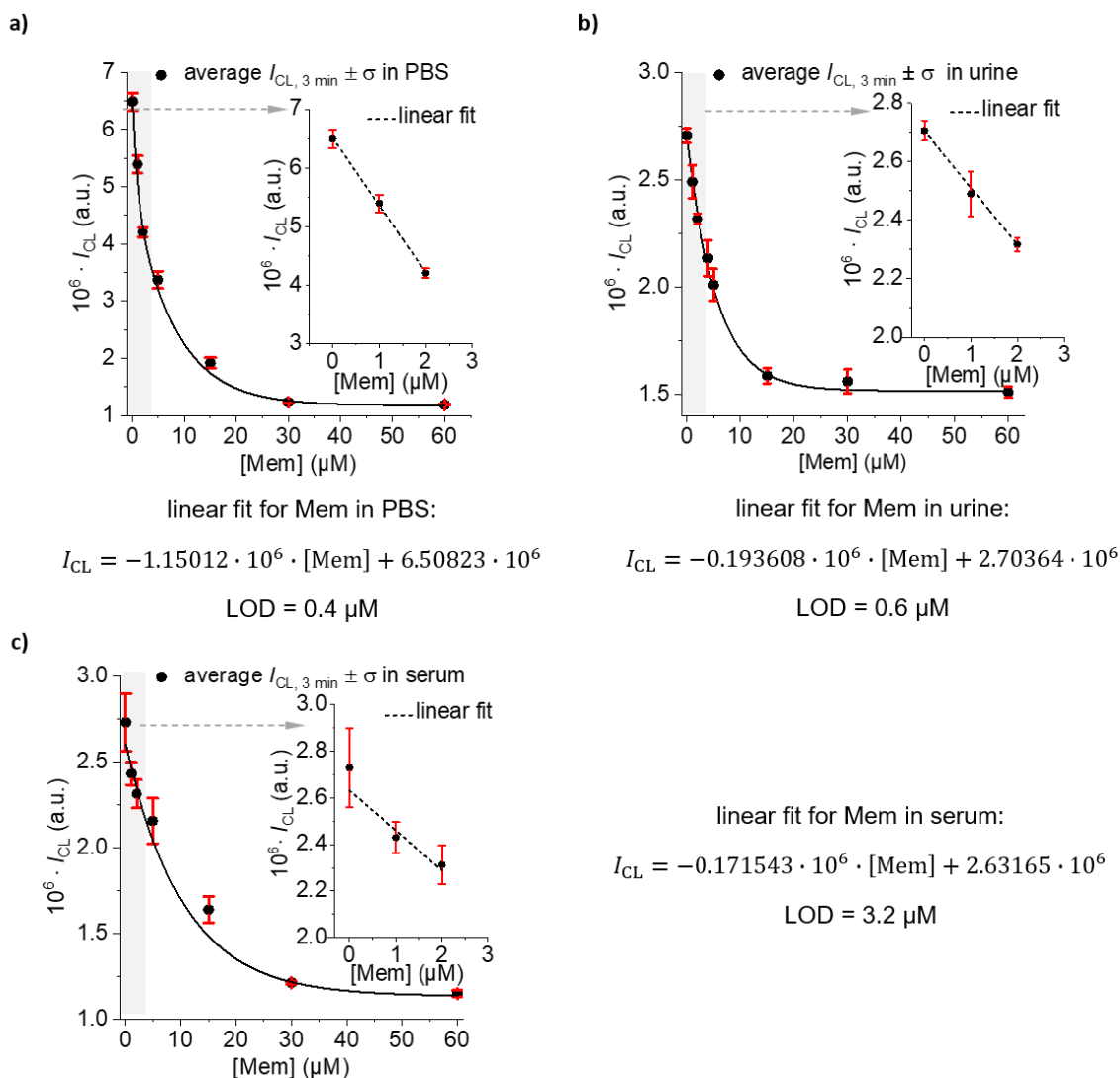
Figure 5.41 Mem-dependent (0 – 60 µM) I_{CL} of CCS (CB8 = 30 µM, DX = 30 µM) were plotted at 3 min. Mem (a) in PBS (10 mM, containing 2.5 vol% DMSO, pH 9.6), (b) in diluted urine (1:1 with 10 mM PBS, containing 2.5 vol% DMSO, pH 9.6), and (c) in deproteinized human serum (diluted 1:3 with 10 mM PBS, containing 2.5 vol% DMSO, pH 9.6). Insets show the corresponding I_{CL} vs. Mem regime (0 – 2 µM) used to calculate the LOD using linear regression.

linear fit for Nan in PBS:

$$I_{CL} = -0.640038 \cdot 10^6 \cdot [\text{Nan}] + 6.39099 \cdot 10^6$$

LOD = 0.8 µM

linear fit for Nan in urine:

$$I_{CL} = -0.125381 \cdot 10^6 \cdot [\text{Nan}] + 3.99224 \cdot 10^6$$

LOD = 3.9 µM

linear fit for Nan in serum:

$$I_{CL} = -0.050111 \cdot 10^6 \cdot [\text{Nan}] + 2.53586 \cdot 10^6$$

LOD = 11.0 µM
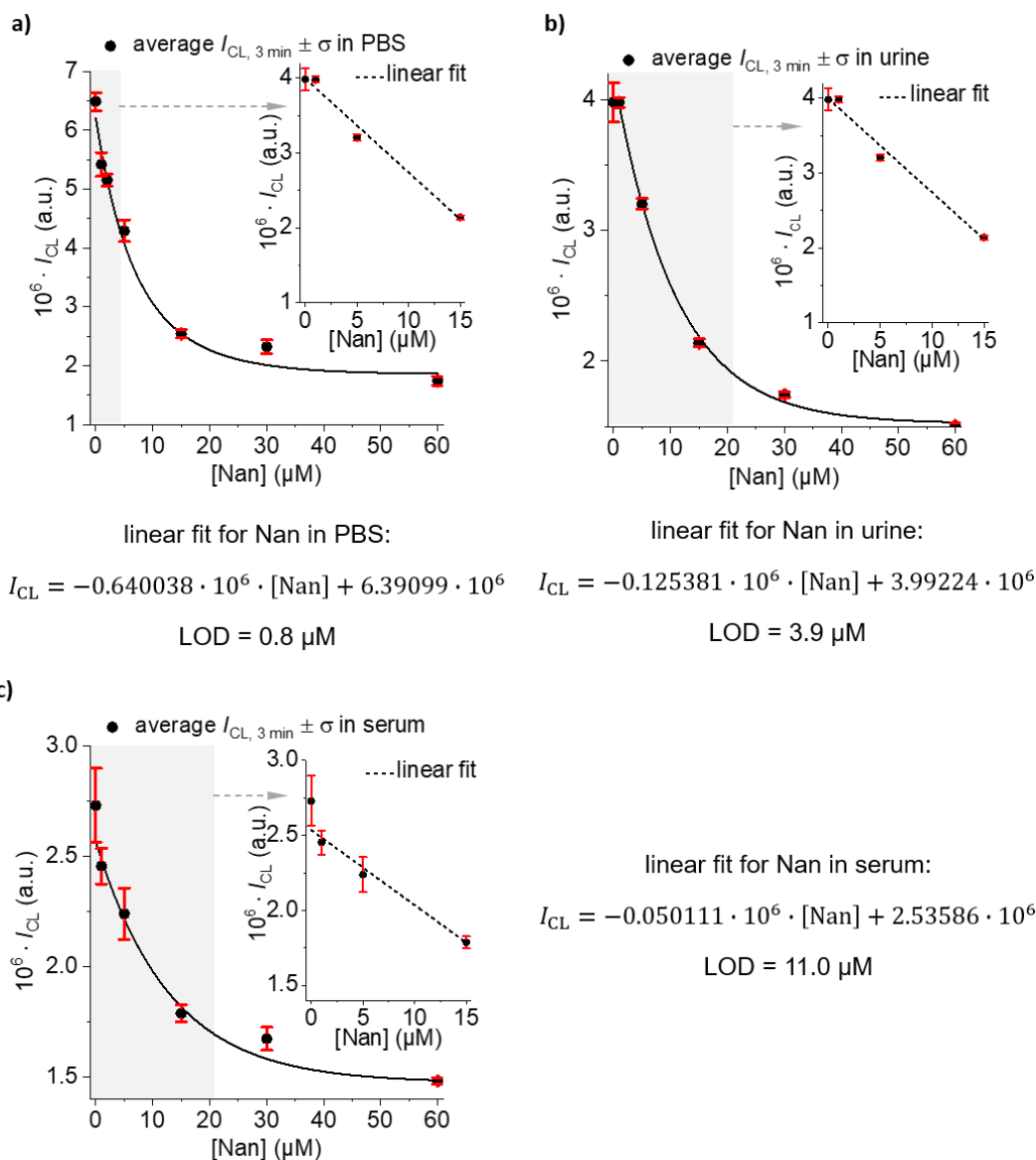
Figure 5.42 Nan-dependent (0 – 60 µM) I_{CL} of CCS (CB8 = 30 µM, DX = 30 µM) were plotted at 3 min. Nan (a) in PBS (10 mM, containing 2.5 vol% DMSO, pH 9.6), (b) in diluted urine (1:1 with 10 mM PBS, containing 2.5 vol% DMSO, pH 9.6), and (c) in deproteinized human serum (diluted 1:3 with 10 mM PBS, containing 2.5 vol% DMSO, pH 9.6). Insets show the corresponding I_{CL} vs. Nan regime used to calculate the LOD using linear regression.

a)

$$I_{em} = -22.43 \cdot [Mem] + 231.19$$

20.2 µM CB8, 120 µM BC
in urine (1:1 diluted with PBS, 10 mM, pH 9.6)

b)

$$I_{CL} = (1.96 \cdot 10^6) \cdot e^{-\frac{[Mem]}{6.42}} + (1.4 \cdot 10^6)$$

average $I_{CL,\ 3\ min} \pm \sigma$

30 µM CB8, 30 µM DX
in urine (1:1 diluted with PBS, 10 mM, pH 9.6)

Figure 5.43 Calibration curves used for the validation experiments. (a) CB8⊃BC$_2$ IDA response curve. (b) CCS I_{CL} (t = 3 min) response curve.

6. Cucurbit[7]uril-based indicator displacement assay for the electrochemical detection of drugs

The results described in this chapter have been published as "Electrochemical detection of drugs via a supramolecular cucurbit[7]uril-based indicator displacement assay" in ACS Sensors, 2023.[257] The experimental data collection and analysis were carried out by me under the supervis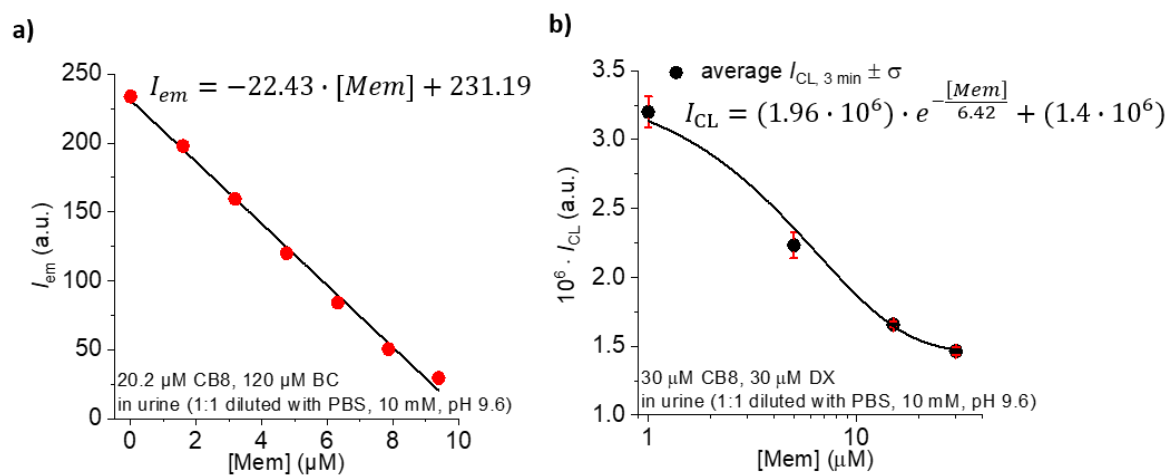ion of Dr. Pierre Picchetti and Priv.-Doz. Dr. Frank Biedermann. The manuscript was written with the contributions of all authors. The co-authors contributed by synthesizing the materials, providing valuable discussions and reviewing the article draft. Sections in this chapter have been reproduced from the published work[257] with permission from the American Chemical Society.

6.1. Introduction

Chemosensors based on host-guest chemistry are widely explored for developing low-cost, robust, and fast-responding analyte sensing assays with real-time monitoring capabilities, offering many new diagnostic opportunities.[5, 70, 258] In optical chemosensors, a spectroscopically detectable signal is generated upon analyte binding event, such as fluorescence response.[6, 212] Since fluorescence emission is generated as a result of photoexcitation, chemosensors based on fluorescence signal readout may encounter major challenges, including high background fluorescence from other emissive components in the sample and light scattering effect, which negatively impacts the performance of the chemosensors. Therefore, employing a signal readout that does not depend on photoexcitation would be advantageous for developing chemosensors with an enhanced signal-to-noise ratio. Based on this context, I was successful in developing a chemosensor based on CL signal readout, as CL is produced by a chemical reaction. This work is described in the previous research project.

Research on electrochemical sensors is gaining much attention for developing disposable, miniaturized, fast-response, cost-effective, and portable sensors for analyte detection.[259-261] Electrochemical sensors are based on redox reactions of the analytes at the working electrode, producing changes in the electrical signal. Using screen-printed electrodes (SPEs) as a sensing platform satisfies the important requirements for detection, including reproducibility, high sensitivity, and the capacity to measure in a few microliters of sample volumes. These

electrodes offer additional benefits, including low cost, compact size, and ease of electrode surface modification.[151, 262]

Macrocyclic hosts, due to their molecular recognition properties, have been used as electrode modifiers in electrochemical sensors to enhance the sensitivity and selectivity of analyte detection.[155, 263] Studies have shown that when organic analytes form host-guest complexes with macrocyclic hosts, there is a significant decrease in their redox current signal. This change is explained as these host molecules protect the analytes from undergoing an electrochemical process.[158, 197, 264] For instance, Ong and co-workers reported that Ferrocene (Fc) generates a reduced current signal upon forming an inclusion complex with CB7.[199] Yu and co-workers showed a CB7-based competitive assay using Fc as the redox indicator, which is immobilized on the gold electrode surface, to investigate the CB7 binding of a redox-inactive guest by analyzing the changes in the oxidation potential of Fc.[158] It was observed that the oxidation potential of Fc shifts to more positive values upon forming a complex with CB7, and the potential responses gradually shift back to the original potential of unbound Fc in the presence of redox-inactive analytes. Although a sensing approach based on this strategy is possible, it necessitates an immobilization process on the electrodes, which is a challenging process due to its limited stability and nonspecific adsorption of analytes.[158, 159]
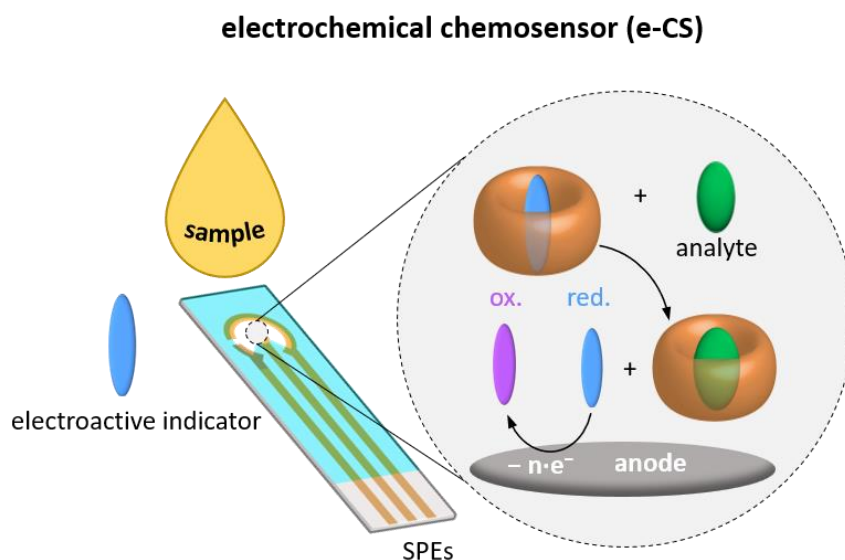

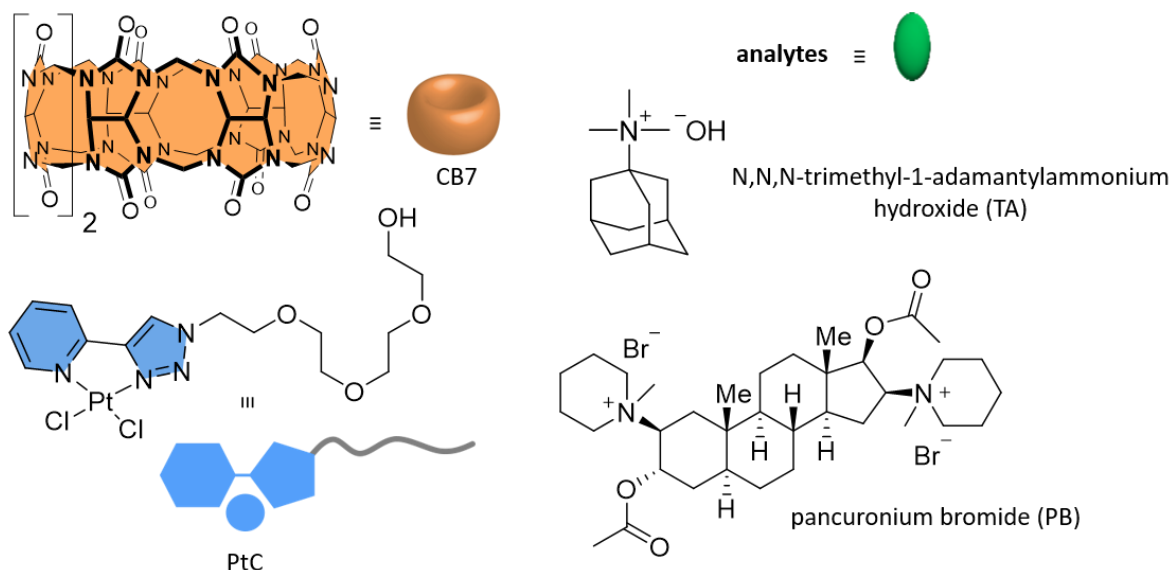**Figure 6.1** Schematic representation of the e-CS functioning principle.

Figure 6.2 Chemical structures of the macrocyclic host CB7, the redox indicator PtC, and the analytes.

In my investigations, I developed an electrochemical chemosensor (e-CS) based on a competitive binding strategy that does not require an immobilization process on the electrode surface and studied the potential of the e-CS to detect redox-inactive analytes at low micromolar concentrations in aqueous solutions and human urine samples. Figure 6.1 shows the schematic representation of the e-CS functioning principle. Specifically, the e-CS was designed by using a redox-active, water-soluble platinum(II) triazole-pyridine complex (PtC) as the redox indicator and CB7 as the macrocyclic host (Figure 6.2). This chapter focuses on the studies involved in the development of the e-CS and its ability to detect drugs in aqueous solutions and urine samples.

6.2. Results and discussion

6.2.1. Design and synthesis of PtC

To develop e-CS, the first step was to find an appropriate redox-active indicator that can bind to CB7. In search of a redox indicator, Pt(II) complexes having 2-(1-R-1H-1,2,3-triazole-4-yl)-pyridine ligands are considered suitable candidates because of the following reasons: Firstly, the ability of the Pt(II) metal centre of the complex to undergo electrochemical oxidation and form Pt(III/IV), preventing auto-oxidation of water. In addition, the triazole-pyridine ligand exhibits lower steric effects than other common Pt(II) ligands like terpyridines and porphyrins, enabling inclusion complex formation with CB7. Therefore, a new triazole-pyridine bearing Pt(II) complex (Figure 6.2), PtC ((2-(2-(2-(2-(4-(pyridine-2-yl)-1H-1,2,3-triazole-1-yl)ethoxy)ethoxy)eth-oxy)ethan-1-ol)dichloroplatinum(II)), was synthesized with the help of Prof.

Dr. Angela Casini's research group in Technical University of Munich (TUM) (see section 6.4.3. in experimental details for the synthesis and characterization of PtC).

6.2.2. Photophysical properties of PtC

Firstly, I investigated the photophysical properties of PtC in water. In the UV-Vis absorption spectrum of PtC, a characteristic absorption band was observed at $\lambda_{ab, max} = 295$ nm (see Figure 6.15 in supplementary data). This band is due to the spin-allowed and ligand-centered transitions, whereas the absorption at $\lambda = 310 - 380$ nm is because of the transition involving mixed metal-to-ligand charge transfer/ligand-centered character.[265, 266] In water, PtC displays a weakly blue-emissive nature ($\lambda_{ex} = 300$ nm, $\lambda_{em, max} = 400$ nm) due to the presence of low-lying metal-centred excited states that undergo efficient non-radiative decay.[267, 268]

6.2.3. Host-guest inclusion complex of PtC with CB7

Next, I studied the photophysical properties of PtC in the presence of CB7. It was observed that the addition of PtC (50 µM) to a solution of CB7 (50 µM) in water (pH 7.0) resulted in a 2.2-fold increase in the emission intensity of PtC (Figure 6.3). In addition, a blue shift in the emission wavelength maximum ($\Delta\lambda \approx 23$ nm) was observed (Figure 6.3). These results confirm the formation of the CB7⊃PtC inclusion complex. Based on this, the blue shift in emission wavelength suggests that the formation of the CB7⊃PtC complex causes the disaggregation of PtC aggregates formed in the water due to the amphiphilic nature of PtC.
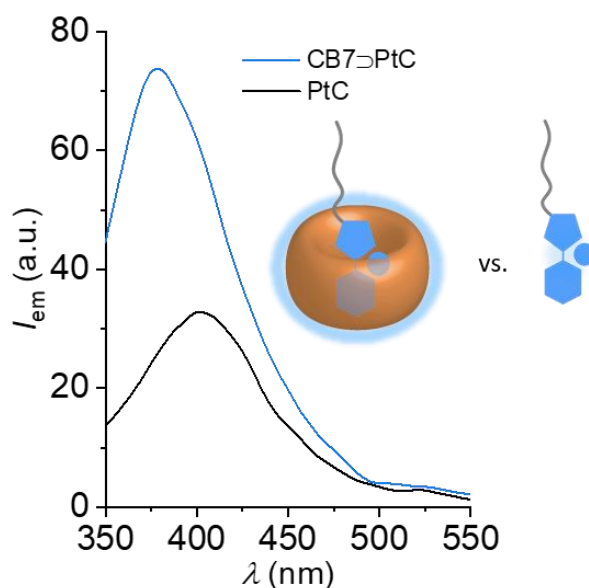

Figure 6.3 Fluorescence emission spectra ($\lambda_{ex} = 300$ nm) of PtC (50 µM) and CB7⊃PtC (50 µM) in water at pH 7.0.

Since there is an enhancement in the fluorescence signal of PtC in the presence of CB7, a fluorescence titration experiment (DBA) was performed to determine the binding affinity of the CB7⊃PtC complex (log K_a = 4.2) in water at pH 7.0 (see section 6.4.4. in experimental details and Figure 6.16 in supplementary data).

Additionally, the ^{1}H NMR spectrum (section 6.4.4. in experimental details and Figure 6.17 in supplementary data) of CB7⊃PtC showed a slight downfield shift for aromatic proton signals of PtC in the presence of CB7, in contrast with cases of complex formation of other organic molecules with CB7, which resulted in upfield signal shifts. Similar unusual behaviour in the chemical shift was also reported in the inclusion complexes of organic dyes such as acridine orange or methylene blue with CB7.[269, 270] As in these organic dyes, amphiphilic PtC possesses a planar head group that induces aggregation in solution by head-to-head stacking. The addition of CB7 results in the disaggregation of PtC aggregates, which has a larger impact on the chemical shifts than the binding event between PtC and CB7. This observation further confirmed the binding of CB7 with the PtC headgroup.

Unlike other electrochemically active indicators having a strong binding affinity with CB7, the moderate binding nature of PtC enables the application of this system to develop displacement assays for the detection of analytes.

6.2.4. Cyclic voltammetry studies of CB7⊃PtC

The next task was to investigate the electrochemical properties of CB7⊃PtC, which was performed using a Metrohm portable bipotentiostat/galvanostat (SpectroECL). SPEs were used for the measurements. In the CV studies, it was observed that the anodic peak current intensity (i_{ox}, from 0.9 to 1 V) for CB7⊃PtC undergoes a strong reduction (almost 25-fold) compared to the free PtC (Figure 6.4). This reduction in intensity can be explained based on the shielding effect provided by CB7, which hinders the oxidation of Pt(II).[271] Therefore, the formation of the CB7⊃PtC complex switches the electrochemical redox activity of PtC to its "OFF" state. Thus, the results obtained from the CV studies further supported the formation of the CB7⊃PtC complex.
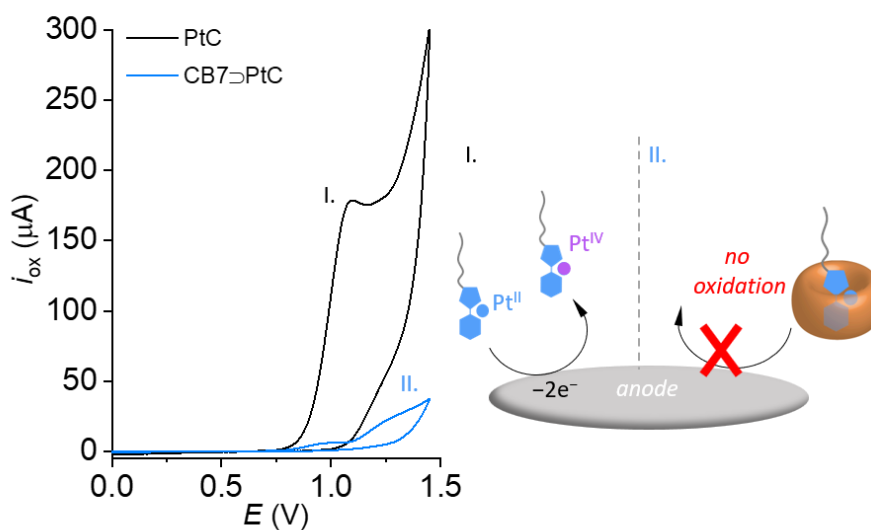
Figure 6.4 CV curves of PtC (200 μM) and CB7⊃PtC (200 μM) in water at pH 7.0 (scan rate: 50 mV/s).

Next, I explored whether the host-guest-induced modulation in the electrochemical activity of PtC could be switched in the presence of a high-affinity CB7 guest. To investigate this, a CB7-binding analyte, N,N,N-trimethyl-1-adamantylammonium hydroxide (TA, log $K_{a,CB7}$ = 12.2, Figure 6.2)[272] was added to a solution containing CB7⊃PtC (200 μM). Interestingly, a noticeable rise in the i_{ox} was observed in the CV measurements (Figure 6.5) due to the displacement of PtC from the CB7 cavity. This increase in the i_{ox} was seen until the equivalence point, indicating the complete displacement of PtC from the CB7 cavity. These results thus paved the way to apply the developed e-CS assay to detect redox-inactive analytes.

Figure 6.5 TA-dependent i_{ox} (at 0.9 V) obtained from CV measurements of CB7⊃PtC (200 μM) in water at pH 7.0 (scan rate: 50 mV/s).

6.2.5. Electrochemical detection of pancuronium bromide

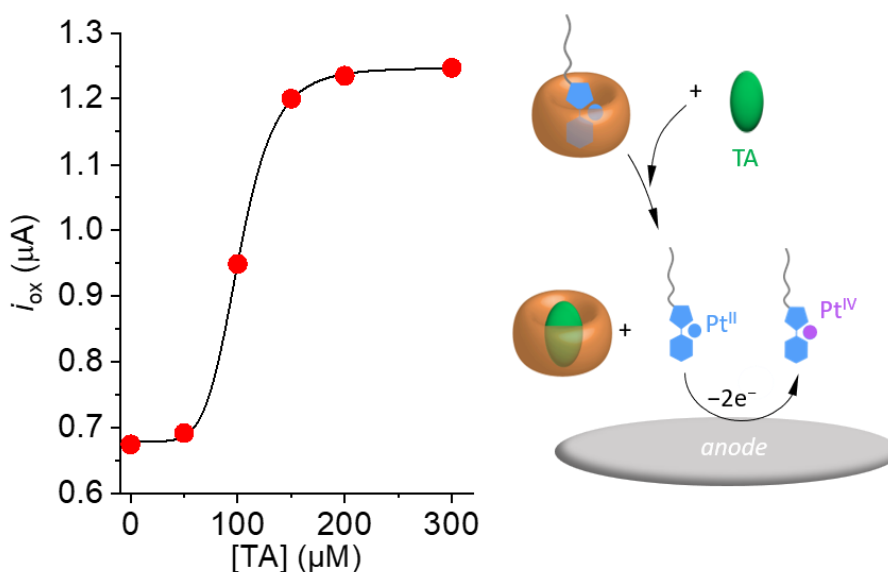Pancuronium bromide (PB, Figure 6.2) is a steroid that is used as a muscle relaxant in general anaesthesia. During normal anaesthesia, the blood contains PB concentrations within the range of 0.3 – 0.5 µM.[273] However, after PB treatment (8 h), the PB concentrations in the patient's urine were approximately 2.4 µM.[274] When overdosed, concentrations of up to 2 mM were detected in both blood and urine.[275] Mainly, the detection of PB in pharmaceutical formulations, illicit preparations, and biosamples is conducted by mass spectrometry combined with liquid chromatographic methods.[274, 275] The absence of reactive functional groups and chromophore units in PB hindered the development of direct or reactive-probe-based assays to detect PB. Therefore, the development of a chemosensor-based detection method for PB calls for potential research. Hence, I took the opportunity to test the developed e-CS for the detection of PB.
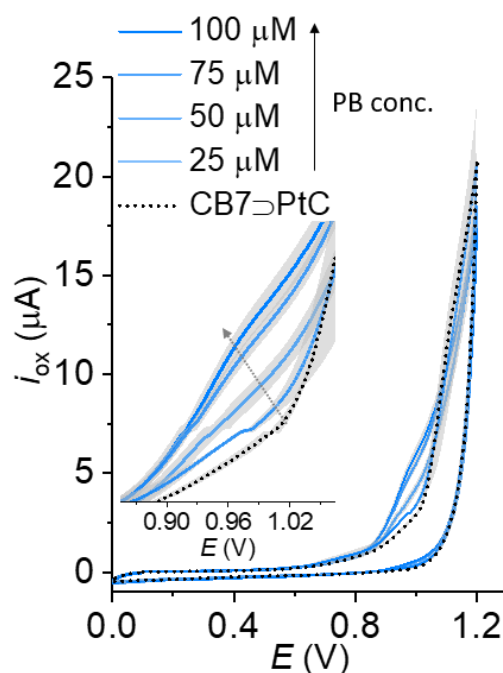
Figure 6.6 CV response curves of e-CS (CB7 = 50 µM, PtC = 50 µM) in PB spiked (0 – 100 µM)-PBS (5 mM, pH 7.0). The average i_{ox} and the corresponding standard deviation (σ) were calculated from three replica measurements; scan rate: 50 mV/s.

As in the first case, CV measurements of CB7⊃PtC (50 µM) were performed in PBS (5 mM, pH 7.0) with increasing concentrations (0 – 100 µM) of PB. As anticipated, a PB-dependent increase in the i_{ox} was observed from 0.9 to 1.1 V (Figure 6.6) due to the competitive binding of PB to CB7 (log $K_{a,CB7}$ = 10.2),[276] thereby resulting in PB-induced displacement of PtC from the CB7 cavity. As a control experiment, CV measurements for free PB were performed and
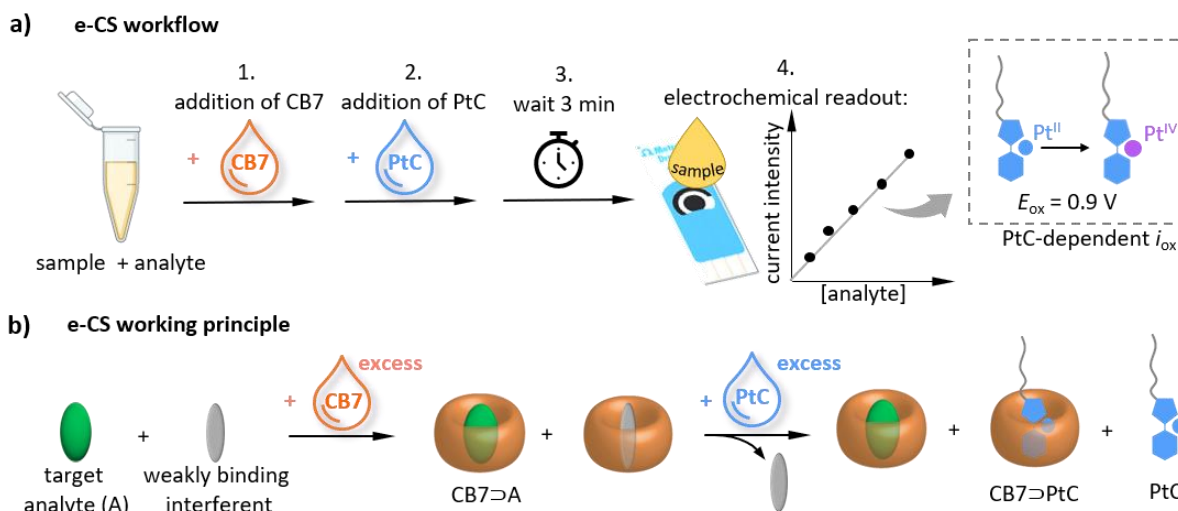
Figure 6.7 (a) Schematic representation of the e-CS workflow (CB7 = 50 µM, PtC = 50 µM). The electrochemical readout is recorded at $E_{ox} = 0.9$ V. (b) Schematic representation of the working principle of e-CS.

no significant i_{ox} was observed (at 0.9 V is 0.8 µA; see Figure 6.18 in supplementary data) as it cannot be oxidized in the potential range studied.

In a typical e-CS procedure, 50 µM CB7 and 50 µM PtC were added sequentially to analyte-spiked solutions (in 5 mM PBS, pH 7.0) (Figure 6.7a). The mixture was thoroughly mixed, and after an equilibration time of 3 min, drop-cast 40 µL of the mixture onto the SPE. As shown in the working principle (Figure 6.7b), the addition of CB7 to the analyte-spiked solution results in the formation of the CB7⊃A complex. Hence, PtC sequesters the remaining unoccupied CB7 by forming the CB7⊃PtC complex. The lower binding affinity of PtC with CB7 compared to the target analyte ensures that no analyte is displaced from the CB7⊃A after its addition to the solution. However, weaker CB7-binding interferents in the sample are displaced from the CB7 cavity by PtC, which is a desirable side effect of the e-CS.

For higher sensitive readings, the chronoamperometric method was adapted to execute the e-CS assay. In the chronoamperometric method, the current of the drop-cast sample was recorded by applying a constant oxidation potential ($E_{ox} = 0.9$ V). As expected, the observed chronoamperometric curves (Figure 6.8a) show an increase in anodic current density (j_{ox}) with increasing PB concentration due to the oxidation of non-complexed PtC. To get a clear picture of the observed increase in j_{ox}, the corresponding PB-dependent j_{ox} at 50 s is shown in Figure 6.8b. As a control experiment, the detection of PB in the absence of CB7, *i.e.* with PtC alone, was not possible as there were no changes in j_{ox} (see Figure 6.19a in supplementary data).

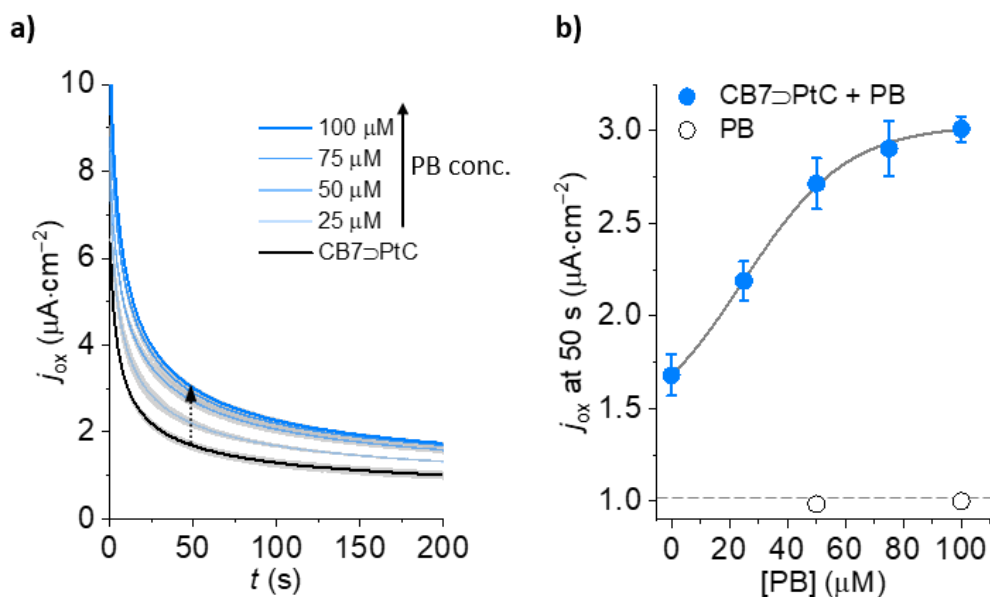**Figure 6.8** (a) Chronoamperometric response curves of e-CS (CB7 = 50 µM, PtC = 50 µM) in PB-spiked (0 – 100 µM) PBS (5 mM, pH 7.0) at E_{ox} = 0.9 V and (b) the corresponding PB-dependent j_{ox} (at 50 s). The average j_{ox} (coloured lines) and the corresponding standard deviation (σ; grey area) were calculated from three replica measurements.

Moreover, PB itself showed no observable increase in j_{ox} (see Figure 6.19b in supplementary data). The LOD of PB in PBS (5 mM, pH 7.0) was calculated to be 17.7 µM from the linear-response range of the obtained chronoamperometric response curve (see section 6.4.5. in experimental details and Figures 6.20a in supplementary data).

In addition to chronoamperometry, staircase voltammetry (SCV) and differential pulse voltammetry (DPV) are employed in electrochemical sensors to achieve higher sensitivity, as these voltammetric methods minimise the occurrence of capacitive charges.[139, 141] Therefore, the SCV method was performed to detect PB in PB-spiked (0 – 200 µM) human urine (1:3 diluted with 5 mM PBS, pH 7.0). Figure 6.9a shows the obtained SCV response curves. Notably, a PB-dependent increase in j_{ox} (at 0.9 V) was observed (Figure 6.9b), enabling the detection of PB in PB-spiked human urine. The detection of PB in the absence of CB7, *i.e.* with PtC alone, was not possible as there was no observable change in j_{ox} (see Figure 6.21a in supplementary data). In addition, the detection of PB without CB7⊃PtC showed no significant increase in j_{ox} (see Figure 6.21b in supplementary data). The DPV method also yielded detection results comparable to those obtained from SCV measurements (see Figure 6.22 in supplementary data).
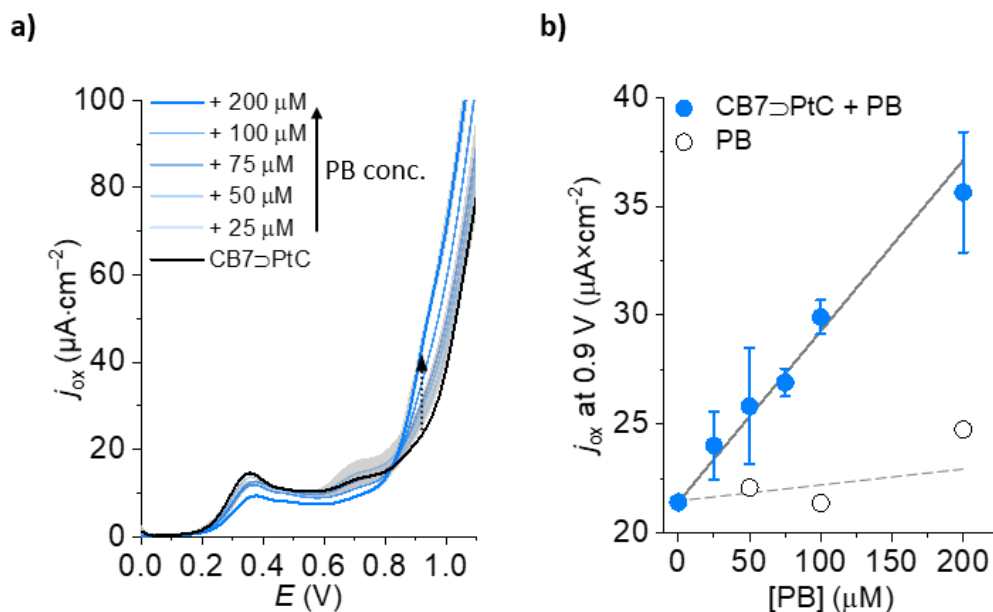
Figure 6.9 (a) SCV response curves of e-CS (CB7 = 50 μM, PtC = 50 μM) in PB-spiked (0 – 200 μM) human urine (1:3 diluted with 5 mM PBS, pH 7.0) and (b) the corresponding PB-dependent j_{ox} (at 0.9 V). The average j_{ox} (coloured lines) and the corresponding standard deviation (σ; grey area) were calculated from three replica measurements.

6.2.6. Performance of the e-CS

The LOD of PB was determined to be 7.6 μM in PB-spiked (0 – 200 μM) human urine, derived from the linear response range of the obtained SCV response curve (see section 6.4.5. in experimental details and Figures 6.20b in supplementary data). Notably, this LOD is considerably lower than the standard concentration levels required to detect the misuse or overdose of PB. In addition, DPV measurement showed a comparable LOD of 6.3 μM for PB-spiked (0 – 200 μM) human urine (see section 6.4.5. in experimental details and Figures 6.22b in supplementary data). It is important to note that the LODs calculated *via* linear regression are approximations, as host-guest interactions follow non-linear relationships.

The optimal concentration of CB7 and PtC was selected through a preliminary screening experiment *via* DPV, where the use of 50 μM CB7⊃PtC yielded a satisfactory LOD of 4.3 μM for PB in PBS (5 mM, pH 7.0) (see Figure 6.23 in supplementary data).

Considering the determined LODs, this approach can be used to detect illicitly prepared PB formulations and overdoses.[275] Remarkably, e-CS is the first chemosensor based on host-guest chemistry to detect PB at low micromolar concentrations (Table 6.1).

Furthermore, to understand the e-CS under the impact of the matrix-to-matrix effect, recovery studies were conducted using PB-spiked (5 – 35 μM) human urine samples from two healthy

voluntary donors. The e-CS showed good recoveries (>85%) in all the tested samples (Table 6.2). In addition, fluorescence (IDA) and LC-MS-based detection methods were conducted to validate the e-CS (see section 6.4.5. in experimental details). The validation results yielded comparable PB concentration values to those obtained in IDA and LC-MS-based detection methods (see Figure 6.24 in supplementary data).

Table 6.1 Comparison of different methods for the detection of PB (n.a. – not applicable).

method	concentration range (μM)	LOD (μM)	sample	ref.
enzyme assay	0.3–2.7	0.002	urine, serum	[277]
fluorescence	0.1–1.3	n.a.	extracts of urine, plasma or blood	[278]
HPLC	546.0–1638.0	8.5	pavulon injections	[279]
	68.2–409.4	6.0		[280]
HPLC-MS	0.0–2.7	0.003	extracts of urine, plasma, blood, and gastric content	[281]
potentiometry	9.9–997.3	n.a.	urine and pharmaceutical samples	[282]
voltammetry (this work)	0.0-200.0	6.3	urine	

Table 6.2 Calculated recoveries for urine-spiked samples from different donors using the e-CS.

spiked conc. [μM]	observed conc. [μM]	recovery
urine donor 1		
5.0	5.6	112%
15.0	13.4	89%
25.0	30.4	122%
35.0	41.9	120%
urine donor 2		
5.0	4.8	96%
15.0	13.7	91%
25.0	29.2	117%
35.0	31.0	88%

6.3. Conclusion

In conclusion, a novel electrochemical chemosensor was successfully developed and applied for the detection of electrochemically inactive analytes. The characteristic properties of the developed chemosensor include the use of commercially available screen-printed electrodes, operation with minimal sample volumes (40 μL), short assay times (6 min), and no requirement for electrode surface immobilization. In this competitive binding approach, the chemosensor ensemble consists of a new Pt(II) complex as the redox-active indicator and cucurbit[7]uril as the macrocyclic host, which enabled the detection of the drug pancuronium bromide in saline media and human urine. To the best of my knowledge, this is the first host-guest-based electrochemical chemosensor to detect pancuronium bromide at low micromolar concentrations. Furthermore, utilizing chemosensors based on electrochemical readout eliminates the limitations associated with optical chemosensors that rely on an external light source for sample excitation. Hence, I believe that this approach could lead to the development of new sensors to detect biologically important analytes that can be used in point-of-care applications.

6.4. Experimental details

6.4.1. Materials and methods

All purchased chemicals and solvents were used as received from suppliers without any further purification. CB7 was synthesized by following the reported procedure[251] and was also purchased from Strem or Sigma. [PtCl$_2$(DMSO)$_2$] was synthesized by following the reported procedures.[283] The 5 mM PBS buffer (137 mM NaCl, 2.7 mM KCl, 10 mM Na$_2$HPO$_4$, and 1.8 mM KH$_2$PO$_4$) was prepared from Gibco PBS tablets and Milli-Q water. The pH of the PBS solution was adjusted to pH 7.0 by adding diluted HCl.

CB7, PtC, PB, and TA stock solutions were prepared in Milli-Q water. The concentration of the CB7 stock solution was determined by fluorescence titration against a known concentration of the MDAP dye (λ_{ex} = 339 nm and λ_{em} = 452 nm) in Milli-Q water.

Urine samples were provided by healthy volunteers and were used within 3 – 4 days after excretion (the urine was stored in the fridge at 4 °C). The collected urine was further diluted (1:3) with 5 mM PBS (pH 7.0) and the pH value was adjusted to pH 7.0 by the addition of diluted HCl for all the measurements. The resulting dilution was filtered through a syringe filter (0.45 μm, PES membrane) before use.

All the experiments involving human participants (urine sample collection from healthy voluntary donors) were in accordance with the formal statement of ethical principles published by the World Medical Association in the Declaration of Helsinki in 1964 and its later amendments or comparable ethical standards.[252, 253] Informed consent was obtained from all individual participants included in the study.[254, 255]

6.4.2. Instrumentation

Nuclear magnetic resonance (NMR) spectroscopy

^{1}H and ^{13}C NMR spectra were recorded on a Bruker AV400 Ultra Shield or on a Bruker Advance 500 spectrometer at 25 °C. The chemical shifts (δ) are given in ppm and refer to residual protons on the corresponding deuterated solvent. For the characterization of symmetric signals, the median point of the signal was chosen and for multiplets, the signal range was used. The multiplicities of the signals were abbreviated as follows: s = singlet, d = doublet, dd =

doublet of doublets, dt = doublet of triplets, td = triplet of doublets, t = triplet, m = multiplet. All coupling constants (J) are stated as modulus in Hertz (Hz).

Electrospray ionization mass spectrometry (ESI-MS)

Mass spectra were recorded on a HESI Thermo Scientific Exactive Plus Orbitrap Mass Spectrometer. 5 nM solutions of the compound in LC-MS grade acetonitrile were prepared and analysed. The spectra were acquired in positive mode optimized parameters are as follows: capillary temperature: 300 °C, aux gas flux: 2.0 L/min, spray voltage: 4.0 V, spray current 0.36 μA, collision RF: 800 Vpp, transfer time: 120 μs, prepulse storage: 10 μs.

UV-Vis absorption spectroscopy

Absorbance spectra were measured at 25 °C in Milli-Q water on a Jasco V-730 double-beam UV-Vis spectrophotometer. For UV-Vis absorption experiments, PMMA cuvettes with a light path of 10 mm and dimensions of 10 × 10 mm and a spectroscopic cut-off at 220 nm were utilized. In addition, the cuvettes were equipped with a magnetic stirrer, allowing rapid mixing.

Fluorescence spectroscopy

Steady-state emission spectra and time-resolved emission profiles for the titration experiments were recorded on a Jasco FP-8300 fluorescence spectrometer equipped with a 450 W Xenon arc lamp, double-grating excitation, and emission monochromators. Emission spectra were corrected for source intensity (lamp and grating) and the emission spectral response (detector and grating) by standard correction curves. All titration and kinetic experiments were carried out at 25 °C by using a water thermostatic cell holder STR-812, while the cuvettes were equipped with a magnetic stirrer, allowing rapid mixing. For fluorescence-based titration experiments, PMMA cuvettes with a light path of 10 mm and dimensions of 10 × 10 mm from Brand with a spectroscopic cut-off at 300 nm were utilized. Fluorescence-based validation experiments were carried out with a CLARIOstar Plus microplate reader using the software-implemented fluorescence method with black isoplates (96-isoplate with black frame and clear well from Perkin Elmer).

Electrochemical measurements

CV, chronoamperometric, and DPV measurements were performed using a Metrohm portable bipotentiostat/galvanostat (SpectroECL - ± 4 V potential range, ± 40 mA maximum measurable current). The electrochemical setup is controlled by DropView SPELEC software. SPEs (DRP-

110 from Metrohm DropSense) were used for the measurements. For DPV measurements, the pulse step was 0.02 V, the pulse height was 0.05 V, the pulse duration was 0.1 s, and the sampling rate was 0.02 V s^{-1}. The area of the working electrode is 0.125 cm^2.

LC-MS measurements

LC-MS measurements were performed on an Agilent 1260 Infinity II system consisting of a quaternary pump (GB7111B), autosampler (G7129A, 100 μL sample loop), a temperature-controlled column oven (G7114A) and a variable UV-Vis detector (G7114 A, VWD, flow cell G7114A 018, d = 10 mm, V = 14 μL). Separation was performed on a C18 HPLC-column (Agilent Poroshell 120 EC-C18 4.6 x 100 mm, 2.7 μm) operating at 40 °C. A gradient (refer to the gradient table below) of eluent A (ACN + 0.1 vol% Et$_3$N) and eluent B (Millipore water + 0.1 vol% formic acid) at a flow rate of 1.00 mL·min^{-1} was used. The flow was directed into an Agilent MSD (G6136BA, AP-ESI ion source). The instrument was calibrated in the m/z range 118–2121 in the positive mode and 113–2233 in the negative mode using a premixed calibration solution (Agilent). The following parameters were used: spray chamber flow: 12 L·min^{-1}, drying gas temperature: 320 K, capillary voltage: 2000 V, fragment or voltage: 25. The MSD was set up in the single ion mode (SIM) at m/z = 284.4 at positive polarization.

time [min]	A [%]	B [%]
0.0	80.0	20.0
1.5	80.0	20.0
9.5	0.0	100.0
9.9	0.0	100.0
9.95	80.0	20.0
11.0	80.0	20.0

6.4.3. Synthesis and characterization of PtC

The synthesis and characterization of PtC were carried out by Prof. Dr. Angela Casini's research group at the Technical University of Munich (TUM).
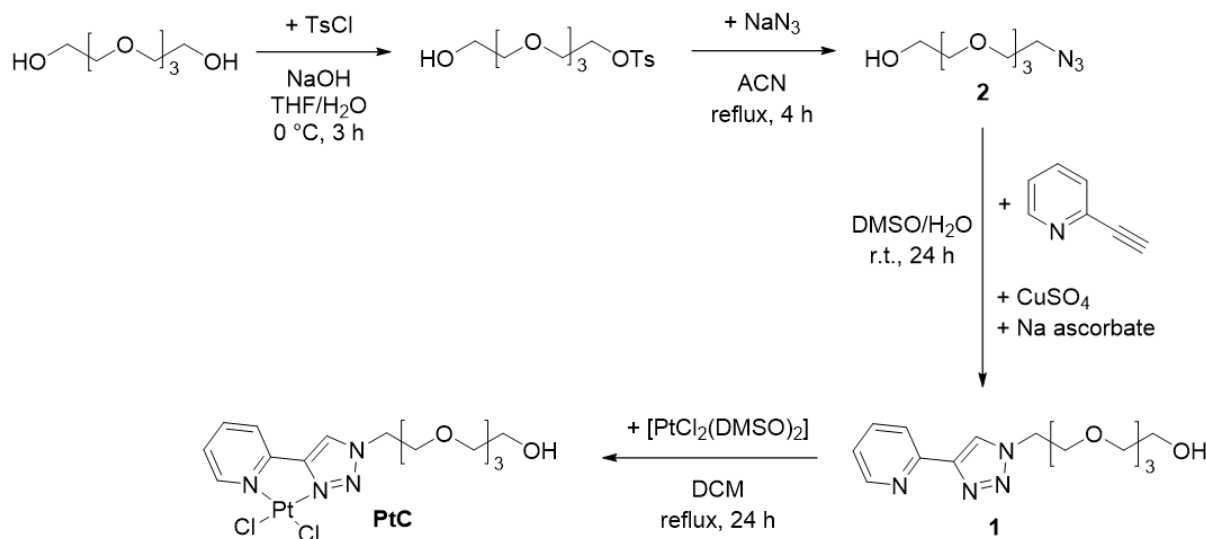

Figure 6.10 Reaction scheme for the synthesis of PtC.

(2-(2-(2-(2-azidoethoxy)ethoxy)ethoxy)ethan-1-ol) (2). It was synthesized according to the previously reported procedure.[265]

^{1}H NMR (400 MHz, CDCl$_3$) δ 3.76 – 3.72 (m, 2H), 3.70 – 3.66 (m, 10H), 3.66 – 3.59 (m, 2H), 3.40 (t, J = 5.0 Hz, 2H) ppm.

(2-(2-(2-(2-(4-(pyridine-2-yl)-1H-1,2,3-triazole-1-yl)ethoxy)ethoxy)ethoxy)ethan-1-ol) (1). In a 25 mL round-bottom flask, **2** (2.19 g, 10.0 mmol), 2-ethynylpyridine (2.06 g, 20.0 mmol), CuSO$_4$·5H$_2$O (125 mg, 5.00 mol%), and sodium ascorbate (1.00 g, 20.0 mol%) were dissolved in DMSO/H$_2$O (2:1 v/v, 12.0 mL) and the mixture was stirred under N$_2$ at room temperature for 24 h. The reaction mixture was poured in 100 mL of 1 M EDTA in aqueous NH$_4$OH (25%) and the mixture was stirred for 1 h. The mixture was extracted with DCM (3 × 50.0 mL), and the combined organics were washed with brine (2 × 50.0 mL) and dried over Na$_2$SO$_4$. The organic solvent was removed under reduced pressure. The residue was purified by flash column chromatography (silica gel, 100% DCM to 5% MeOH with 1% TEA) to yield a yellowish oil (2.0 g, 62%).

^{1}H NMR (400 MHz, CD$_3$CN) δ 8.64 – 8.58 (m, 1H), 8.38 (s, 1H), 8.11 (dt, J = 7.9, 1.2 Hz, 1H), 7.86 (td, J = 7.8, 1.9 Hz, 1H), 7.31 (ddd, J = 7.6, 4.9, 1.3 Hz, 1H), 4.61 (t, J = 5.1 Hz, 2H), 3.97 – 3.89 (m, 2H), 3.65 – 3.50 (m, 11H), 3.47 (t, J = 4.1 Hz, 2H) ppm. **^{13}C NMR** (100 MHz,

CD$_3$CN) δ 151.46, 150.50, 148.72, 137.92, 124.18, 123.72, 120.51, 73.22, 71.10, 71.03, 70.94, 70.91, 69.83, 61.86, 51.03 ppm. **Elemental analysis** (%) found: C, 55.66; H, 6.91; N, 17.12, calculated for C$_{15}$H$_{22}$N$_4$O$_4$: C, 55.89; H, 6.88; N, 17.38. **MS** (HR-ESI), m/z [M+Na]$^+$ calc. 345.1533; found 345.1521.
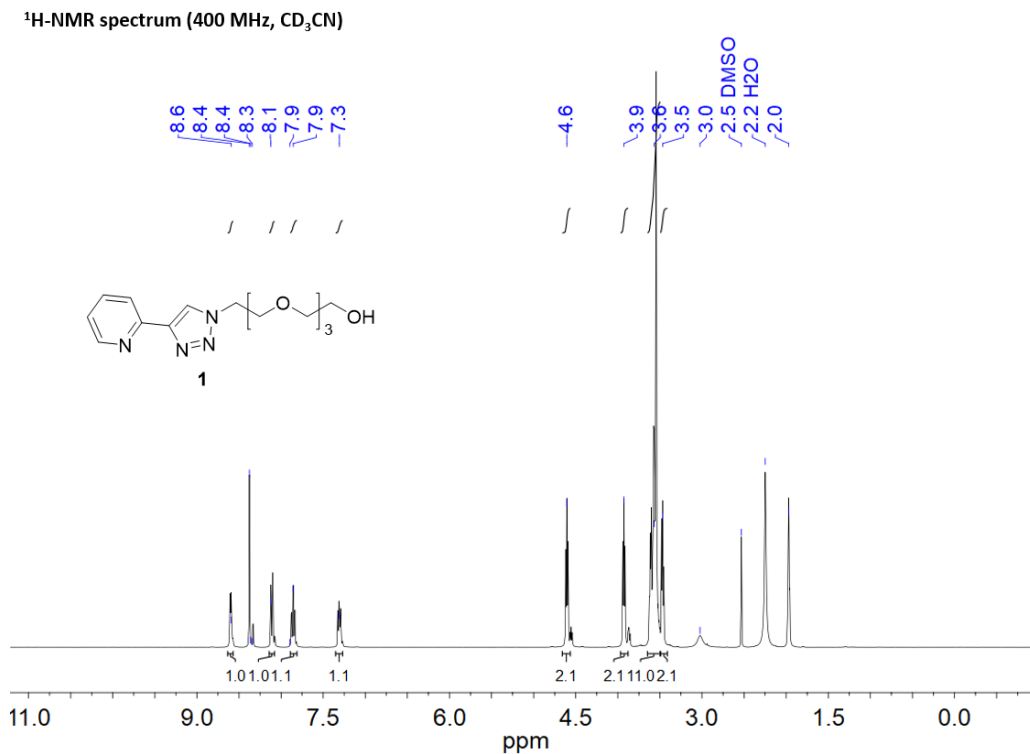
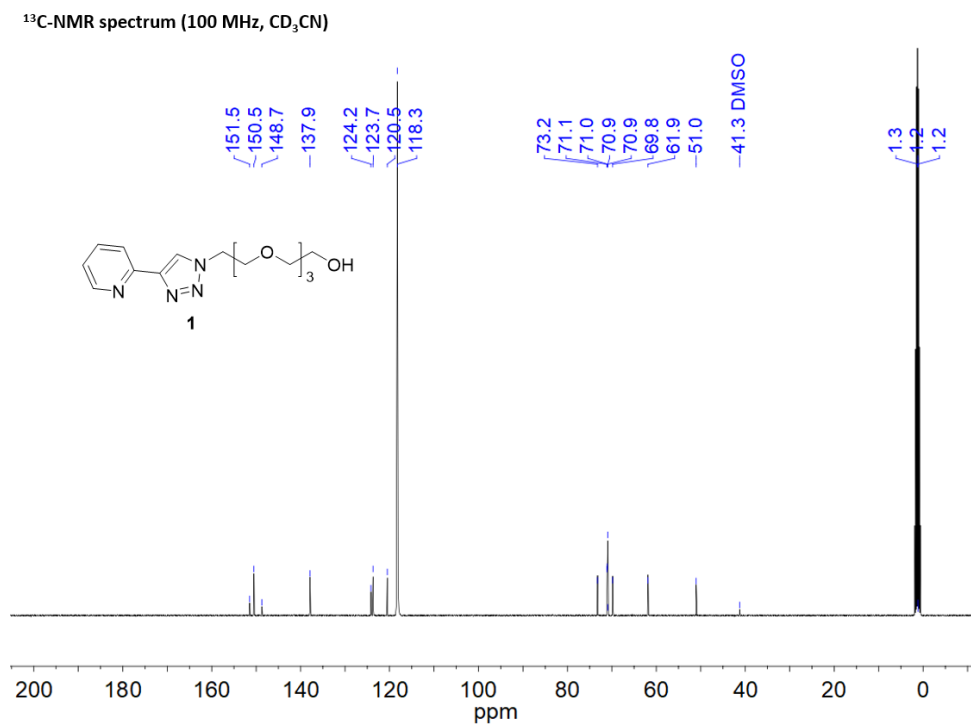**Figure 6.11** ^{1}H NMR (400 MHz) spectrum of **1** in CD$_3$CN.

Figure 6.12 ^{13}C NMR (100 MHz) spectrum of **1** in CD$_3$CN.

Additional information on the synthesis and analysis is available in the Chemotion repository:

https://dx.doi.org/10.14272/reaction/SA-FUHFF-UHFFFADPSC-GJRAKKLOML-UHFFFADPSC-NUHFF-NUHFF-NUHFF-ZZZ

(2-(2-(2-(2-(4-(pyridine-2-yl)-1H-1,2,3-triazole-1-yl)ethoxy)ethoxy)ethoxy)ethan-1-ol)dichloroplatinum(II) (PtC). In a 100 mL round-bottom flask, **1** (322 mg, 1.00 mmol) and [PtCl$_2$(DMSO)$_2$] (422 mg, 1.00 mmol) were dissolved in DCM (20.0 mL) and the resulting solution was stirred for 24 h under reflux. After the reaction mixture was cooled down to room temperature, hexane (50.0 mL) was added, and the resulting precipitate was filtered. The obtained solid was redissolved in a minimum amount of DCM and precipitated by adding diethyl ether to yield the compound as a yellow solid (510 mg, 87%).

^{1}H NMR (400 MHz, CD$_3$CN) δ 9.48 (d, J = 5.7 Hz, 1H), 8.76 (s, 1H), 8.21 (td, J = 7.8, 1.5 Hz, 1H), 8.04 (d, J = 7.7 Hz, 1H), 7.58 (ddd, J = 7.5, 5.9, 1.5 Hz, 1H), 4.71 (t, J = 5.0 Hz, 2H), 3.97 (t, J = 5.0 Hz, 2H), 3.70 – 3.62 (m, 2H), 3.61 – 3.53 (m, 8H), 3.49 (dd, J = 5.8, 4.1 Hz, 2H), 2.79 (t, J = 5.6 Hz, 1H) ppm. **^{13}C NMR** (100 MHz, CD$_3$CN) δ 150.74, 149.81, 149.56, 141.31, 127.14, 126.58, 122.84, 118.26, 73.16, 71.03, 70.85, 70.86, 68.92, 61.81, 53.81 ppm. **Elemental analysis** (%) found: C, 30.66; H, 3.52; N, 9.39, calculated for C$_{15}$H$_{22}$Cl$_2$N$_4$O$_4$Pt: C, 30.62; H, 3.77; N, 9.52. **MS** (HR-ESI), m/z [M+Na]$^+$: 610.0547.
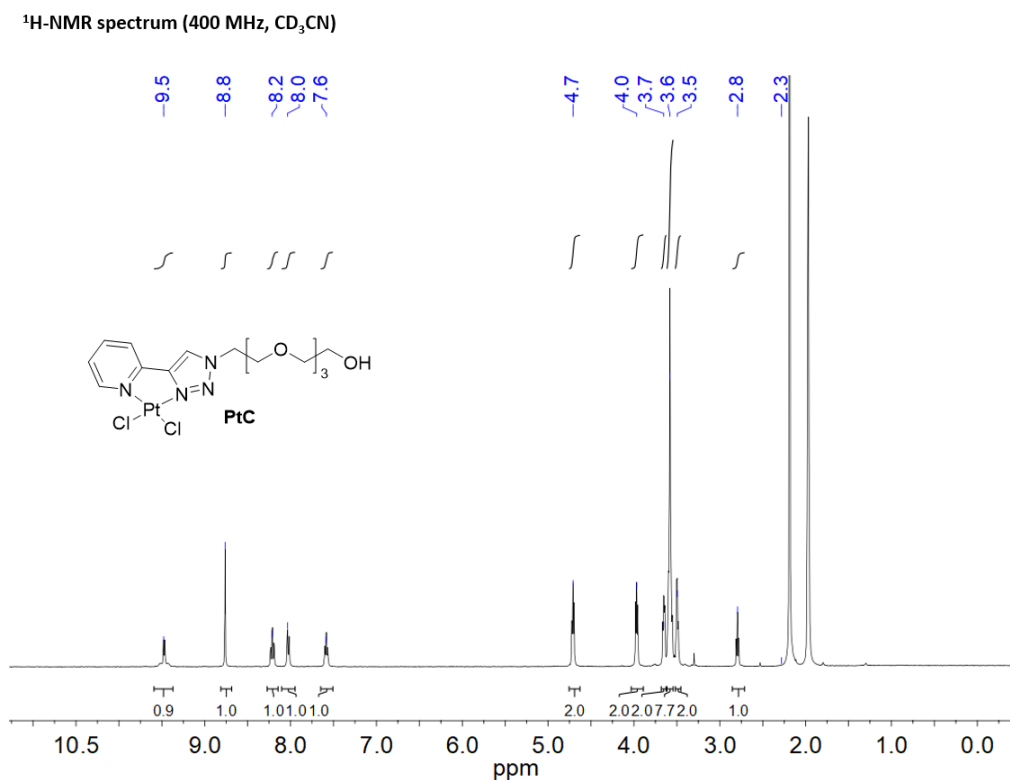
Figure 6.13 ^{1}H NMR (400 MHz) spectrum of **PtC** in CD$_3$CN.

¹³C-NMR spectrum (100 MHz, CD₃CN)

Figure 6.14 ¹³C NMR (100 MHz) spectrum of **PtC** in CD₃CN.

Additional information on the synthesis and analysis is available in the Chemotion repository:

https://dx.doi.org/10.14272/reaction/SA-FUHFF-UHFFFADPSC-QQPOZDZNHN-UHFFFADPSC-NUHFF-LUHFF-NUHFF-ZZZ

6.4.4. Binding studies of PtC with CB7

CB7⊃PtC binding constant determination by fluorescent titration. The binding constant for CB7⊃PtC was determined by DBA, following a reported procedure.[237] The binding isotherm is obtained by fluorescent titration of PtC (50 µM) with increasing concentration of CB7 stock solution in Milli-Q water at 25 °C (λ_{ex} = 300 nm, λ_{em} = 378 nm). (see Figure 6.16 in supplementary data).

$$H + G \leftrightarrows HG \quad\quad H + D \leftrightarrows HD \quad\quad\quad\quad \text{Eq. 1}$$
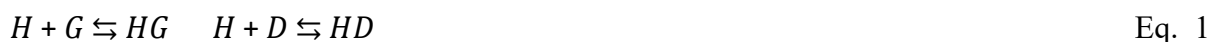
$$I_{em} = \alpha HD \cdot [HD] + \alpha D \cdot [D] \quad\quad\quad\quad \text{Eq. 2}$$

$$K_a\,(HD) = [HD] / [H] \cdot [D] \quad\quad\quad\quad \text{Eq. 3}$$

$$[D]_0 = [D] + [HD] \quad\quad\quad\quad \text{Eq. 4}$$

The obtained binding isotherm was fitted to a binding model derived from Eq. 1–4 to obtain the binding constant (K_a, CB7). All numerical solutions were determined by using the Wolfram Mathematica software (https://github.com/ASDSE/thermosimfit).

NMR-based binding studies of PtC with CB7. ^{1}H NMR spectrum of PtC (500 µM) and mixture of CB7 (500 µM) and PtC (500 µM) was performed in D_2O solvent (see Figure 6.17 in supplementary data).

6.4.5. Performance studies of e-CS

Determination of the LOD values

The linear range of the PB-spiked solutions (PBS and urine) curves was fitted with a linear regression curve. The LOD was calculated using the following equation:

$$LOD = 3.3 \cdot \left(\frac{\sigma_{jox\ at\ 0.9\ V\ of\ CB7 \supset PtC}}{|\ slope\ of\ linear\ fit\ |} \right)$$

Validation and recovery studies

Fluorescence-based validation of the e-CS. The validation studies of the e-CS were performed by fluorescence-based detection of PB following the reported procedure by Poklis and coworkers.[278] To the PB-spiked solution of known concentration (in 5 mM PBS, pH 7.0), rose bengal (50 µM, from a 118 µM stock solution in 0.45 M K_2HPO_4) and $CHCl_3$ (300 µL) were added (V_{final} = 600 µL). The resulting mixture was briefly shaken (2 s) and subsequently

centrifuged at 8000 rpm for 2 min. Subsequently, 200 µL of the CHCl$_3$ layer was transferred to a 96-well isoplate. The fluorescence intensities were measured at 576 nm (λ_{ex} = 546 nm). For validation, the obtained calibration curve was used to determine the PB concentration of the unknown samples. The same unknown samples were determined with the SCV calibration curve. Both the fluorescence-based and e-CS were able to determine the concentration of the unknown samples with good recoveries (see Figure 6.24a and b in supplementary data). The recoveries were calculated from the following equation.

$$\% \ recovery = \frac{[PB]observed - [PB]before \ spiking}{[PB]expected} \times 100$$

LC-MS-based validation of the e-CS. To perform LC-MS-based validation, I followed the reported procedure by Vorce and coworkers.[284] PB-spiked samples in PBS (5 mM, pH 7.0) were used without further treatment and analysed by LC-MS. Both the LC-MS and e-CS were able to determine the concentration of the unknown samples with good recoveries (see Figure 6.24a and c in supplementary data).
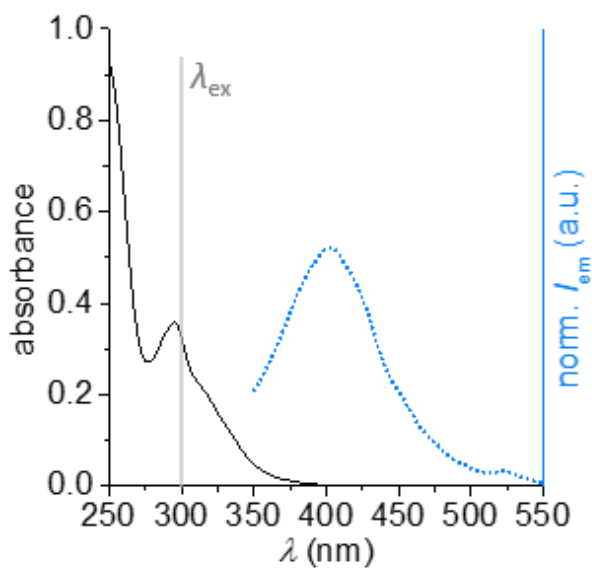
6.5. Supplementary data

Figure 6.15 Absorption and normalized emission spectra (λ_{ex} = 300 nm) of PtC (200 μM) in Milli-Q water.

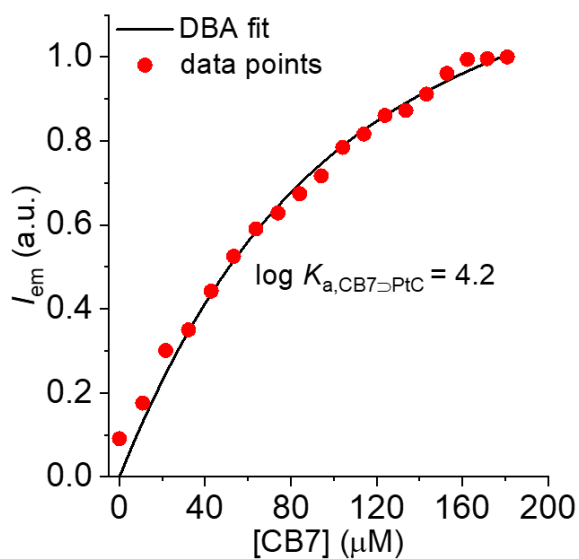**Figure 6.16** Representative DBA isotherm determined by the fluorescent titration experiment of PtC (50 μM) with increasing concentration of CB7 in water (pH 7.0) at 25 °C (λ_{ex} = 300 nm, λ_{em} = 378 nm). The estimated fitting error in log K_a is 0.15.
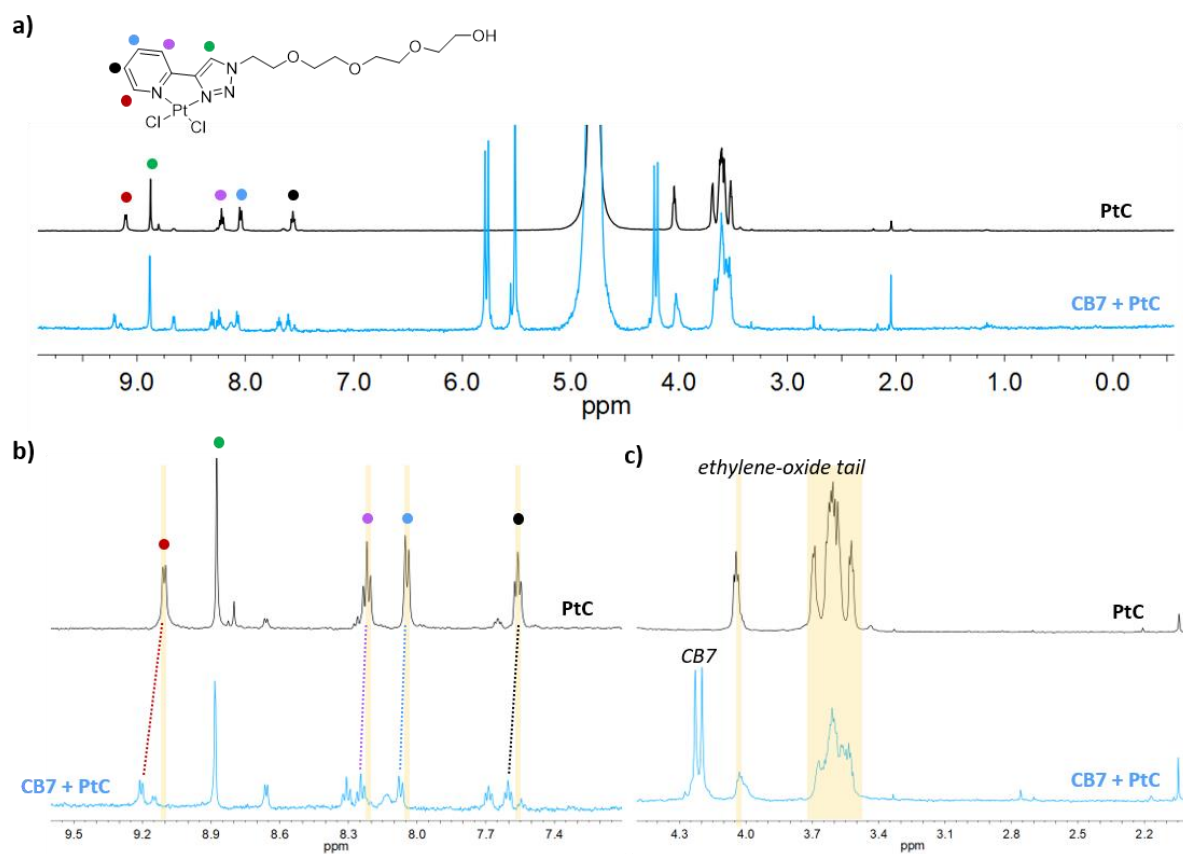
Figure 6.17 (a) ^{1}H NMR spectrum (500 MHz, D$_2$O) of PtC (500 µM) and the mixture of PtC and CB7 (both 500 µM). (b) and (c) Shown are magnified regions of the ^{1}H NMR spectrum of PtC (500 µM) and the mixture of PtC and CB7 (both 500 µM).
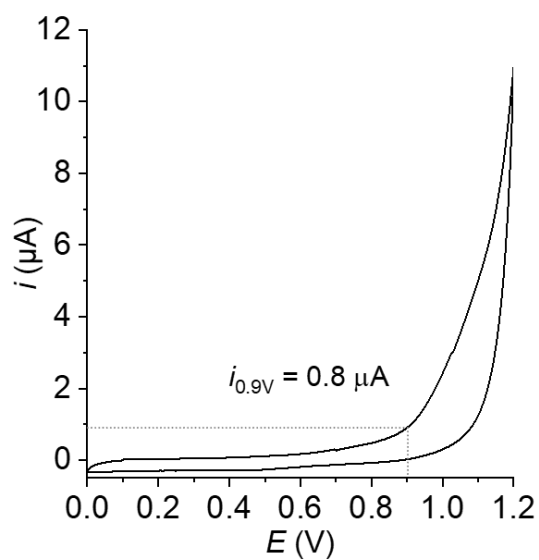
Figure 6.18 CV spectrum of PB (50 µM) in water (scan rate = 50 mV/s).
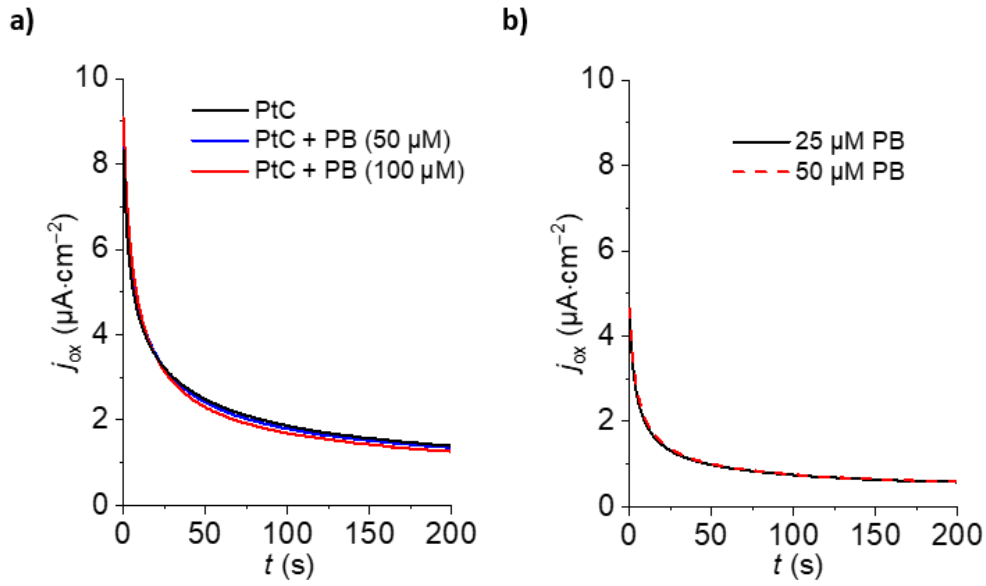
Figure 6.19 (a) Chronoamperometric response curves of PtC (50 μM) without CB7 and in the presence of PB. (b) Chronoamperometric response curves of PB.
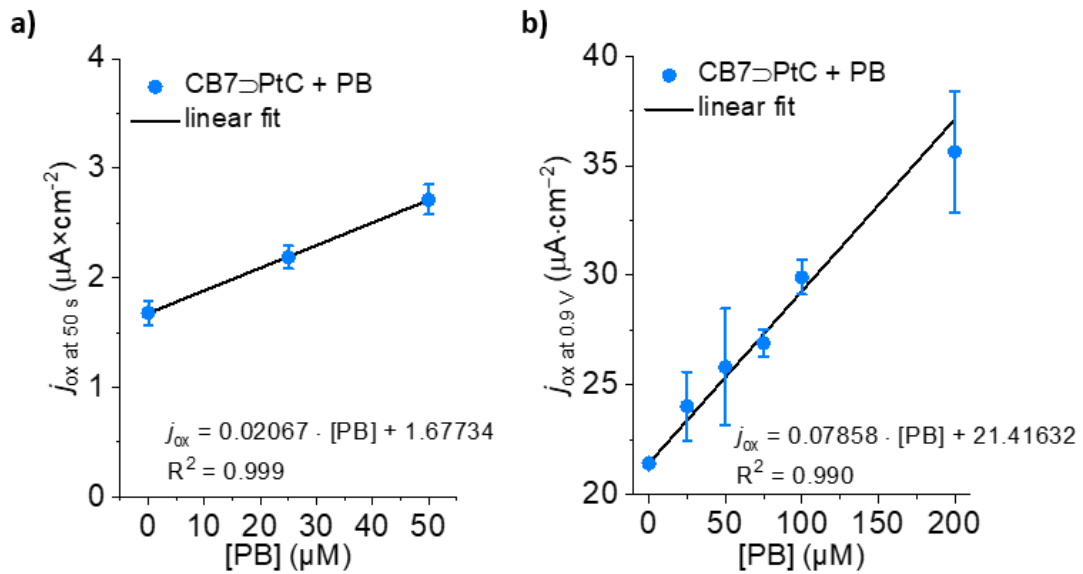
Figure 6.20 (a) The corresponding linear regime of the chronoamperometric response curves used to calculate the LOD. (b) The corresponding linear regime of the SCV response curves used to calculate the LOD.
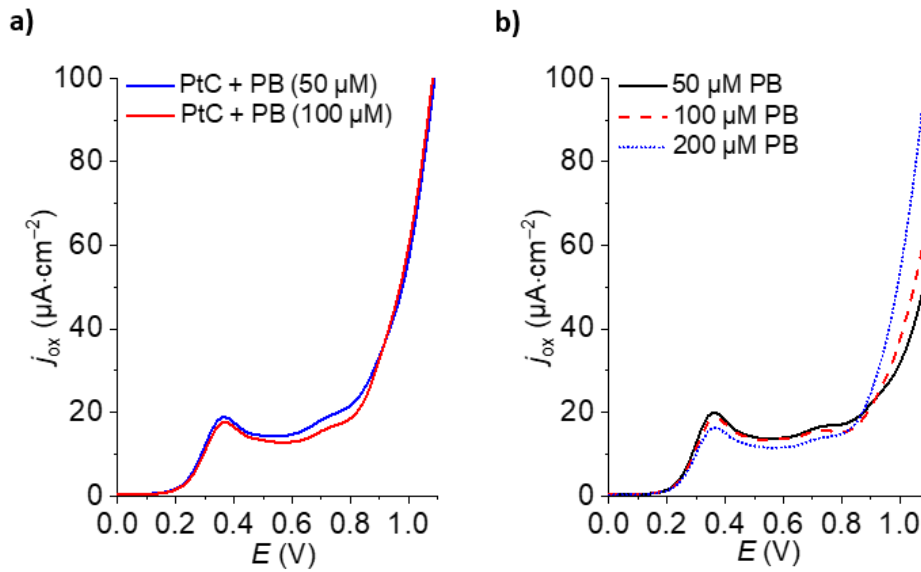
Figure 6.21 (a) SCV response curves of PtC (50 μM) without CB7 and in the presence of PB. (b) SCV response curves of PB.
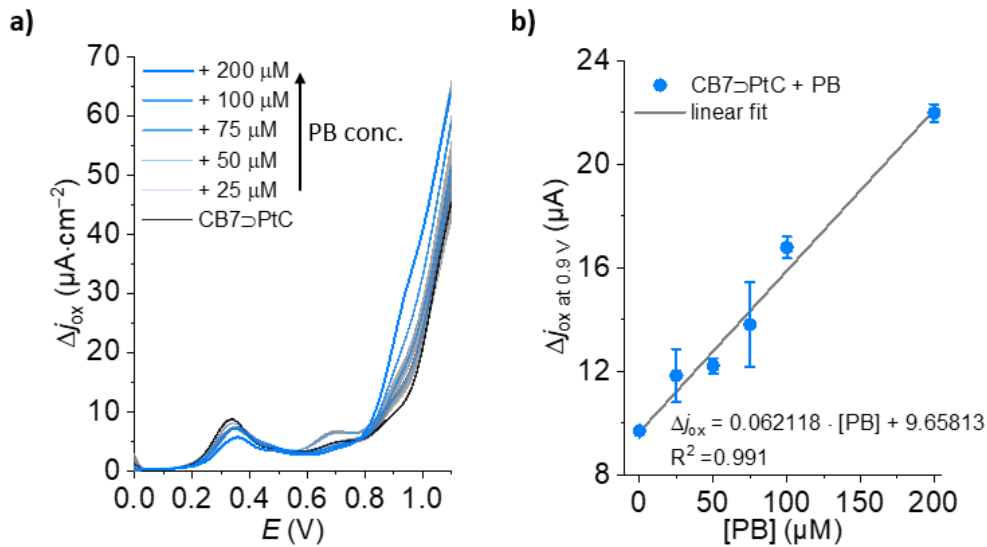
Figure 6.22 (a) DPV response curves of e-CS (CB7 = 50 μM, PtC = 50 μM) in PB-spiked (0 – 200 μM) human urine (1:3 diluted with 5 mM PBS, pH 7.0) and (b) the corresponding linear regime of the DPV response curves used to calculate the LOD. The average Δj_{ox} (coloured lines) and the corresponding standard deviation (σ; grey areas) were calculated from three replica measurements.
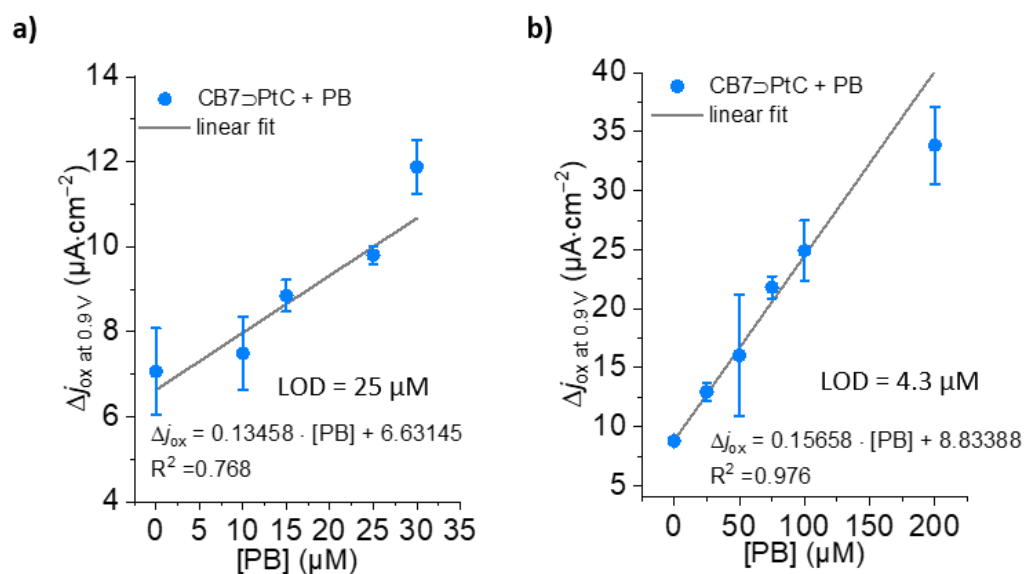
Figure 6.23 DPV response in PB-spiked PBS (5 mM, pH 7.0) with (a) 25 µM CB7⊃PtC and with (b) 50 µM CB7⊃PtC. The average Δj_{ox} and the corresponding standard deviation were calculated from three replica measurements.

a)   *e-CS*

sample	spiked conc. [μM]	detected conc. [μM]	recovery
1	15.0	11.8	79 %
2	30.0	30.0	100 %
3	50.0	47.4	95 %

b)   *fluorescence analysis*

sample	spiked conc. [μM]	detected conc. [μM]	recovery
1	15.0	13.3	89 %
2	30.0	36.4	121 %
3	50.0	50.9	102%

c)   *LC-MS analysis*

sample	spiked conc. [μM]	detected amount [pmol]	detected conc. [μM]	recovery
1	15.0	78.0 ± 3.8	15.6 ± 0.7	104 ± 4.6 %
2	30.0	162.7 ± 4.0	32.5 ± 0.8	108 ± 2.6 %
3	50.0	284.4 ± 5.5	56.8 ± 1.1	113 ± 2.2 %

Figure 6.24 Calibration curve and sample analysis of PB-spiked samples. (a) e-CS results. (b) Fluorescence-based detection (IDA) results. (c) LC-MS-based detection results. Errors are calculated from three replica measurements.

Figure 6.25 Positive MS spectrum of PB. Insets: Shown are the UV-Vis traces and the mass selective detector (MSD) response. The MSD response was used to establish the calibration function and detect PB.

7. Conclusion and outlook

Supramolecular chemosensors based on host-guest chemistry are emerging as a potential sensing platform for molecular diagnostics, offering practical solutions for routine check-ups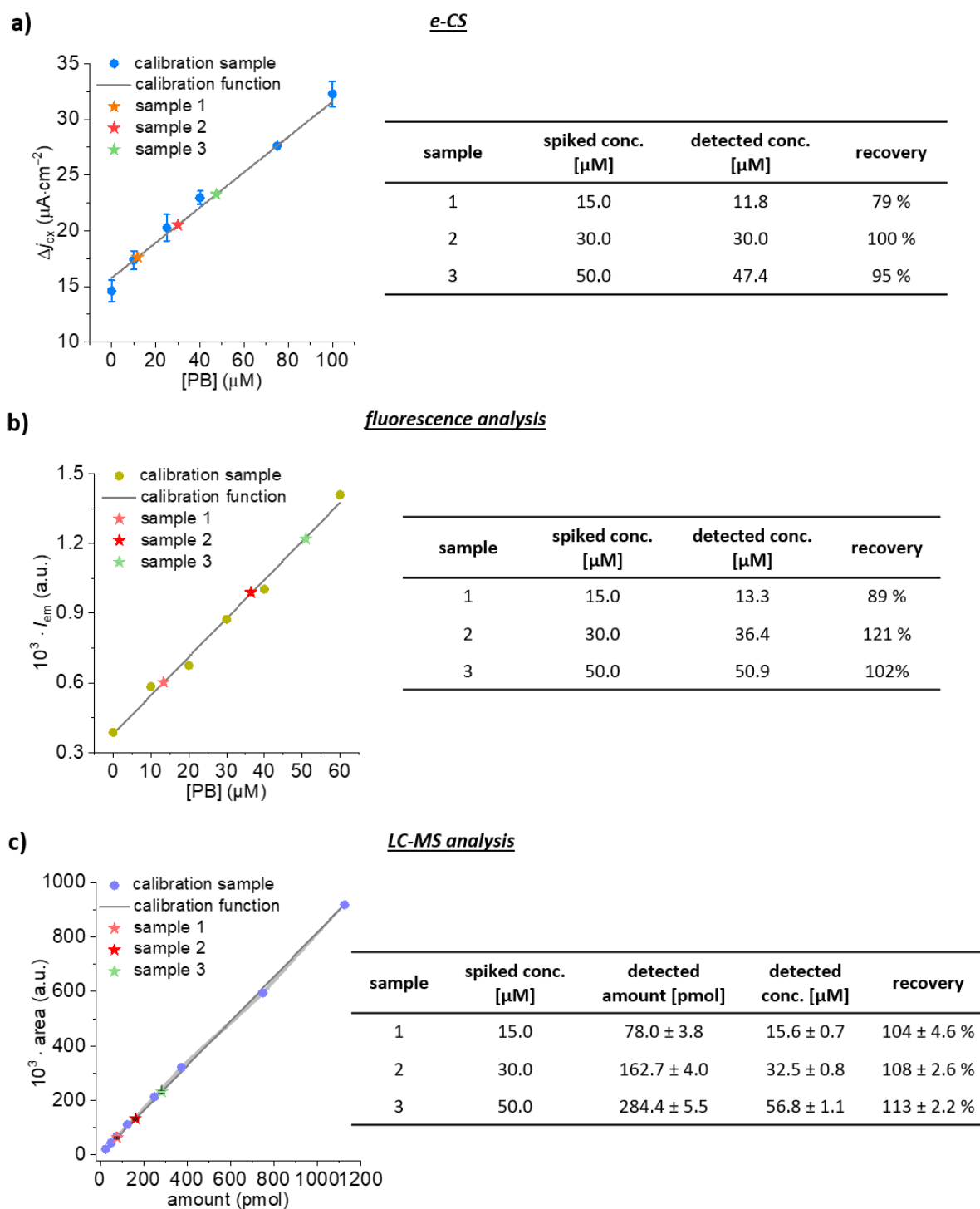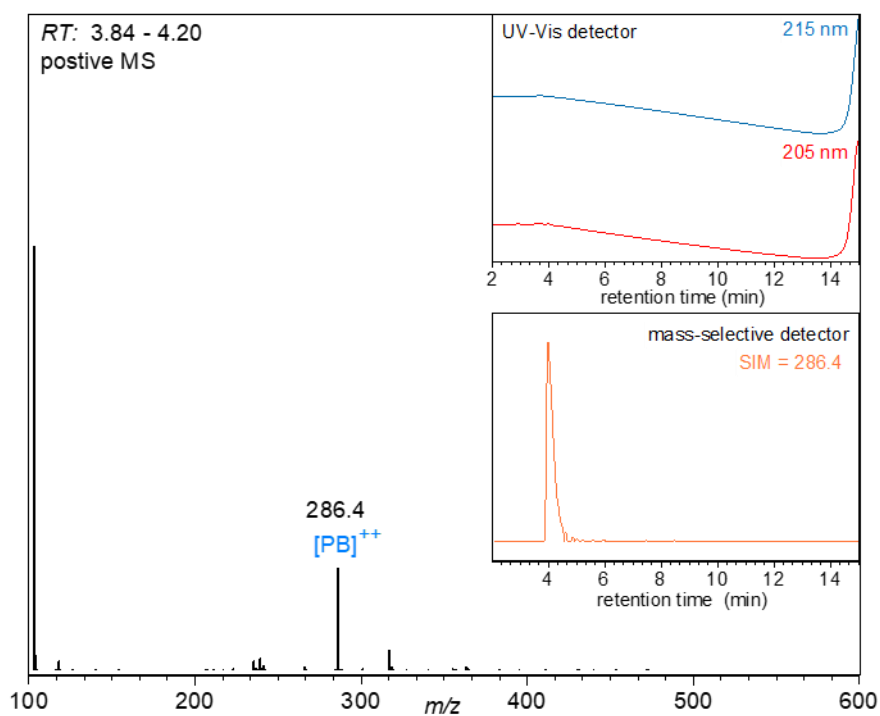 in clinics, at point-of-care units, and in-home settings due to their cost-effectiveness, robustness, high-throughput analysis, and fast-responding nature. Chemosensors consisting of cucurbit[*n*]urils (CB*n*) as the macrocyclic hosts for performing analyte recognition are extensively investigated owing to the characteristic properties of CB*n*, such as exceptional binding affinities to a broad range of biologically relevant analytes and excellent physical and chemical properties. Fluorescence-based sensing strategies are adopted in most CB*n*-based chemosensors. However, the signal-to-noise ratio in these chemosensors is often sub-optimal due to the light interference from background fluorescence caused by emissive components in the sample.

In this doctoral thesis, supramolecular CB*n*-based chemosensors employing novel signal transduction methods for the detection of biologically relevant analytes in biofluids and saline buffers were successfully developed. Specifically, chemiluminescence- and electrochemical-based detection methods have been investigated to develop chemiluminescent chemosensors and electrochemical chemosensors, respectively. These developed sensors can be a useful alternative to the existing fluorescent chemosensors.

Chemiluminescence is the emission of light from chemical reactions. It is widely used as a signal readout in clinical diagnostics, for example, in immunoassays, and provides ultralow sensitivity. Considering the promising applications of chemiluminescence-based systems, developing chemosensors that employ chemiluminescence-based detection methods was investigated. In the first part of the thesis, a supramolecular assay based on a chemiluminescent chemosensor was developed using CB8 as the macrocyclic host and phenoxy 1,2-dioxetane as the chemiluminescent dye and was successfully implemented for the detection of drug molecules in saline media and biofluids (human urine and deproteinized human serum). The ability of CB8 to function as a chemiluminescence performance enhancer for commercially available chemiluminescent probes was shown, which opens further opportunities to modify the existing chemiluminescent assays. Furthermore, a chemiluminescence resonance energy transfer-based assay was realized using CB7-dye conjugate and phenoxy 1,2-dioxetane, which enabled the detection of a herbicide in water.

Electrochemical sensors are emerging as a powerful sensing technique owing to their capability to design miniaturized, disposable, portable, and cost-effective sensors that enable highly sensitive detection of analytes. There are several literature examples of electrochemical sensors that utilize macrocyclic hosts as recognition units for accumulating target analytes on the electrode surfaces. Nevertheless, the design of these electrochemical sensors demands immobilization methods on the electrode surfaces, which are challenging due to the cumbersome process involved, non-specific adsorption of molecules, and stability issues. In this aspect, a new design principle for an electrochemical sensor, which does not require an immobilization process on the electrode surface, was demonstrated in the second part of the thesis and, thus, circumvents the limitations of the existing electrochemical sensors based on host-guest chemistry. Notably, the developed electrochemical sensor can be directly used with commercially available screen-printed electrodes. Specifically, in this work, a CB7-based indicator displacement assay using a platinum(II) triazole-pyridine complex as the electroactive indicator was developed and was applied for the electrochemical detection of redox-inactive analytes in aqueous buffer and human urine.

Overall, the CBn-based chemosensor designs presented in this thesis can offer further opportunities to develop novel supramolecular chemosensors for sensing applications.

As an outlook, exploring liposome-encapsulated chemosensors and their potential application in membrane-selective sensing of analytes would be interesting, as these systems are known to detect analytes more sensitively compared to non-encapsulated chemosensors. For instance, the encapsulation of chemiluminescent chemosensors inside liposomes and studying their sensitive and selective detection of analytes can be envisioned.

Another promising approach is developing chemiluminescent sensing assays combined with signal amplification mechanisms. Specifically, the idea is that the presence of one target molecule can alter the activation of many chemiluminescent dyes, thereby resulting in an amplified signal-to-noise ratio. This can be achieved by employing an enzyme inhibitor, which also acts as an indicator of CBn-based indicator displacement assay. In this strategy, the release of enzyme inhibitors from the CBn cavity upon target analyte binding is expected to act on the enzymes present in the medium and thereby switch off the enzyme activity. Consequently, the chemiluminescence signal is expected to switch off in this method.

These approaches can facilitate the development of robust, cost-effective, and fast-response chemosensors based on host-guest chemistry, offering practical applications for molecular diagnostics.

8. Additional information

pH Meter

The pH of buffer solutions was measured with a FiveEasy Plus pH meter from Mettler Toledo at 25 °C. Hydrochloric acid or sodium hydroxide solution was used for pH adjustments.

Centrifuge

Centrifugation was carried out at room temperature or 4 °C for the serum deproteinization using a centrifuge by Sigma, type 2-16KL.

Pipettes

Volume transfer was performed by Eppendorf research plus single- or 8-channel pipettes with disposable tips (epT.I.P.S.).

Balances

Samples were weighed in Sartorius TE214S and Mettler Toledo XS204 balances (mass > 1.0 g). For samples with mass < 1.0 g, Sartorius SE2-F balance was used.

9. List of abbreviations

Å	Angstrom
A	Analyte
ABA	Associative binding assay
ACN	Acetonitrile
AO	Acridine orange
ALP	Alkaline phosphatase
ATR	Attenuated total reflectance
aq.	Aqueous
BC	Berberine chloride
BET	Back electron transfer
β-CD	β-cyclodextrin
CB5	Cucurbit[5]uril
CB6	Cucurbit[6]uril
CB7	Cucurbit[7]uril
CB8	Cucurbit[8]uril
CBn	Cucurbit[n]uril
CCS	Chemiluminescence-based chemosensor
CDCl$_3$	Deuterated chloroform
CE	Counter electrode
CIEEL	Chemically initiated electron exchange luminescence
CL	Chemiluminescence
CLA	*Cypridina* luciferin analog
CF-N$_3$	Carboxyfluorescein azide
conc.	Concentration
CRET	Chemiluminescence resonance energy transfer
CD	Circular dichroism
CDP-Star	disodium 2-chloro-5-(4-methoxyspiro[1,2-dioxetane-3,2′-(5-chlorotricyclo[3.3.1.1$^{3.7}$]decan])-4-yl]-1-phenyl phosphate
CD$_3$CN	Acetonitrile-D$_3$
CO$_2$	Carbon dioxide
CV	Cyclic voltammetry

CuSO$_4$	Copper(II) sulfate
d	Doublet
dd	Doublet of doublets
dt	Doublet of triplets
D	Dye
DA	Dopamine
DAPI	4',6-diamidino-2-phenylindole
DASPI	(*trans*-4-[4-(dimethylamino)-styryl]-1-methylpyridinium iodide
DBA	Direct binding assay
DCM	Dichloromethane
D$_2$O	Deuterium oxide
DMSO	Dimethyl sulfoxide
DNA	Deoxyribonucleic acid
DPV	Differential pulse voltammetry
DX	3-(4-methoxyspiro[1,2-dioxetane-3,2'tricyclo[3.3.1.1^{3,7}]decan]-4-yl)phenol
EDTA	Ethylenediaminetetraacetic acid
EPI	Epinephrine
ESI-MS	Electrospray ionization mass spectrometry
ET	Energy transfer
e-CS	Electrochemical chemosensor
eq.	Equivalent
eT	Electron transfer
EtOAc	Ethyl acetate
Eq.	Equation
EWG	Electron-withdrawing group
eV	Electron volt
e.g.	exemplari gratia, for example
F	Faraday constant
FARMA	Fluorescent artificial receptor membrane assay
FRET	Fluorescence resonance energy transfer
Fc	Ferrocene
g	gram
G	Guest

GDA	Guest displacement assay
H	Host
H⊃G	Host-guest complex
H⊃D	Host-dye complex
Hz	Hertz
Hex	Hexane
HCl	Hydrochloric acid
HR-ESI	High-resolution electrospray ionization
H_2S	Hydrogen sulfide
HPLC	High-performance liquid chromatography
h	hours
i.e.	id est, that is to say
I_A	Anodic current
I_C	Cathodic current
I_{CL}	Chemiluminescence intensity
IDA	Indicator displacement assay
IC	Internal conversion
IR	Infrared
ISC	Intersystem crossing
J	Coupling constant
K	Kelvin
KCl	Potassium chloride
KH_2PO_4	Dipotassium phosphate
LC-MS	Liquid chromatography-mass spectrometry
LOD	Limit of detection
LDA	Lithium diisopropylamide
L	Litre
M	Molar
MB	Methylene blue
MDAP	2,7-dimethyldiazapyrenium dication
MeOH	Methanol
$MgSO_4$	Magnesium sulfate
Mem	Memantine hydrochloride

MPCP	*N*-Methyl-4-pyridinylium[2.2]paracyclophane
MSD	Mass selective detector
m	Multiplet
mm	Millimetre
min	Minute
mmol	Millimoles
mg	Milligram
mL	Millilitre
mM	Millimolar
mV	Millivolt
MHz	Megahertz
MPCP	*N*-methyl-4-pyridinylium[2.2]paracyclophane
MV^{2+}	Methyl viologen dichloride
nm	Nanometre
nM	Nanomolar
N_2	Nitrogen
NaCl	Sodium chloride
NaOH	Sodium hydroxide
$NaHCO_3$	Sodium bicarbonate
NH_4OH	Ammonium hydroxide
Na_2SO_4	Sodium sulfate
Na_2HPO_4	Disodium hydrogen phosphate
Nan	Nandrolone
NH_3	Ammonia
NMR	Nuclear magnetic resonance
NE	Norepinephrine
O_2	Oxygen
PB	Pancuronium bromide
PBS	Phosphate buffered saline
PC	Packing coefficient
PCA	Principal component analysis
PDI	Perylene bisdiimide
PDO	Phenoxy 1,2-dioxetane

PG	Protecting group
pH	Potential of hydrogen (scale of acidity /basicity)
pK_a	Negative base-10 logarithm of the acid dissociation constant
ppm	Parts per million
PtC	(2-(2-(2-(2-(4-(pyridine-2-yl)-1H-1,2,3-triazole-1-yl)ethoxy)ethoxy)ethoxy)ethan-1-ol)dichloroplatinum(II)
Q	Reaction quotient
r.t.	Room temperature
rpm	Revolutions per minute
R	Universal gas constant
R.E.	Reference electrode
RNA	Ribonucleic acid
RSD	Relative standard deviation
R_f	Retention factor
ssDNA	Single-stranded deoxyribonucleic acid
s	seconds
SAMs	Self-assembled monolayers
SPE	Screen-printed electrode
SCV	Staircase voltammetry
SIM	Single ion mode
t	Triplet
td	Triplet of doublets
T	Temperature
TA	N,N,N-trimethyl-1-adamantylammonium hydroxide
TBATB	Tetrabutylammonium tribromide
TBAF	Tetrabutylammonium fluoride
TBDMSCl	tert-Butyldimethylsilyl chloride
TCPO	bis(2,4,6-trichlorophenyl)oxalate
TEA	Triethylamine
THF	Tetrahydrofuran
TMCD	trimethyl β-cyclodextrin
TRIS	Tris (hydroxymethyl) aminomethane hydrochloride
TsCl	p-toluenesulfonyl chloride

List of abbreviations

TiCl$_4$	Titanium tetrachloride
U	Units
UV-Vis	Ultraviolet-visible
vol	Volume
V	Volt
VR	Vibrational relaxation
W	Watt
W.E.	Working electrode
K_a	Binding constant
°C	Degree Celsius
E	Measured potential
E^0	Standard potential
E_{ox}	Oxidation potential
$E_{1/2}$	Half-way potential
$E^{\circ\prime}$	Formal reduction potential
E_F	Final potential
E_S	Starting potential
E_{SW}	Switching potential
E_p	Pulse height
t_p	Pulse time
σ	Standard deviation
µA	Microampere
µL	Microliter
µm	Micrometer
µM	Micromolar
δ	Chemical shifts
s	Singlet
t	Triplet
ε	Molar extinction coefficient
$λ$	Wavelength
$λ_{ex}$	Excitation wavelength
$λ_{em}$	Emission wavelength
i_{ox}	Anodic peak current intensity

j_{ox} Anodic current density

10. References

1. J.-M. Lehn, *Science*, **1985**, 227, 849-856.

2. S. Kubik, in *Supramol. Chem.*, De Gruyter, Berlin, Boston, **2021**, pp. 555-582.

3. J.-M. Lehn, *Angew. Chem., Int. Ed. Engl.*, **1988**, 27, 89-112.

4. M. J. Webber and R. Langer, *Chem Soc Rev*, **2017**, 46, 6600-6620.

5. X. Ma and Y. Zhao, *Chem. Rev.*, **2015**, 115, 7794-7839.

6. J. Krämer, R. Kang, L. M. Grimm, L. De Cola, P. Picchetti and F. Biedermann, *Chem. Rev.*, **2022**, 122, 3459-3636.

7. S. Kubik, in *Supramol. Chem.*, De Gruyter, Berlin, Boston, **2021**, pp. 37-100.

8. F.-G. Banica, *Chemical sensors and biosensors: fundamentals and applications*, John Wiley & Sons, **2012**.

9. P. Mehrotra, *J. Oral Biol. Craniofac. Res.*, **2016**, 6, 153-159.

10. B. Wang and E. V. Anslyn, *Chemosensors : Principles, Strategies, and Applications*, John Wiley & Sons, Incorporated, **2011**.

11. G. N. Konstantinou, in *Food Allergens: Methods and Protocols*, eds. J. Lin and M. Alcocer, Springer New York, New York, NY, **2017**, pp. 79-94.

12. H. Bisswanger, *Sci. Perspect.*, **2014**, 1, 41-55.

13. S. Ranallo, A. Porchetta and F. Ricci, *Anal. Chem.*, **2019**, 91, 44-59.

14. A. P. F. Turner, *Chem Soc Rev*, **2013**, 42, 3184-3196.

15. S. B. Murugaiyan, R. Ramasamy, N. Gopal and V. Kuzhandaivelu, *Adv. Biomed. Res.*, **2014**, 3, 67.

16. L. C. Clark Jr. and C. Lyons, *Ann. N. Y. Acad. Sci.*, **1962**, 102, 29-45.

17. N. J. Ronkainen, H. B. Halsall and W. R. Heineman, *Chem Soc Rev*, **2010**, 39, 1747-1763.

18. V. Naresh and N. Lee, *Sensors (Basel)*, **2021**, 21.

19. M. Staiano, A. Pennacchio, A. Varriale, A. Capo, A. Majoli, C. Capacchione and S. D'Auria, in *Methods in Enzymology*, eds. R. B. Thompson and C. A. Fierke, Academic Press, **2017**, vol. 589, pp. 115-131.

20. M. Barreiros dos Santos, L. Rodriguez-Lorenzo, R. Queirós and B. Espiña, in *Microfluidics and Biosensors in Cancer Research: Applications in Cancer Modeling and Theranostics*, eds. D. Caballero, S. C. Kundu and R. L. Reis, Springer International Publishing, Cham, **2022**, pp. 3-29.

References

21. H. H. Nguyen, S. H. Lee, U. J. Lee, C. D. Fermin and M. Kim, *Materials (Basel)*, **2019**, 12.

22. G. Rocchitta, A. Spanu, S. Babudieri, G. Latte, G. Madeddu, G. Galleri, S. Nuvoli, P. Bagella, M. I. Demartis, V. Fiore, R. Manetti and P. A. Serra, *Sensors*, **2016**, 16, 780.

23. R. A. Copeland, in *Enzymes*, **2000**, pp. 42-75.

24. M. A. Morales and J. M. Halpern, *Bioconjugate Chem.*, **2018**, 29, 3231-3239.

25. C. I. L. Justino, A. C. Duarte and T. A. P. Rocha-Santos, *Trends Anal. Chem.*, **2016**, 85, 36-60.

26. R. Monosik, M. Stredansky, J. Tkac and E. Sturdik, *Food Anal. Methods*, **2012**, 5, 40-53.

27. B. D. Leca-Bouvier and L. J. Blum, in *Recognition Receptors in Biosensors*, ed. M. Zourob, Springer New York, New York, NY, **2010**, pp. 177-220.

28. G. S. Wilson and Y. Hu, *Chem. Rev.*, **2000**, 100, 2693-2704.

29. J. P. Chambers, B. P. Arulanandam, L. L. Matta, A. Weis and J. J. Valdes, *Curr. Issues Mol. Biol.*, **2008**, 10, 1-12.

30. N. Nikolaus and B. Strehlitz, *Mikrochim. Acta*, **2008**, 160, 15-55.

31. G. Dhawan, G. Sumana and B. D. Malhotra, *Biochem. Eng. J.*, **2009**, 44, 42-52.

32. H. Liu, J. Ge, E. Ma and L. Yang, in *Biomaterials in Translational Medicine*, eds. L. Yang, S. B. Bhaduri and T. J. Webster, Academic Press, **2019**, pp. 213-255.

33. C. I. L. Justino, A. C. Freitas, R. Pereira, A. C. Duarte and T. A. P. Rocha Santos, *Trends Anal. Chem.*, **2015**, 68, 2-17.

34. G. Evtugyn, in *Biosensors: Essentials*, Springer Berlin Heidelberg, Berlin, Heidelberg, **2014**, pp. 21-97.

35. P. B. Luppa, L. J. Sokoll and D. W. Chan, *Clin. Chim. Acta.*, **2001**, 314, 1-26.

36. A. K. Trilling, J. Beekwilder and H. Zuilhof, *Analyst*, **2013**, 138, 1619-1627.

37. M. S. Wilson, *Anal. Chem.*, **2005**, 77, 1496-1502.

38. M. C. Morris, J. Depollier, J. Mery, F. Heitz and G. Divita, *Nat. Biotechnol.*, **2001**, 19, 1173-1176.

39. A. Sassolas, B. D. Leca-Bouvier and L. J. Blum, *Chem. Rev.*, **2008**, 108, 109-139.

40. K. J. Odenthal and J. J. Gooding, *Analyst*, **2007**, 132, 603-610.

41. F. R. R. Teles and L. P. Fonseca, *Talanta*, **2008**, 77, 606-623.

42. Y. Du and S. Dong, *Anal. Chem.*, **2017**, 89, 189-215.

43. B. Huo, Y. Hu, Z. Gao and G. Li, *Talanta*, **2021**, 222, 121565.

44. M. Pedrero, S. Campuzano and J. M. Pingarrón, *Sensors*, **2009**, 9, 5503-5520.

References

45.   I. Palchetti and M. Mascini, *Analyst*, **2008**, 133, 846-854.

46.   D. Dell'Atti, S. Tombelli, M. Minunni and M. Mascini, *Biosens. Bioelectron.*, **2006**, 21, 1876-1879.

47.   K. Chang, S. Deng and M. Chen, *Biosens. Bioelectron.*, **2015**, 66, 297-307.

48.   V. M. Mirsky and A. Yatsimirsky, *Artificial receptors for chemical sensors*, John Wiley & Sons, **2010**.

49.   J. Wankar, N. G. Kotla, S. Gera, S. Rasala, A. Pandit and Y. A. Rochev, *Adv. Funct. Mater.*, **2020**, 30, 1909049.

50.   A. S. Braegelman and M. J. Webber, *Theranostics*, **2019**, 9, 3017-3040.

51.   A. A. Karim, Q. Dou, Z. Li and X. J. Loh, *Chem. Asian J.*, **2016**, 11, 1300-1321.

52.   R. Pinalli, A. Pedrini and E. Dalcanale, *Chem Soc Rev*, **2018**, 47, 7006-7026.

53.   S. Dong, B. Zheng, F. Wang and F. Huang, *Acc. Chem. Res.*, **2014**, 47, 1982-1994.

54.   J. Zhou, G. Yu and F. Huang, *Chem Soc Rev*, **2017**, 46, 7021-7053.

55.   E. M. Peck and B. D. Smith, in *Synthetic Receptors for Biomolecules: Design Principles and Applications*, ed. B. Smith, The Royal Society of Chemistry, **2015**, p. 0.

56.   H.-J. Schneider, *Angew. Chem. Int. Ed.*, **2009**, 48, 3924-3977.

57.   S. Kubik, in *Supramol. Chem.*, De Gruyter, Berlin, Boston, **2021**, pp. 101-244.

58.   L. Escobar and P. Ballester, *Chem. Rev.*, **2021**, 121, 2445-2514.

59.   J. Murray, K. Kim, T. Ogoshi, W. Yao and B. C. Gibb, *Chem Soc Rev*, **2017**, 46, 2479-2496.

60.   Q. Shi, X. Wang, B. Liu, P. Qiao, J. Li and L. Wang, *Chem. Commun.*, **2021**, 57, 12379-12405.

61.   D.-S. Guo, V. D. Uzunova, K. I. Assaf, A. I. Lazar, Y. Liu and W. M. Nau, *Supramol. Chem.*, **2016**, 28, 384-395.

62.   X. Shu, K. Xu, D. Hou and C. Li, *Isr. J. Chem.*, **2018**, 58, 1230-1240.

63.   R. N. Dsouza, U. Pischel and W. M. Nau, *Chem. Rev.*, **2011**, 111, 7941-7980.

64.   M. T. Albelda, J. C. Frías, E. García-España and H.-J. Schneider, *Chem Soc Rev*, **2012**, 41, 3859-3877.

65.   S. K. Sahoo, D. Sharma, R. K. Bera, G. Crisponi and J. F. Callan, *Chem Soc Rev*, **2012**, 41, 7195-7227.

66.   O. F. Sayo, L. Mark, A. F. Kristin, H. Xiaodong, M. P. Aleeta and M. W. Isiah, *Curr. Anal. Chem.*, **2007**, 3, 171-181.

References

67. D. Wu, A. C. Sedgwick, T. Gunnlaugsson, E. U. Akkaya, J. Yoon and T. D. James, *Chem Soc Rev*, **2017**, 46, 7105-7123.

68. Z. Kotková, J. Kotek, D. Jirák, P. Jendelová, V. Herynek, Z. Berková, P. Hermann and I. Lukeš, *Chemistry*, **2010**, 16, 10094-10102.

69. Y. Li, J. Wen, J. Li, Z. Wu, W. Li and K. Yang, *ACS Sens.*, **2021**, 6, 3882-3897.

70. L. You, D. Zha and E. V. Anslyn, *Chem. Rev.*, **2015**, 115, 7840-7892.

71. T. L. Mako, J. M. Racicot and M. Levine, *Chem. Rev.*, **2019**, 119, 322-477.

72. S. L. Wiskur, H. Ait-Haddou, J. J. Lavigne and E. V. Anslyn, *Acc. Chem. Res.*, **2001**, 34, 963-972.

73. A. C. Sedgwick, J. T. Brewster, T. Wu, X. Feng, S. D. Bull, X. Qian, J. L. Sessler, T. D. James, E. V. Anslyn and X. Sun, *Chem Soc Rev*, **2021**, 50, 9-38.

74. S. Sinn and F. Biedermann, *Isr. J. Chem.*, **2018**, 58, 357-412.

75. S. Sinn, J. Krämer and F. Biedermann, *Chem. Commun.*, **2020**, 56, 6620-6623.

76. F. Biedermann, D. Hathazi and W. M. Nau, *Chem. Commun.*, **2015**, 51, 4977-4980.

77. B. Wang, E. V. Anslyn in *Chemosensors*, John Wilet & Sons, Inc., **2011**, pp. 227-228.

78. J. R. Lakowicz, in *Principles of Fluorescence Spectroscopy*, Springer US, Boston, MA, **2006**, pp. 1-26.

79. B. Valeur and M. N. Berberan-Santos, in *Molecular Fluorescence*, **2012**, pp. 53-74.

80. M. Kasha, *Faraday Discuss.*, **1950**, 9, 14-19.

81. R. Parkesh, E. B. Veale and T. Gunnlaugsson, in *Chemosensors*, John Wilet & Sons, Inc., **2011**, pp. 229-252.

82. G. N. Lewis and M. Kasha, *J. Am. Chem. Soc.*, **1944**, 66, 2100-2116.

83. M. Formica, V. Fusi, L. Giorgi and M. Micheloni, *Coord. Chem. Rev.*, **2012**, 256, 170-192.

84. G. Ghale and W. M. Nau, *Acc. Chem. Res.*, **2014**, 47, 2150-2159.

85. C. Jiang, Z. Song, L. Yu, S. Ye and H. He, *Trends Anal. Chem.*, **2020**, 133, 116086.

86. J.-F. Chen, Q. Lin, Y.-M. Zhang, H. Yao and T.-B. Wei, *Chem. Commun.*, **2017**, 53, 13296-13311.

87. M. Vacher, I. Fdez. Galván, B.-W. Ding, S. Schramm, R. Berraud-Pache, P. Naumov, N. Ferré, Y.-J. Liu, I. Navizet, D. Roca-Sanjuán, W. J. Baader and R. Lindh, *Chem. Rev.*, **2018**, 118, 6927-6974.

88. M. A. Tzani, D. K. Gioftsidou, M. G. Kallitsakis, N. V. Pliatsios, N. P. Kalogiouri, P. A. Angaridis, I. N. Lykakis and M. A. Terzidis, *Molecules*, **2021**, 26, 7664.

89. Z. Wang, J. Huang, J. Huang, B. Yu, K. Pu and F.-J. Xu, *Aggregate*, **2021**, 2, e140.

References

90. I. Navizet, Y.-J. Liu, N. Ferré, D. Roca-Sanjuán and R. Lindh, *ChemPhysChem*, **2011**, 12, 3064-3076.

91. N. Hananya and D. Shabat, *Angew. Chem. Int. Ed.*, **2017**, 56, 16454-16463.

92. R. Blau, O. Shelef, D. Shabat and R. Satchi-Fainaro, *Nat. Rev. Bioeng.*, **2023**, 1, 648-664.

93. I. Bronstein, J. Fortin, P. E. Stanley, G. S. A. B. Stewart and L. J. Kricka, *Anal. Biochem.*, **1994**, 219, 169-181.

94. L. Chen, Y. Chen, W. Zhou, J. Li, Y. Zhang and Y. Liu, *Chem. Commun.*, **2020**, 56, 8857-8860.

95. C. Dodeigne, L. Thunus and R. Lejeune, *Talanta*, **2000**, 51, 415-439.

96. O. Green, T. Eilon, N. Hananya, S. Gutkin, C. R. Bauer and D. Shabat, *ACS Cent. Sci.*, **2017**, 3, 349-358.

97. N. Hananya and D. Shabat, *ACS Cent. Sci.*, **2019**, 5, 949-959.

98. L. J. Kricka, *Anal. Chim. Acta*, **2003**, 500, 279-286.

99. G. C. Van de Bittner, E. A. Dubikovskaya, C. R. Bertozzi and C. J. Chang, *Proc. Natl. Acad. Sci. U.S.A.*, **2010**, 107, 21316-21321.

100. A. Roda and M. Guardigli, *Anal. Biochem.*, **2012**, 402, 69-76.

101. A. Roda, P. Pasini, M. Mirasoli, E. Michelini and M. Guardigli, *Trends Biotechnol.*, **2004**, 22, 295-303.

102. W. R. G. Baeyens, S. G. Schulman, A. C. Calokerinos, Y. Zhao, A. M. García Campaña, K. Nakashima and D. De Keukeleire, *J. Pharm. Biomed. Anal.*, **1998**, 17, 941-953.

103. G. Merényi, J. Lind and T. E. Eriksen, *J. biolumin. chemilumin.*, **1990**, 5, 53-56.

104. S. M. Silva, F. Casallanovo Jr, K. H. Oyamaguchi, L. F. L. M. Ciscato, C. V. Stevani and W. J. Baader, *Luminescence*, **2002**, 17, 313-320.

105. M. Nakano, K. Sugioka, Y. Ushijima and T. Goto, *Anal. Biochem.*, **1986**, 159, 363-369.

106. D. Lee, S. Khaja, J. C. Velasquez-Castano, M. Dasari, C. Sun, J. Petros, W. R. Taylor and N. Murthy, *Nat. Mater.*, **2007**, 6, 765-769.

107. N. Zhang, K. P. Francis, A. Prakash and D. Ansaldi, *Nat. Med.*, **2013**, 19, 500-505.

108. M. Yang, J. Huang, J. Fan, J. Du, K. Pu and X. Peng, *Chem Soc Rev*, **2020**, 49, 6800-6815.

109. A. P. Schaap and S. D. Gagnon, *J. Am. Chem. Soc.*, **1982**, 104, 3504-3506.

110. A. P. Schaap, H. Akhavan and L. J. Romano, *Clin. Chem.*, **1989**, 35, 1863-1864.

References

111. A. P. Schaap, M. D. Sandison and R. S. Handley, *Tetrahedron Lett.*, **1987**, 28, 1159-1162.

112. A. P. Schaap, R. S. Handley and B. P. Giri, *Tetrahedron Lett.*, **1987**, 28, 935-938.

113. A. P. Schaap, T.-S. Chen, R. S. Handley, R. DeSilva and B. P. Giri, *Tetrahedron Lett.*, **1987**, 28, 1155-1158.

114. W. Adam, I. Bronstein, A. V. Trofimov and R. F. Vasil'ev, *J. Am. Chem. Soc.*, **1999**, 121, 958-961.

115. L. Yue and Y.-J. Liu, *J. Chem. Theory Comput.*, **2013**, 9, 2300-2312.

116. S. Gnaim, O. Green and D. Shabat, *Chem. Commun.*, **2018**, 54, 2073-2085.

117. M. Matsumoto, Y. Mizoguchi, T. Motoyama and N. Watanabe, *Tetrahedron Lett.*, **2001**, 42, 8869-8872.

118. N. Hananya, A. Eldar Boock, C. R. Bauer, R. Satchi-Fainaro and D. Shabat, *J. Am. Chem. Soc.*, **2016**, 138, 13438-13446.

119. U. Haris and A. R. Lippert, *ACS Sens.*, **2023**, 8, 3-11.

120. O. Green, S. Gnaim, R. Blau, A. Eldar-Boock, R. Satchi-Fainaro and D. Shabat, *J. Am. Chem. Soc.*, **2017**, 139, 13243-13248.

121. M. Roth-Konforti, O. Green, M. Hupfeld, L. Fieseler, N. Heinrich, J. Ihssen, R. Vorberg, L. Wick, U. Spitz and D. Shabat, *Angew. Chem. Int. Ed.*, **2019**, 58, 10361-10367.

122. B. Gu, C. Dong, R. Shen, J. Qiang, T. Wei, F. Wang, S. Lu and X. Chen, *Sens. Actuators B Chem.*, **2019**, 301, 127111.

123. I. Bronstein, B. Edwards and J. C. Voyta, *J. biolumin. chemilumin.*, **1989**, 4, 99-111.

124. J.-A. Richard, L. Jean, A. Romieu, M. Massonneau, P. Noack-Fraissignes and P.-Y. Renard, *Org. Lett.*, **2007**, 9, 4853-4855.

125. L. Liu and R. P. Mason, *PLOS ONE*, **2010**, 5, e12024.

126. J. Cao, R. Lopez, J. Thacker, J. Moon, C. Jiang, S. Morris, J. Bauer, P. Tao, R. Mason and A. Lippert, *Chem. Sci.*, **2015**, 6, 1979-1985.

127. J. Cao, J. Campbell, L. Liu, R. P. Mason and A. R. Lippert, *Anal. Chem.*, **2016**, 88, 4995-5002.

128. S. Gnaim, A. Scomparin, A. Eldar-Boock, C. R. Bauer, R. Satchi-Fainaro and D. Shabat, *Chem. Sci.*, **2019**, 10, 2945-2955.

129. S. He, W. Shi, X. Zhang, J. Li and Y. Huang, *Talanta*, **2010**, 82, 377-383.

130. S. R. Bayly, G. Z. Chen and P. D. Beer, in *Chemosensors*, **2011**, pp. 297-328.

131. D. Mandler, *Anal. Biochem.*, **2010**, 398, 2771-2772.

132. W. Vonau, in *Encyclopedia of Applied Electrochemistry*, eds. G. Kreysa, K.-i. Ota and R. F. Savinell, Springer New York, New York, NY, **2014**, pp. 1692-1697.

133. E. Bakker and E. Pretsch, *Trends Anal. Chem.*, **2001**, 20, 11-19.

134. O. Özbek, C. Berkel and Ö. Isildak, *Crit. Rev. Anal. Chem*, **2022**, 52, 768-779.

135. M. Parrilla, M. Cuartero and G. A. Crespo, *Trends Anal. Chem.*, **2019**, 110, 303-320.

136. R. De Marco, G. Clarke and B. Pejcic, *Electroanalysis*, **2007**, 19, 1987-2001.

137. L. Khalafi, A. M. Cunningham, L. E. Hoober-Burkhardt and M. Rafiee, *J. Chem. Educ.*, **2021**, 98, 3957-3961.

138. C. Sandford, M. A. Edwards, K. J. Klunder, D. P. Hickey, M. Li, K. Barman, M. S. Sigman, H. S. White and S. D. Minteer, *Chem. Sci.*, **2019**, 10, 6404-6422.

139. S. Ramotowska, A. Ciesielska and M. Makowski, *Molecules*, **2021**, 26, 3478.

140. A. J. Bard, L. R. Faulkner and H. S. White, *Electrochemical methods: fundamentals and applications*, John Wiley & Sons, **2022**.

141. J. Osteryoung, *Acc. Chem. Res.*, **1993**, 26, 77-83.

142. A. Chen and B. Shah, *Analytical Methods*, **2013**, 5, 2158-2173.

143. S. A. Ozkan, J.-M. Kauffmann and P. Zuman, in *Electroanalysis in Biomedical and Pharmaceutical Sciences: Voltammetry, Amperometry, Biosensors, Applications*, Springer Berlin Heidelberg, Berlin, Heidelberg, **2015**, pp. 45-81.

144. C. Francesco, *J. New Dev. Chem.*, **2020**, 2, 20-28.

145. V. Mirceski, S. Skrzypek and L. Stojanov, *ChemTexts*, **2018**, 4, 17.

146. A. Amine and H. Mohammadi, in *Encyclopedia of Analytical Science (Third Edition)*, eds. P. Worsfold, C. Poole, A. Townshend and M. Miró, Academic Press, Oxford, **2019**, pp. 85-98.

147. F. S. Felix and L. Angnes, *J. Pharm. Sci.*, **2010**, 99, 4784-4804.

148. M. Rafiee, D. J. Abrams, L. Cardinale, Z. Goss, A. Romero-Arenas and S. S. Stahl, *Chem Soc Rev*, **2024**, 53, 566-585.

149. M. Labib, E. H. Sargent and S. O. Kelley, *Chem. Rev.*, **2016**, 116, 9001-9090.

150. M. Li, D.-W. Li, G. Xiu and Y.-T. Long, *Curr. Opin. Electrochem.*, **2017**, 3, 137-143.

151. J. S. Stefano, L. O. Orzari, H. A. Silva-Neto, V. N. de Ataíde, L. F. Mendes, W. K. T. Coltro, T. R. Longo Cesar Paixão and B. C. Janegitz, *Curr. Opin. Electrochem.*, **2022**, 32, 100893.

152. A. García-Miranda Ferrari, S. J. Rowley-Neale and C. E. Banks, *Talanta Open*, **2021**, 3, 100032.

153. R. A. S. Couto, J. L. F. C. Lima and M. B. Quinaz, *Talanta*, **2016**, 146, 801-814.

154. M. del Pozo, J. Mejías, P. Hernández and C. Quintana, *Sens. Actuators B Chem.*, **2014**, 193, 62-69.

155. M. del Pozo, P. Hernández, L. Hernández and C. Quintana, *J. Mater. Chem.*, **2011**, 21, 13657-13663.

156. C. Quintana, S. Suárez and L. Hernández, *Sens. Actuators B Chem.*, **2010**, 149, 129-135.

157. E. Wajs, N. Fernández and A. Fragoso, *Analyst*, **2016**, 141, 3274-3279.

158. L. Qi, R. Wang and H. Z. Yu, *Anal. Chem.*, **2020**, 92, 2168-2175.

159. M. W. J. Beulen, M. I. Kastenberg, F. C. J. M. van Veggel and D. N. Reinhoudt, *Langmuir*, **1998**, 14, 7463-7467.

160. S. J. Barrow, S. Kasera, M. J. Rowland, J. del Barrio and O. A. Scherman, *Chem. Rev.*, **2015**, 115, 12320-12406.

161. J. Lagona, P. Mukhopadhyay, S. Chakrabarti and L. Isaacs, *Angew. Chem. Int. Ed.*, **2005**, 44, 4844-4870.

162. W. A. Freeman, W. L. Mock and N. Y. Shih, *J. Am. Chem. Soc.*, **1981**, 103, 7367-7368.

163. J. Kim, I.-S. Jung, S.-Y. Kim, E. Lee, J.-K. Kang, S. Sakamoto, K. Yamaguchi and K. Kim, *J. Am. Chem. Soc.*, **2000**, 122, 540-541.

164. L. Cao, M. Šekutor, P. Y. Zavalij, K. Mlinarić-Majerski, R. Glaser and L. Isaacs, *Angew. Chem. Int. Ed.*, **2014**, 53, 988-993.

165. F. Biedermann, W. M. Nau and H.-J. Schneider, *Angew. Chem. Int. Ed.*, **2014**, 53, 11158-11171.

166. F. Biedermann, V. D. Uzunova, O. A. Scherman, W. M. Nau and A. De Simone, *J. Am. Chem. Soc.*, **2012**, 134, 15318-15323.

167. G. Huber, F.-X. Legrand, V. Lewin, D. Baumann, M.-P. Heck and P. Berthault, *ChemPhysChem*, **2011**, 12, 1053-1055.

168. K. A. Kellersberger, J. D. Anderson, S. M. Ward, K. E. Krakowiak and D. V. Dearden, *J. Am. Chem. Soc.*, **2001**, 123, 11316-11317.

169. Y. Miyahara, K. Abe and T. Inazu, *Angew. Chem. Int. Ed.*, **2002**, 41, 3020-3023.

170. J. W. Lee, S. Samal, N. Selvapalam, H.-J. Kim and K. Kim, *Acc. Chem. Res.*, **2003**, 36, 621-630.

171. A. I. Lazar, F. Biedermann, K. R. Mustafina, K. I. Assaf, A. Hennig and W. M. Nau, *J. Am. Chem. Soc.*, **2016**, 138, 13022-13029.

References

172. J. Vázquez , P. Remón , R. N. Dsouza, A. I. Lazar, J. F. Arteaga, W. M. Nau and U. Pischel, *Chem. Eur. J.*, **2014**, 20, 9897-9901.

173. W. Li and A. E. Kaifer, *Organometallics*, **2013**, 32, 6091-6097.

174. M. Y. Hur, J. Murray and K. Kim, in *Cucurbiturils and Related Macrocycles*, ed. K. Kim, The Royal Society of Chemistry, **2019**, p. 0.

175. A. Day, A. P. Arnold, R. J. Blanch and B. Snushall, *J. Org. Chem.*, **2001**, 66, 8094-8100.

176. D. Lucas, T. Minami, G. Iannuzzi, L. Cao, J. B. Wittenberg, P. Anzenbacher, Jr. and L. Isaacs, *J. Am. Chem. Soc.*, **2011**, 133, 17966-17976.

177. S. Y. Jon, N. Selvapalam, D. H. Oh, J. K. Kang, S. Y. Kim, Y. J. Jeon, J. W. Lee and K. Kim, *J. Am. Chem. Soc.*, **2003**, 125, 10186-10187.

178. N. Dong, J. He, T. Li, A. Peralta, M. R. Avei, M. Ma and A. E. Kaifer, *J. Org. Chem.*, **2018**, 83, 5467-5473.

179. F. Biedermann and H.-J. Schneider, *Chem. Rev.*, **2016**, 116, 5216-5300.

180. S. Mecozzi and J. Rebek, Julius, *Chem. Eur. J.*, **1998**, 4, 1016-1022.

181. W. M. Nau, M. Florea and K. I. Assaf, *Isr. J. Chem.*, **2011**, 51, 559-577.

182. K. I. Assaf and W. M. Nau, *Chem Soc Rev*, **2015**, 44, 394-418.

183. V. D. Uzunova, C. Cullinane, K. Brix, W. M. Nau and A. I. Day, *Org. Biomol. Chem.*, **2010**, 8, 2037-2042.

184. N. Saleh, I. Ghosh and W. M. Nau, in *Supramolecular Systems in Biomedical Fields*, ed. H.-J. Schneider, The Royal Society of Chemistry, **2013**, p. 0.

185. A. Aktanova, T. Abramova, E. Pashkina, O. Boeva, L. Grishina, E. Kovalenko and V. Kozlov, *Nanomaterials*, **2021**, 11, 1356.

186. A. Praetorius, D. M. Bailey, T. Schwarzlose and W. M. Nau, *Org. Lett.*, **2008**, 10, 4089-4092.

187. A. E. Kaifer, W. Li and S. Yi, *Isr. J. Chem.*, **2011**, 51, 496-505.

188. K. M. Park, J. Kim, Y. H. Ko, Y. Ahn, J. Murray, M. Li, A. Shrinidhi and K. Kim, *Bull. Chem. Soc. Jpn.*, **2017**, 91, 95-99.

189. M. E. Bush, N. D. Bouley and A. R. Urbach, *J. Am. Chem. Soc.*, **2005**, 127, 14511-14517.

190. J. M. Chinai, A. B. Taylor, L. M. Ryno, N. D. Hargreaves, C. A. Morris, P. J. Hart and A. R. Urbach, *J. Am. Chem. Soc.*, **2011**, 133, 8810-8813.

191. W. Li, A. T. Bockus, B. Vinciguerra, L. Isaacs and A. R. Urbach, *Chem. Commun.*, **2016**, 52, 8537-8540.

References

192. S. Kasera, Z. Walsh, J. del Barrio and O. A. Scherman, *Supramol. Chem.*, **2014**, 26, 280-285.

193. S. Zhang, K. I. Assaf, C. Huang, A. Hennig and W. M. Nau, *Chem. Commun.*, **2019**, 55, 671-674.

194. A. Prabodh, D. Bauer, S. Kubik, P. Rebmann, F. G. Klärner, T. Schrader, L. Delarue Bizzini, M. Mayor and F. Biedermann, *Chem. Commun.*, **2020**, 56, 4652-4655.

195. A. Prabodh, Y. Wang, S. Sinn, P. Albertini, C. Spies, E. Spuling, L.-P. Yang, W. Jiang, S. Bräse and F. Biedermann, *Chem. Sci.*, **2021**, 12, 9420-9431.

196. V. Iglesias, M. R. Avei, S. Bruña, I. Cuadrado and A. E. Kaifer, *J. Org. Chem.*, **2017**, 82, 415-419.

197. W. S. Jeon, K. Moon, S. H. Park, H. Chun, Y. H. Ko, J. Y. Lee, E. S. Lee, S. Samal, N. Selvapalam, M. V. Rekharsky, V. Sindelar, D. Sobransingh, Y. Inoue, A. E. Kaifer and K. Kim, *J. Am. Chem. Soc.*, **2005**, 127, 12984-12989.

198. Y. Ling, J. T. Mague and A. E. Kaifer, *Chem. Eur. J.*, **2007**, 13, 7908-7914.

199. W. Ong and A. E. Kaifer, *Organometallics*, **2003**, 22, 4181-4183.

200. D. Sobransingh and A. E. Kaifer, *Langmuir*, **2006**, 22, 10540-10544.

201. Y. H. Ko, E. Kim, I. Hwang and K. Kim, *Chem. Commun.*, **2007**, 1305-1315.

202. H.-J. Kim, W. S. Jeon, Y. H. Ko and K. Kim, *Proc. Natl. Acad. Sci. U.S.A.*, **2002**, 99, 5007-5011.

203. H. Li, H. Xie, Y. Cao, X. Ding, Y. Yin and G. Li, *Anal. Chem.*, **2013**, 85, 1047-1052.

204. R. N. Dsouza, A. Hennig and W. M. Nau, *Chem. Eur. J.*, **2012**, 18, 3444-3459.

205. A. Hennig, H. Bakirci and W. M. Nau, *Nat. Methods.*, **2007**, 4, 629-632.

206. D. M. Bailey, A. Hennig, V. D. Uzunova and W. M. Nau, *Chem. Eur. J.*, **2008**, 14, 6069-6077.

207. G. Ghale, V. Ramalingam, A. R. Urbach and W. M. Nau, *J. Am. Chem. Soc.*, **2011**, 133, 7528-7535.

208. W. M. Nau, G. Ghale, A. Hennig, H. Bakirci and D. M. Bailey, *J. Am. Chem. Soc.*, **2009**, 131, 11558-11570.

209. G. Ghale, A. G. Lanctôt, H. T. Kreissl, M. H. Jacob, H. Weingart, M. Winterhalter and W. M. Nau, *Angew. Chem. Int. Ed.*, **2014**, 53, 2762-2765.

210. F. Biedermann, G. Ghale, A. Hennig and W. M. Nau, *Commun. Biol.*, **2020**, 3, 383.

211. N. M. Kumar, P. Picchetti, C. Hu, L. M. Grimm and F. Biedermann, *ACS Sens.*, **2022**, 7, 2312-2319.

212. T. W. Bell and N. M. Hext, *Chem Soc Rev*, **2004**, 33, 589-598.

213. A. Ueno, T. Kuwabara, A. Nakamura and F. Toda, *Nature*, **1992**, 356, 136-137.

214. T. Ogoshi, M. Hashizume, T.-a. Yamagishi and Y. Nakamoto, *Chem. Commun.*, **2010**, 46, 3708-3710.

215. L. J. Bauer and C. D. Gutsche, *J. Am. Chem. Soc.*, **1985**, 107, 6063-6069.

216. L.-P. Yang, X. Wang, H. Yao and W. Jiang, *Acc. Chem. Res.*, **2020**, 53, 198-208.

217. N. i. Saleh, A. L. Koner and W. M. Nau, *Angew. Chem. Int. Ed.*, **2008**, 47, 5398-5401.

218. S. K. Konda, R. Maliki, S. McGrath, B. S. Parker, T. Robinson, A. Spurling, A. Cheong, P. Lock, P. J. Pigram, D. R. Phillips, L. Wallace, A. I. Day, J. G. Collins and S. M. Cutts, *ACS Med. Chem. Lett.*, **2017**, 8, 538-542.

219. A. L. Koner and W. M. Nau, *Supramol. Chem.*, **2007**, 19, 55-66.

220. E. Masson, X. Ling, R. Joseph, L. Kyeremeh-Mensah and X. Lu, *RSC Adv.*, **2012**, 2, 1213-1247.

221. S. Chatterjee and F. Liang, *ChemistrySelect*, **2023**, 8, e202204833.

222. Q. Duan, R. Chen, S. Deng, C. Yang, X. Ji, G. Qi, H. Li, X. Li, S. Chen, M. Lou and K. Lu, *Front. Chem.*, **2023**, 11.

223. A. Simeonov and M. I. Davis., Interference with Fluorescence and Absorbance, **2015**.

224. Q. Wang, L. Li and B. Xu, *Chem. Eur. J.*, **2009**, 15, 3168-3172.

225. E. Masson, Y. M. Shaker, J.-P. Masson, M. E. Kordesch and C. Yuwono, *Org. Lett.*, **2011**, 13, 3872-3875.

226. C. M. Geiselhart, H. Mutlu, P. Tzvetkova and C. Barner-Kowollik, *Polym. Chem.*, **2020**, 11, 4213-4220.

227. I. Bronstein and L. J. Kricka, *J. Clin. Lab. Anal.*, **1989**, 3, 316-322.

228. A. Fan, Z. Cao, H. Li, M. Kai and J. Lu, *Anal. Sci.*, **2009**, 25, 587-597.

229. C. A. Marquette and L. J. Blum, *Bioanalysis*, **2009**, 1, 1259-1269.

230. M. Matsumoto, *J. Photochem. Photobiol.*, **2004**, 5, 27-53.

231. W. Adam, D. Reinhardt and C. R. Saha-Möller, *Analyst*, **1996**, 121, 1527-1531.

232. M. A. Partearroyo, H. Ostolaza, F. M. Goñi and E. Barberá-Guillem, *Biochem. Pharmacol.*, **1990**, 40, 1323-1328.

233. J. Liu, J. Jiang, Y. Dou, F. Zhang, X. Liu, J. Qu and Q. Zhu, *Org. Biomol. Chem.*, **2019**, 17, 6975-6979.

234. A. Prabodh, S. Sinn, L. Grimm, Z. Miskolczy, M. Megyesi, L. Biczók, S. Bräse and F. Biedermann, *Chem. Commun.*, **2020**, 56, 12327-12330.

235. Z. Miskolczy, L. Biczók and G. Lendvay, *Phys. Chem. Chem. Phys.*, **2018**, 20, 15986-15994.

References

236. N. Watanabe, H. Takatsuka, H. K. Ijuin and M. Matsumoto, *Tetrahedron*, **2020**, 76, 131203.

237. S. Sinn, E. Spuling, S. Bräse and F. Biedermann, *Chem. Sci.*, **2019**, 10, 6584-6593.

238. D. M. Robinson and G. M. Keating, *Drugs*, **2006**, 66, 1515-1534.

239. C. Wu and J. R. Kovac, *Curr. Urol. Rep.*, **2016**, 17, 72.

240. S. Sakamoto, W. Putalun, S. Vimolmangkang, W. Phoolcharoen, Y. Shoyama, H. Tanaka and S. Morimoto, *J. Nat. Med.*, **2018**, 72, 32-42.

241. S. Nagasawa, D. Yajima, S. Torimitsu, F. Chiba and H. Iwase, *Forensic Sci. Int.*, **2015**, 257, e12-e15.

242. W. Klein-Schwartz and G. M. Oderda, *Drugs Aging*, **1991**, 1, 67-89.

243. R. M. N. Kohler and M. I. Lambert, *Br J Sports Med.*, **2002**, 36, 325.

244. F. Kamel, *Science*, **2013**, 341, 722-723.

245. L. A. Vermeulen and M. E. Thompson, *Nature*, **1992**, 358, 656-658.

246. P. Jagadesan, S. R. Valandro and K. S. Schanze, *Mater. Chem. Front.*, **2020**, 4, 3649-3659.

247. E.-C. Lee, H.-J. Kim and S. Y. Park, *Chem. Asian J.*, **2019**, 14, 1457-1461.

248. C. Hu, L. Grimm, A. Prabodh, A. Baksi, A. Siennicka, P. A. Levkin, M. M. Kappes and F. Biedermann, *Chem. Sci.*, **2020**, 11, 11142-11153.

249. M. A. Cejas and F. M. Raymo, *Langmuir*, **2005**, 21, 5795-5802.

250. C. A. Daykin, P. J. D. Foxall, S. C. Connor, J. C. Lindon and J. K. Nicholson, *Anal. Biochem.*, **2002**, 304, 220-230.

251. C. Marquez, H. Fang and W. M. Nau, *IEEE Transactions on NanoBioscience*, **2004**, 3, 39-45.

252. *Jama*, **2013**, 310, 2191-2194.

253. S. Holm, in *The International Encyclopedia of Ethics*, ed. H. LaFollette, Wiley-Blackwell, **2013**.

254. L. P. Nijhawan, M. D. Janodia, B. S. Muddukrishna, K. M. Bhat, K. L. Bairy, N. Udupa and P. B. Musmade, *J Adv Pharm Technol Res*, **2013**, 4, 134-140.

255. S. Manti and A. Licari, *Breathe (Sheff)*, **2018**, 14, 145-152.

256. D. Jiao, F. Biedermann and O. A. Scherman, *Org. Lett.*, **2011**, 13, 3044-3047.

257. N. M. Kumar, P. Gruhs, A. Casini, F. Biedermann, G. Moreno-Alcántar and P. Picchetti, *ACS Sens.*, **2023**, 8, 2525-2532.

258. M. A. Beatty and F. Hof, *Chem Soc Rev*, **2021**, 50, 4812-4832.

259. J. Kim, A. S. Campbell, B. E.-F. de Ávila and J. Wang, *Nat. Biotechnol.*, **2019**, 37, 389-406.

260. W. Gao, S. Emaminejad, H. Y. Y. Nyein, S. Challa, K. Chen, A. Peck, H. M. Fahad, H. Ota, H. Shiraki, D. Kiriya, D.-H. Lien, G. A. Brooks, R. W. Davis and A. Javey, *Nature*, **2016**, 529, 509-514.

261. G. Peng, U. Tisch, O. Adams, M. Hakim, N. Shehada, Y. Y. Broza, S. Billan, R. Abdah-Bortnyak, A. Kuten and H. Haick, *Nat. Nanotechnol.*, **2009**, 4, 669-673.

262. B. Pérez-Fernández, A. Costa-García and A. d. l. E.-. Muñiz, *Biosensors*, **2020**, 10, 32.

263. H. Luo, L.-X. Chen, Q.-M. Ge, M. Liu, Z. Tao, Y.-H. Zhou and H. Cong, *J. Incl. Phenom. Macrocycl. Chem.*, **2019**, 95, 171-198.

264. M. H. Tootoonchi, S. Yi and A. E. Kaifer, *J. Am. Chem. Soc.*, **2013**, 135, 10804-10809.

265. G. Moreno-Alcántar, A. Aliprandi, R. Rouquette, L. Pesce, K. Wurst, C. Perego, P. Brüggeller, G. M. Pavan and L. De Cola, *Angew. Chem. Int. Ed.*, **2021**, 60, 5407-5413.

266. M. Mydlak, M. Mauro, F. Polo, M. Felicetti, J. Leonhardt, G. Diener, L. De Cola and C. A. Strassert, *Chem Mater.*, **2011**, 23, 3659-3667.

267. J. A. Weinstein, D. C. Grills, M. Towrie, P. Matousek, A. W. Parker and M. W. George, *Chem. Commun.*, **2002**, 382-383.

268. J. A. G. Williams, in *Photochemistry and Photophysics of Coordination Compounds II*, eds. V. Balzani and S. Campagna, Springer Berlin Heidelberg, Berlin, Heidelberg, **2007**, pp. 205-268.

269. J. Liu, N. Jiang, J. Ma and X. Du, *Eur. J. Org. Chem.*, **2009**, 2009, 4931-4938.

270. P. Montes-Navajas, A. Corma and H. Garcia, *ChemPhysChem*, **2008**, 9, 713-720.

271. C. Yao, H. Lin, B. Daly, Y. Xu, W. Singh, H. Q. N. Gunaratne, W. R. Browne, S. E. J. Bell, P. Nockemann, M. Huang, P. Kavanagh and A. P. de Silva, *J. Am. Chem. Soc.*, **2022**, 144, 4977-4988.

272. S. Liu, C. Ruspic, P. Mukhopadhyay, S. Chakrabarti, P. Y. Zavalij and L. Isaacs, *J. Am. Chem. Soc.*, **2005**, 127, 15959-15967.

273. Colin A. Shanks, Andrew A. Somogyi and Edward J. Triggs, *Anesthesiol.*, **1979**, 51, 111-118.

274. T. R. Baker, P. Vouros, D. Rindgen and J. A. J. Martyn, *Biomed. Mass Spectrom.*, **1990**, 19, 69-74.

References

275.　C. H. M. Kerskes, K. J. Lusthof, P. G. M. Zweipfenning and J. P. Franke, *J. Anal. Toxicol.*, **2002**, 26, 29-34.

276.　M. A. Gamal-Eldin and D. H. Macartney, *Can. J. Chem.*, **2014**, 92, 243-249.

277.　V. P. Stankov-Jovanović, S. D. Nikolić-Mandić, L. M. Mandić and V. D. Mitić, *Anal. Biochem.*, **2006**, 385, 1462-1469.

278.　A. Poklis and E. G. Melanson, *J. Anal. Toxicol.*, **1980**, 4, 275-280.

279.　M. Zecevic, L. Zivanovic and A. Stojkovic, *J. Chromatogr. A*, **2002**, 949, 61-64.

280.　P. L. García, F. P. Gomes, M. I. R. M. Santoro and E. R. M. Kedor-Hackmann, *Anal. Lett.*, **2008**, 41, 1895-1908.

281.　H. Sayer, O. Quintela, P. Marquet, J.-L. Dupuy, J.-M. Gaulier and G. Lachâtre, *J. Anal. Toxicol.*, **2004**, 28, 105-110.

282.　A. A. Salem, B. N. Barsoum and D. M. El Said, *Helv. Chim. Acta*, **2005**, 88, 861-872.

283.　R. Romeo, L. M. Scolaro, V. Catalano and S. Achar, in *Inorganic Syntheses*, **1998**, pp. 153-158.

284.　S. P. Vorce, C. T. Mallak and A. Jacobs, *J. Anal. Toxicol.*, **2008**, 32, 422-427.

11.   Appendix

11.1.   Patents, publications and conference contributions

Patents

Novel chemosensors and their use in electrochemical detection methods, European patent application number 23175726.1 – Issued on May 2023.

Scientific publications

<u>N. M. Kumar</u>, P. Gruhs, A. Casini, F. Biedermann, G. Moreno-Alcántar and P. Picchetti, Electrochemical Detection of Drugs via a Supramolecular Cucurbit[7]uril-Based Indicator Displacement Assay. *ACS Sens.,* **2023**, *8*, 2525-2532.

<u>N. M. Kumar</u>, P. Picchetti, C. Hu, L. M. Grimm and F. Biedermann, Chemiluminescent Cucurbit[*n*]uril-Based Chemosensor for the Detection of Drugs in Biofluids. *ACS Sens.*, **2022**, *7*, 2312-2319.

P. Picchetti, M. V. Balli, S. Baker, <u>N. M. Kumar</u>, P. Gruhs, L. Prodi and F. Biedermann, Unimolecular Cucurbit[7]uril-Based Indicator Displacement Assay with Dual Signal-Readout for the Detection of Drugs. *Manuscript submitted to Analysis & Sensing (accepted)*.

V. Mahram, <u>N. M. Kumar</u>, P. Weslie, J. Krämer, F. Idiris and F. Biedermann, From Cuvette to Microplate: A Transition Guide for Accurate and Reproducible Binding Constant Determination in Supramolecular Chemistry. *Manuscript in preparation*.

K. S. Harikrishnan, N. Krishnan, <u>N. M. Kumar</u>, A. Krishna, G. Raj, D. Perumal, J. Kalathil, J. Krishna and R. Varghese, Galactose Grafted Two-Dimensional Nanosheets as a Scaffold for the In Situ Synthesis of Silver Nanoparticles: A Potential Catalyst for the Reduction of Nitroaromatics. *Chem. Eur. J.*, **2021**, *27*, 14100-14107.

N. Krishnan, D. Perumal, S. Atchimnaidu, K. S. Harikrishnan, M. Golla, <u>N. M. Kumar</u>, J. Kalathil, J. Krishna, D. K. Vijayan and R. Varghese, Galactose-Grafted 2D Nanosheets from the Self-Assembly of Amphiphilic Janus Dendrimers for the Capture and Agglutination of Escherichia coli. *Chem. Eur. J.*, **2020**, *26*, 1037-1041.

Conference contributions

Flash talk and Poster presentation - <u>Nilima Manoj Kumar</u>, Stephan Sinn, Katharina Wendler, Joana Krämer and Frank Biedermann, SupraChem, 2024, Ulm, Germany. *SUPRABANK –The Repository for Supramolecular Interactions*.

Poster presentation - <u>Nilima Manoj Kumar</u>, Pierre Picchetti, Changming Hu, Laura M. Grimm and Frank Biedermann, Supramolecular Chemistry Days for Young Researchers, 2023, Cagliari, Italy. *Chemiluminescent Cucurbit[n]uril-Based Chemosensor for the Detection of Drugs in Biofluids*.

Flash talk and Poster presentation - <u>Nilima Manoj Kumar</u>, Pierre Picchetti, Changming Hu, Laura M. Grimm and Frank Biedermann, European-Winter School on Physical Organic Chemistry (E-WISPOC), 2022, Ischia, Italy. *Chemiluminescent Cucurbit[n]uril-Based Chemosensor for the Detection of Drugs in Biofluids*.

11.2. Acknowledgements